Journal of Research of the National Bureau of Standards Vol. 49, No. 5, November 1952 Research Paper 2365

Analytical and Experimental Studies With Idealized Gas Turbine Combustors[1]

Fillmer W. Ruegg and Howard J. Klug

Problems of flow, heat release, and mixing in gas turbine combustion chambers are discussed and analyzed. The analysis is based on an idealized or equivalent chamber in which the end result is the same as in the conventional chamber, but in which the functions are separate and distinct. A large primary zone is advantageous, but the combustion process still is burdened by an inverse relationship between primary air and fuel. Conditions favorable to combustion in the primary zone over the whole range of operation are realized by means of a mechanical control. Agreement between analysis and experiment was demonstrated by tests of a chamber with a mechanical control. Comparison of the field of mixing of primary flame gas and secondary air with other studies of mixing revealed a general similarity, but a slower rate of mixing that is ascribed to the effects of a large difference of temperature or density in these experiments.

1. Introduction

Although jet propulsion for aircraft has become a practical reality, many problems connected with it are still only partially solved. One of these problems is the development of combustion chambers for turbojet engines that will give satisfactory performance under all service conditions. Satisfactory performance implies that a continuous supply of exhaust gas at the desired temperature is furnished the turbine, and that response to demands for changes of conditions is positive and occurs in a minimum of time. Other desirable characteristics are high combustion efficiency, small loss of pressure, uniformity of temperature in the exhaust, minimum size and weight consistent with required performance and life, and ease of manufacture and maintenance. Some compromises have been necessary in designing combustion chambers, since some of these features have been found to be obtained only at the expense of others.

Problems of flow and combustion in conventional combustion chambers are so complicated and interrelated that development of chambers has progressed largely by empirical methods. Although development by these methods has produced immediate results, in the long run a fundamental understanding of the problem is advantageous and will promote design on a more rational basis. It is the purpose of this paper to separate and examine some of the functions of conventional gas turbine combustion chambers in an attempt to arrive at a better understanding of their influence on the performance of the chamber as a whole.

2. Nomenclature

A = Area, ft².
c = Effectiveness of mixing.
C = Coefficient in mixing length equation.
c_p = Specific heat at constant pressure, Btu/lb°F.
d, D = Diameter, ft.
g = Standard acceleration of gravity, ft/sec².
l = Mixing length, ft.
L = Length of potential core, ft.
p = Absolute static pressure, lb/ft².
p_t = Absolute total pressure, lb/ft².
$q = \frac{1}{2}\rho V^2$; dynamic pressure, lb/ft².
r = Radius, ft.
r_m = Radius at which T (or V) is halfway between T (or V) at axis and that of secondary stream, ft.
R = Gas constant, ft-lb/lb ° F.
T = Absolute temperature, ° R.
V = Velocity, ft/sec.
W = Weight flow per unit time, lb/sec.
x = Axial distance from station 3, ft.
y = Lateral distance, ft.
z = Upper limit of probability integral.
ϵ = Emissivity.
η_b = Combustion efficiency.
ρ = Density, slugs/ft³.
σ = Scale factor.
τ = Turbulent shear stress, lb/ft².

SUBSCRIPTS

1 to 4 = Stations in the chamber.
f = Fuel.
i = Indicated.
p = Primary.
s = Secondary.

3. Combustion Chamber

Combustion chambers for gas turbines have been developed and modified according to the requirements of the system in which they are intended to be used. Although each chamber may be different from any other, it appears that most designs differ in detail only, and not in principle. An examination of the conventional combustion chamber reveals that there are four main functions that it must perform, (1) separation of the air into primary and secondary streams, (2) maintenance of a stable pilot zone, (3) combustion of fuel with the primary air, and (4) mixing of the burned gases with secondary air.

Design features may be illustrated by the schematic drawing in figure 1. A protected, turbulent zone of low velocity is established at A inside of the dome of the perforated liner, and when fuel is injected into this zone a mixture is formed which is capable of sustaining a stable flame. More air enters the liner between A and B and combustion proceeds as it

[1] The work described in this report was sponsored by the Bureau of Aeronautics, Department of the Navy.

223977—52——1

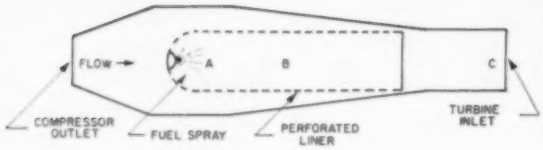

FIGURE 1. *The conventional chamber.*

A, Turbulent zone of low velocity; A to B, primary zone; B to C, mixing of secondary air with products of combustion from primary zone.

mixes with fuel. Velocity of the mixture in this zone is probably higher than the velocity of the flame in the mixture, but combustion is piloted by the flame from A. The air that takes part in the combustion in this zone is known as primary air. Secondary air enters and mixes with the products of combustion between B and C, thereby reducing the gas temperature to a safe operating level. Completeness of combustion is promoted if the air is admitted gradually into the liner and in a manner so that it does not quench the flame and cause blowout.

There is no assurance that all of the air that enters the liner between A and B takes part in the combustion process, and therefore it may be said that the separation into primary and secondary air is not distinct.

Gas turbine combustors must be capable of operating over a wide range of exhaust to inlet temperature ratio, and generally this flexibility is attained by injecting atomized liquid fuel into the pilot zone at A. This method of fuel injection provides heterogeneous mixtures that are capable of supporting stable combustion, even though their quality may differ substantially from stoichiometric. It does not follow that combustion must always be efficient with this system. Actually, it may be good over only a narrow range of conditions, and may become poor when others are imposed.

Loss of pressure due to flow friction is high, and problems of flow and combustion are complicated and interrelated. Flow is turbulent, and in some regions within the primary zone, it may actually be in an upstream direction. Combustion and mixing within the liner nowhere occur as distinct, individual processes. Although these conditions appear to be beneficial from the standpoint of performance and flexibility, they make a detailed analysis of the conventional chamber almost an impossibility.

If a chamber is designed to carry out the functions enumerated above as separate and distinct operations, then an analysis of its performance becomes possible. A chamber designed for this purpose may be called an idealized or equivalent chamber, equivalent in the sense that the end result is the same as in the conventional chamber. The differences between this chamber, represented by figure 2, and one of conventional design are apparent. Stations A, B, and C in each figure represent locations where the same respective operations are performed. In this equivalent chamber the air is separated into two distinct streams, and the drop in pressure due to flow friction that each experiences is made to occur

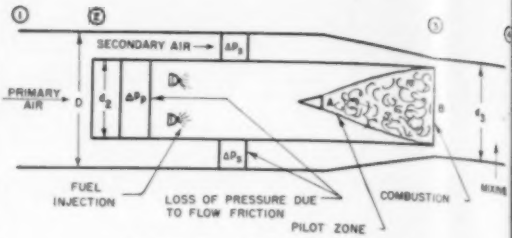

FIGURE 2. *The equivalent chamber.*

A, Turbulent zone of low velocity; A to B, primary zone; B to C, mixing of secondary air with products of combustion from primary zone.

in a manner that is subject to analysis. A throttling process is assumed for the primary air, and the secondary air is assumed to go through a throttling process followed by a reversible expansion. Fuel is injected and combustion is stablized after the primary throttling process, and is assumed to be complete within the primary zone. The size of the pilot zone has been diminished to that which would exist at a flame holder, and combustion may be said to occur as in ramjet chambers. Since combustion is made to occur at a fixed temperature ratio in a stream that has a uniform, measureable velocity, the process is subject to treatment by both analytical and experimental methods. Mixing of the burned gas with secondary air occurs only after combustion is complete, and the changes resulting from this process also may be predicted and measured.

4. Analysis of the Equivalent Combustion Chamber

The method used in the analysis depends on the fact that each function of the combustion chamber is considered to be performed as a distinct, individual operation. Changes of temperature, pressure, etc., are calculated for each, and from these the performance of the chamber as a whole is derived.

Before these calculations may be made, it is necessary to specify some of the conditions at which the chamber is required to operate. Although any practical chamber must be able to operate over a wide range of conditions, there is usually some condition where it performs best, and it is desirable that this should coincide with the condition that is used most often in service. For the purpose of this analysis, an exhaust to inlet temperature ratio of 3.2 is a suitable specification, because it is close to that used in practice and is also a convenient working condition for experimental purposes.

As combustion is usually best when the mixture of air and fuel is at or near stoichiometric, this condition may be used as the basis of a second specification. A mixture of this quality would give an exhaust to inlet temperature ratio of about 7.25 across the primary zone.

Some loss of pressure in conventional chambers occurs when the air flows through the perforations of the liner. In order to approximate this condition in the chamber represented in figure 2, it is necessary

to introduce loss of pressure in the flow of air in a manner that its effects can be determined analytically and experimentally. Once the magnitude of the loss of pressure due to friction is specified, the configuration of the chamber may be calculated to satisfy all of the above specifications, provided the conditions of the flow in the chamber are also specified. However, the solution of the problem would apply only to the set of conditions of flow that were specified. Because an infinite number of conditions is possible and as all of them cannot possibly be handled, it is necessary to make a choice. The problem is simplified if it is considered that the velocity of flow in the chamber approaches zero, and this assumption is used throughout these analyses. Combustion chambers of gas turbines are operated at relatively low velocities; hence such an assumption would not cause serious errors.

Other simplifying assumptions may be made without serious error. These are: rise of temperature in the primary zone may be accomplished without adding fuel to the flowing stream; specific heat, c_p, of the gas is independent of temperature; loss of pressure due to friction does not occur except where stated; velocity of flow is uniform in each zone across planes in the duct normal to the flow; and secondary air receives no heat before it mixes with the gas at high temperature from the primary zone.

The problems of flow, heat release, and mixing may be handled by using Bernoulli's equation and the conservation of momentum equation. Since it is considered that the velocity of flow approaches zero, Bernoulli's equation for incompressible, frictionless flow may be written

$$p+\tfrac{1}{2}\rho V^2=p_t, \tag{1}$$

where p_t and ρ are constant at all points in the flow. The conservation of momentum equation for heat release or mixing is

$$p+\rho V^2=\text{constant}, \tag{2}$$

and when heat release occurs where V approaches zero, eq 2 may be written

$$\lim_{V_1\to 0}\frac{p_1-p_2}{\frac{\rho_1 V_1^2}{2}}=2\left(\frac{T_2}{T_1}-1\right). \tag{2a}$$

The subscripts 1 and 2 in eq 2a indicate the state of the gas before and after heat release, respectively. When these equations are applied to cases where V_1 is appreciable, it is equivalent to considering that the fluid is incompressible, or that density is dependent only on temperature. The condition for continuity of flow may be written

$$\rho AV=\text{constant}. \tag{3}$$

Equations 1, 2, and 3 and the gas law, $p=g\rho RT$, are sufficient for the analysis of the problems of flow in the equivalent combustion chamber.

4.1. Effect of Size of the Primary Zone

Two design conditions of temperature rise in the chamber have been specified, but nothing has been said about the size of the primary zone. It would be possible to specify arbitrarily a size based on results of practical experience, but there is no assurance that the decision on this basis would be the most logical. A determination of the effect of size of the primary zone by analytical means probably would provide a sound basis on which to make a choice of size. This determination is attempted in the analysis that follows.

A list of the design conditions, in which the numerical subscripts refer to the stations in the chamber indicated in figure 2, is presented below. The subscripts p and s refer to primary and secondary air, respectively.

(1) $T_4/T_1=3.2$; (2) $T_{3,p}/T_1=7.25$; (3) $\Delta p_s/q_{2,s}=2=$loss of pressure due to flow friction; (4) $\Delta p_p/q_{2,p}=10=$loss of pressure due to flow friction; (5) $p_{3,s}=p_{3,p}$.

At low velocity, loss of pressure due to friction may be expressed as a constant number of velocity heads, q, where $q=\frac{1}{2}\rho V^2$. The losses indicated in the third and fourth specifications were chosen in an attempt to approximate those in practical chambers. The fifth specification is that pressure is uniform across the plane of station 3. Tollmien [1] [2] calculated that the pressure at the plane of the discharge of a free, round jet differs from the ambient by an amount equal to about one-tenth percent of the dynamic pressure of the jet. A pressure difference of this small magnitude would have no significance in the present analysis. A variation of serious magnitude probably would not be encountered except where the velocity of flow in the primary stream at station 3 equaled the acoustic velocity in the stream. Conditions such as this are not encountered in present-day engines, and consequently are not considered here.

The above specifications provide sufficient information to permit a calculation of the effect of liner size, d_2, on the problems of flow, heat release, and mixing in the equivalent chamber.

If W_p and W_s are the rates of flow of the primary and secondary streams, respectively, then when mixing of these streams occurs between stations 3 and 4, a heat balance may be written

$$W_p(T_{3,p}-T_4)c_p=W_s(T_4-T_1)c_p. \tag{4}$$

Noting that c_p is assumed to be independent of temperature, eq 4 may be written

$$\frac{W_p}{W_p+W_s}=\frac{\frac{T_4}{T_1}-1}{\frac{T_{3,p}}{T_1}-1}, \tag{5}$$

and when the first and second specifications are substituted, the right member of eq 5 is equal to

[2] Figures in brackets indicate the literature references at the of this paper.

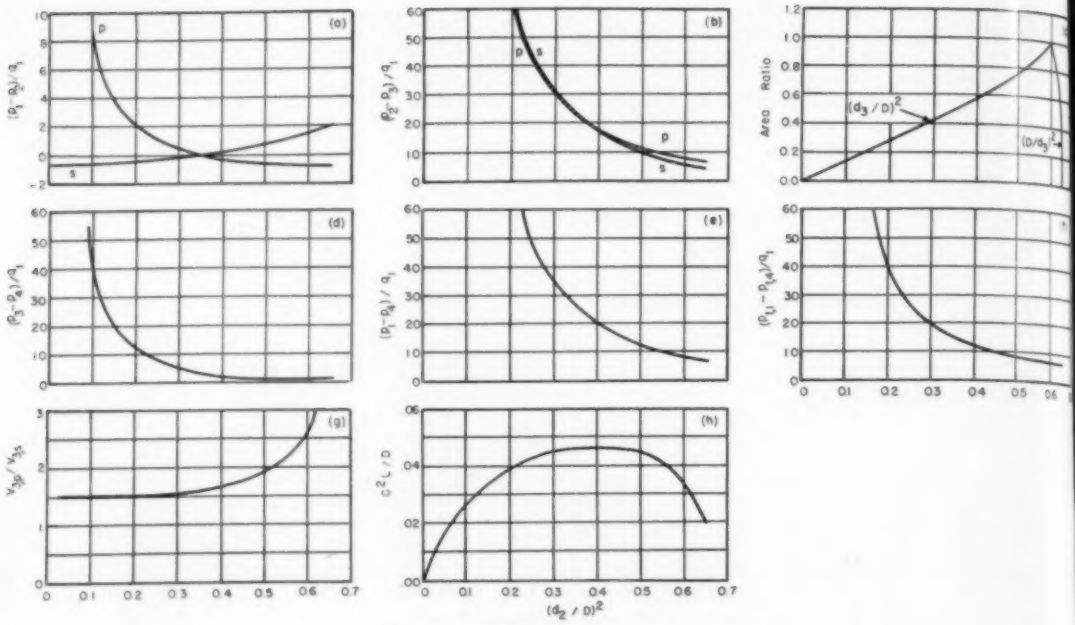

FIGURE 3. *Effect of size of primary zone.*

0.35. In other words, 35 percent of the air must enter the primary zone to fulfill the conditions of specifications (1) and (2). The air that enters the primary zone can be regarded as the central core of the stream at station 1. Since it is considered that the properties of the flow are uniform at this station, the diameter of this central core of primary air can be expressed by the equation

$$(d_1/D)^2=\frac{W_p}{W_p+W_s}. \tag{6}$$

Bernoulli's equation, eq 1, may be used to determine the changes of pressure between stations 1 and 2 as d_2 is changed. Thus

$$p_1-p_2=q_2-q_1=q_1\left(\frac{V_2^2}{V_1^2}-1\right), \tag{7}$$

and the ratio of the velocities for both primary and secondary air may be determined by the continuity equation as follows:

$$\left(\frac{V_{2,p}}{V_1}\right)^2=\frac{q_{2,p}}{q_1}=\left(\frac{d_1/D}{d_2/D}\right)^4 \tag{8}$$

$$\left(\frac{V_{2,s}}{V_1}\right)^2=\frac{q_{2,s}}{q_1}=\left(\frac{1-d_1^2/D^2}{1-d_2^2/D^2}\right)^2. \tag{9}$$

Since $(d_1/D)^2=W_p/(W_p+W_s)$, the pressure changes may be expressed by the equations

$$p_1-p_{2,p}=q_1\left[\frac{\left(\frac{W_p}{W_p+W_s}\right)^2}{\left(\frac{d_2}{D}\right)^4}-1\right], \tag{10}$$

$$p_1-p_{2,s}=q_1\left[\left(\frac{1-\frac{W_p}{W_p+W_s}}{1-\frac{d_2^2}{D^2}}\right)^2-1\right]. \tag{11}$$

These were evaluated and plotted versus $(d_2/D)^2$ in figure 3, a. When $(d_2/D)^2$ is greater than 0.35, the primary air diffuses into the primary zone, its velocity decreases, and its pressure increases. When $(d_2/D)^2=0.6$, the velocity of the primary air as established by eq 8 is about 58 percent of V_1.

Loss of pressure in the primary zone is the sum of that due to friction and combustion. This may be written

$$(p_2-p_3)_p=\Delta p_p+2q_{2,p}\left(\frac{T_{3,p}}{T_1}-1\right), \tag{12}$$

where the second term on the right side is determined by eq 2a, which is the loss due to combustion on the basis of the momentum equation. $q_{2,p}/q_1$ is given by eq 8, and the pressure loss thus may be expressed in terms of q_1 by the following equation:

$$\frac{(p_2-p_3)_p}{q_1}=\left[\frac{\Delta p_p}{q_{2,p}}+2\left(\frac{T_{3,p}}{T_1}-1\right)\right]\left(\frac{d_1/D}{d_2/D}\right)^4 \tag{13}$$

his was evaluated and the results are plotted in ure 3, b.

Calculation of the change of pressure in the econdary air is based on the assumption that $p_{3,p}=p_{3,s}$. In order to fulfill this condition, it is ecessary to change d_3 with d_2, and the required ange may be evaluated by using eq 1 and 3. hange of pressure in the secondary air may be ritten

$$p_{2,s}-p_{3,s}=q_{3,s}-q_{2,s}+\Delta p_s, \tag{14}$$

nd this may be solved for $p_{3,s}$. Eq 7 and 12 may be ombined to yield

$$p_{3,p}=p_1+q_1-q_{2,p}-\Delta p_p-2q_{2,p}\left(\frac{T_{3,p}}{T_1}-1\right), \tag{15}$$

nd since it is considered that $p_{3,p}=p_{3,s}$, the right de of eq 15 may be substituted for $p_{3,s}$ in q 14. By this method the following relation is erived,

$$q_{3,s}=(p_1-p_3)+(q_{2,s}-\Delta p_s)-(p_1-p_2)_s. \tag{16}$$

ow $q_{3,s}$ may be related to q_1 by the continuity quation, and this relation leads to

$$\frac{q_{3,s}}{q_1}=\left(\frac{D^2-d_1^2}{d_3^2-d_2^2}\right)^2, \tag{17}$$

nd when this is solved for $(d_3/D)^2$, the following is erived

$$\left(\frac{d_3}{D}\right)^2=\frac{1-\frac{d_1^2}{D^2}}{\left(\frac{q_{3,s}}{q_1}\right)^{1/2}}+\frac{d_2^2}{D^2}. \tag{18}$$

These equations furnish sufficient information to valuate the change of pressure and of d_3 as d_2 is hanged. Thus eq 14 and 16 evaluate $(p_{2,s}-p_{3,s})$ nd eq 16 and 18 evaluate $(d_3/D)^2$. Changes of pressure between stations 2 and 3 are plotted in figure , b, and $(d_3/D)^2$ is plotted in figure 3, c. Both are lotted against $(d_2/D)^2$, which defines the size of the rimary zone. Figure 3, b, shows that the pressure oss decreases rapidly as the size of the primary zone s increased. However, the velocity in the secondary one becomes high, and a point is reached (when $(d_2/D)^2=0.6$) where the loss in pressure across the hrottle is so high that there is no need for more drop n pressure by expansion in the nozzle at station 3. t this point $d_3=D$. If the primary zone were made till larger, the loss of pressure in the secondary air ould be so high that an enlargement or diffuser ould be necessary to recover and thus maintain the quality of pressure across station 3. Thus d_3 would ave to become larger than D, and this is shown in igure 3, c, by the curve of $(D/d_3)^2$, where this ratio ecomes zero when $(d_2/D)^2=0.65$. For all practical purposes, it may be said that the area of the primary one in this chamber cannot exceed 60 percent of the otal area. This area of the primary zone depends, of course, on the relative pressure losses in the primary and secondary zones. For example, if no friction loss were assumed, the maximum area would be 66 percent, whereas if both the assumed losses were doubled, the maximum area would decrease to 58 percent of the total.

At station 3 the primary air at high temperature and the secondary air begin to mix, and the resulting changes of pressure may be calculated by the equation for the conservation of momentum. For this case it may be written

$$(p_3+2q_{3,s})\left(1-\frac{d_2^2}{d_3^2}\right)+(p_3+2q_{3,p})\frac{d_2^2}{d_3^2}=p_4+2q_4. \tag{19}$$

This equation may be arranged to the more convenient form

$$\frac{p_3-p_4}{q_1}=2\frac{q_4}{q_1}-2\frac{q_{3,s}}{q_1}\left(1-\frac{d_2^2}{d_3^2}\right)-2\frac{q_{3,p}}{q_1}\left(\frac{d_2}{d_3}\right)^2,$$

and the change of pressure is determined by evaluating each of the separate terms and taking the sum. These terms may be evaluated by using the continuity equation and the gas law, and always considering that ρ is dependent only on temperature. Thus

$$2\frac{q_4}{q_1}=2\frac{T_1}{T_4}\left(\frac{T_4}{T_1}\frac{D^2}{d_3^2}\right)^2=2\frac{T_4}{T_1}\left(\frac{D}{d_3}\right)^4, \tag{20}$$

$$2\frac{q_{3,s}}{q_1}\left(1-\frac{d_2^2}{d_3^2}\right)=2\left(\frac{D^2-d_1^2}{d_3^2-d_2^2}\right)^2\left(1-\frac{d_2^2}{d_3^2}\right), \tag{21}$$

$$2\frac{q_{3,p}}{q_1}\left(\frac{d_2}{d_3}\right)^2=2\frac{T_1}{T_{3,p}}\left(\frac{d_1^2}{d_2^2}\frac{T_{3,p}}{T_1}\right)^2\left(\frac{d_2}{d_3}\right)^2=2\frac{T_{3,p}}{T_1}\frac{d_1^4}{d_2^2d_3^2}. \tag{22}$$

The values of these terms were determined from the previous relations, and the sum expressed as $(p_3-p_4)/q_1$ is plotted versus $(d_2/D)^2$ in figure 3, d. The over-all change of pressure from station 1 to 4, which was evaluated by a summation of the successive changes, is plotted versus $(d_2/D)^2$ in figure 3, e.

Although the over-all change of pressure is informative, it does not allow ready comparison with the change of pressure of other combustion chambers. In order to make a comparison on this basis, it would be necessary for each chamber to have inlet and exhaust ducts of the same relative size. However, if the loss of pressure is expressed in the fundamentally more useful form of total pressure, a comparison is possible without this information about size. Loss of total pressure may be written

$$\frac{p_{t,1}-p_{t,4}}{q_1}=\frac{p_1-p_4}{q_1}-\frac{q_4}{q_1}+1. \tag{23}$$

The first two terms on the right side were evaluated previously (see fig. 3, e, and eq 20), and the loss of total pressure was determined and is plotted versus $(d_2/D)^2$ in figure 3, f. Inspection of this curve reveals the advantage of a liner of large size. When the liner of this chamber occupies 60 percent of the total area, the loss of pressure is about half that when the liner occupies 35 percent of the area.

Little is known about the factors that control the rate of mixing of gas streams under conditions that exist in combustion chambers. In practical chambers the rate is accelerated by the turbulent flow of the air through the perforations of the liner. Although this is accomplished at the expense of loss of pressure, it is compensated for by the consequent reduction in length of the chamber. One of the factors that may influence the rate of mixing is the ratio of the velocity of the gas streams at station 3. The ratio of $q_{3,p}/q_{3,s}$ may be determined from eq 21 and 22, and noting that $T_{3,p}/T_1=7.25$, the velocity ratio may be derived, and equals

$$\frac{V_{3,p}}{V_{3,s}}=\frac{T_{3,p}}{T_1}\left(\frac{d_1}{d_2}\right)^2\frac{\left(\frac{d_3}{D}\right)^2-\left(\frac{d_2}{D}\right)^2}{1-\left(\frac{d_1}{D}\right)^2}. \tag{24}$$

This was evaluated and the ratio is plotted versus $(d_2/D)^2$ in figure 3, g. It increases with an increase of the size of the liner, notwithstanding the fact that $V_{2,p}$, and therefore $V_{3,p}$, decreases. The degree of expansion required in the secondary stream also decreases, and $V_{3,s}$ decreases at a greater rate than $V_{3,p}$.

Squire and Trouncer [2] analyzed the problem of incompressible mixing of a round jet in a general stream, and the results were used here in an attempt to determine the effect of liner size on the mixing of the primary and secondary streams. Although the conditions existing in a combustion chamber differ in many respects from those assumed in the analysis, it is possible that the two cases would exhibit similar behavior.

In the analysis [2] the momentum transfer theory was used to determine the way in which velocity is transferred between two round streams. Turbulent shear stress, τ, defined by the equation

$$\tau=\rho l^2\left(\frac{dV}{dr}\right)^2 \tag{25}$$

was equated to the change of momentum flux of the mixing region with axial distance. Mixing length, l, was assumed equal to the width of the mixing region multiplied by a constant of proportionality, C. The constant C was considered a characteristic of the turbulent motion, and appeared in the end result as a constant to be evaluated experimentally. It was also assumed that the variation of velocity across the mixing region was similar to that determined by the cosine equation

$$\frac{V-V_s}{V_{r=0}-V_s}=\frac{1}{2}\left(1+\cos\frac{\pi r}{2r_m}\right), \tag{26}$$

where r_m is the radius at which velocity is half way between axial and secondary stream velocity. Regions in the flow and significance of terms in eq 26 are illustrated in figure 4.

Extent of the potential core of undisturbed primary stream, L/d_2, was found to increase as the ratio

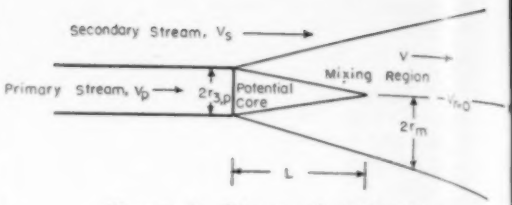

FIGURE 4. *Diagram of mixing field.*

of primary to secondary stream velocity, $V_{3,p}/V_{3,s}$, decreased and approached unity. Beyond L, the rate of decay of velocity along the axis was not influenced greatly by $V_{3,p}/V_{3,s}$, and therefore for the present present purposes L may be regarded as an inverse measure of the effectiveness of the mixing process in bringing the two streams to a uniform state. In other words, at a given value of axial distance x, $(x>L)$, decay along the axis would be less complete when L is large.

Squire and Trouncer present values of L/d_2 and $V_{3,p}/V_{3,s}$, and in this analysis the variation of $V_{3,p}/V_{3,s}$ with d_2/D has been determined. A combination of the two sets of information will allow determination of L as a function of d_2, and this is presented in figure 3, h. In their analysis the constant C was regarded as independent of $V_{3,p}/V_{3,s}$, and this same assumption is made here. At small values of d_2, L is also small, and mixing would probably be good. As d_2 is increased, $V_{3,p}/V_{3,s}$ increases slowly, but not sufficiently to counterbalance increase of d_2, and L increases. However, a point is reached where $V_{3,p}/V_{3,s}$ increases at a rate sufficient to counterbalance increase of d_2, and L begins to decrease. When $(d_2/D)^2=0.6$, L is well below the maximum, and it may be said that mixing probably would be relatively effective at this condition. In connection with these conclusions, it must be remembered that there are differences between the conditions assumed in the theory and those existing in a chamber. A large difference of temperature, confinement of the mixing region by the walls of the chamber, and a relatively large primary stream would probably influence the mixing in a manner that would require experimental determination.

This analysis has indicated the effect of the size of the primary zone on the problems of flow, heat release, and mixing in the equivalent chamber. A primary zone of large size appears to offer the advantages of low velocity in the primary zone, and reduced loss of pressure across the chamber. Low velocity probably would simplify the problem of maintenance of a stable flame, and a reduction in the loss of pressure would increase the "mechanical efficiency" of the chamber and thereby increase the over-all efficiency of the engine in which it would be used. With regard to the problem of mixing, the analysis indicates no serious disadvantage attached to a large primary zone. Maximum area of the primary zone in the equivalent chamber is found to be 60 percent of the total chamber area. Measurements of practical chambers indicate that the area

of the primary zone is generally about 60 percent of the total, and this point of similarity between analysis and practice is gratifying. For these reasons the size of the primary zone is fixed at the maximum value in the analysis that follows.

4.2. Analysis of Operation of the Equivalent Combustion Chamber

The only means of control over the over-all temperature ratio in conventional chambers is by the variation of the rate of fuel injection into the primary zone. This may be approximated for purposes of analysis by assuming that the temperature ratio, $T_{3,p}/T_1$, in the primary zone is allowed to change, while holding the configuration of the chamber constant, as determined above. Before proceeding to the calculations, it is advantageous to list the following complete specifications for this combustion chamber:

(1) $d_2^2=0.6D^2$; (2) $d_3=D$; (3) $\Delta p_s/q_{2,s}=2$=loss of pressure due to flow friction; (4) $\Delta p_p/q_{2,p}=10$=loss of pressure due to flow friction; (5) $p_{3,s}=p_{3,p}$; (6) T_4/T_1 varies with $T_{3,p}/T_1$.

The problem is to evaluate the distribution of air between the primary and secondary zones on the basis that $p_{3,p}$ will always equal $p_{3,s}$. Exhaust to inlet temperature ratio, T_4/T_1, can be determined once the distribution is known. Loss of pressure in the primary zone is given by eq 12, and by using eq 1, $p_{2,p}$ may be written in terms of p_1, as follows:

$$p_{2,p}=p_1+q_1-q_{2,p}. \tag{27}$$

Combining these two equations gives

$$(p_1-p_3)_p=q_{2,p}\left(\frac{\Delta p_p}{q_{2,p}}+2\,\frac{T_{3,p}}{T_1}-1\right)-q_1. \tag{28}$$

Loss of pressure in the secondary air is given by eq 14, and by evaluating $p_{2,s}$ in terms of p_1 and combining, there results

$$p_1-p_{3,s}=2q_{2,s}+q_{3,s}-q_1. \tag{29}$$

Equating 28 and 29 on the assumption that $p_{3,p}=p_{3,s}$ yields

$$q_{2,p}\left(\frac{\Delta p_p}{q_{2,p}}+2\,\frac{T_{3,p}}{T_1}-1\right)=2q_{2,s}+q_{3,s}. \tag{30}$$

Since d_3 is specified equal to D, $q_{2,s}=q_{3,s}$, and eq 30 will yield a relation between $q_{2,p}$, $q_{2,s}$ and $T_{3,p}/T_1$, as follows:

$$\frac{q_{2,s}}{q_{2,p}}=\frac{\Delta p_p/q_{2,p}+2(T_{3,p}/T_1)-1}{(\Delta p_s/q_{2,s})+1}. \tag{31}$$

This equation, when combined with the equation of continuity of flow,

$$(\rho VA)_1=\frac{W_p}{g}+\frac{W_s}{g}=(\rho VA)_{2,p}+(\rho VA)_{2,s} \tag{32}$$

will yield a relation that will predict how the air divides between the primary and secondary zones as $T_{3,p}/T_1$ is changed. Thus the continuity equation may be written in the form

$$\frac{W_p}{W_p+W_s}=\frac{1}{1+\dfrac{V_{2,s}}{V_{2,p}}\,\dfrac{D^2-d_2^2}{d_2^2}} \tag{33}$$

and since $V_{2,s}/V_{2,p}=(q_{2,s}/q_{2,p})^{1/2}$, the fraction of air going into the primary zone is

$$\frac{W_p}{W_p+W_s}=\frac{1}{1+\left[\dfrac{\Delta p_p/q_{2,p}+2(T_{3,p}/T_1)-1}{\Delta p_s/q_{2,s}+1}\right]^{1/2}\left(\dfrac{D^2}{d_2^2}-1\right)}. \tag{34}$$

Equation 5 expresses the relation between T_4/T_1 and $W_p/(W_p+W_s)$, and this may be combined with eq 34 to yield

$$\frac{T_4}{T_1}=1+\frac{\dfrac{T_{3,p}}{T_1}-1}{1+\left[\dfrac{\Delta p_p/q_{2,p}+2(T_{3,p}/T_1)-1}{\Delta p_s/q_{2,s}+1}\right]^{1/2}\left(\dfrac{D^2}{d_2^2}-1\right)}. \tag{35}$$

This expresses the relation between the overall temperature ratio and the temperature ratio in the primary zone, and is plotted in figure 5, a. The relation between T_4/T_1 and $W_p/(W_p+W_s)$ is plotted in figure 5, b.

Inspection of these curves reveals some interesting information concerning the operation of the chamber. Although $T_{3,p}/T_1$ increases with T_4/T_1, the fraction of air going into the primary zone decreases. This may be interpreted to mean that as more fuel is injected into the primary zone, the flow of air into it will decrease. Thus the length of the flame will increase with T_4/T_1, and at values higher than the design condition it may extend downstream beyond the primary zone. Mixing with secondary air may not be complete by the time the gas enters the turbine, and the turbine may be exposed to gas at excessively high temperatures. A further possibility is that the conditions may not be favorable for combustion beyond the primary zone. The flame may be quenched by the large quantity of excess air, and combustion efficiency will then be low. In addition, the pilot zone may become so rich in fuel that it will not support combustion, and rich blowout will occur.

Conversely, at low values of T_4/T_1, the mixture in the primary zone will be lean in fuel, and combustion may be poor. As T_4/T_1 is decreased, a point will be reached where the mixture in the primary zone will be too lean to support combustion, and lean blowout will occur. Moreover, the velocity in the primary zone increases and adds to the difficulty. These effects are observed in testing of practical chambers, although not exclusively because of the reasons enumerated.

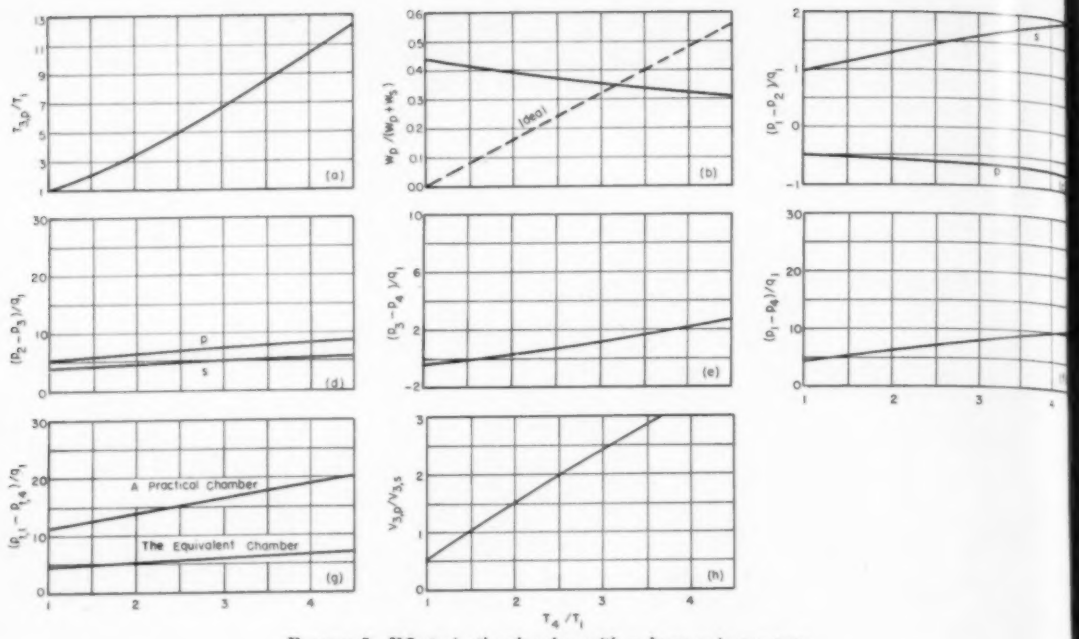

FIGURE 5. *Effects in the chamber with a large primary zone.*

In contrast to the air distribution determined above, a distribution is shown based on maintenance of near stoichiometric conditions in the primary zone. Equation 5 was used with a constant value of $T_{3,p}/T_1$ equal to 7.25, and the dotted curve labeled "ideal" in figure 5, b, is the result. This ideal distribution is radically different and points out the fact that the conventional chamber has proper distribution only at the design condition, that is, at the value of T_4/T_1 where the two curves cross.

Both the type of mixture of air and fuel and the velocity of the air in the combustion chamber influence the lean and rich limits of combustion. Heterogeneous mixtures are used exclusively because the range of combustible limits is relatively wide compared to that of homogeneous mixtures. It is probably true that low velocity tends to widen the limits in all chambers of this type.

When the distribution of the air is known, the changes of pressure and velocity in the chamber may be determined. Because the fraction of air going into the primary zone changes with T_4/T_1, it is evident that the streamlines of this air will diverge or converge on going from station 1 to 2, depending on the quantity that is flowing. If this fraction is smaller than that of the fraction of the area included by the primary zone, the streamlines will diverge, and the air will diffuse into the primary zone. Change of pressure between stations 1 and 2 may be determined as before by eq 5 to 11, remembering in this case that the fraction of primary air is the variable. A plot of these is presented in figure 5, c, for both primary and secondary air streams. At all values of T_4/T_1 the primary air in this chamber diffuses into the primary zone, whereas the secondary air expands.

The changes of pressure between stations 2 and 3 are evaluated by combining eq 28 and 10 for the primary zone, and 28 and 11 for the secondary zone. Thus by this method

$$p_{2,p}-p_3=(p_1-p_3)-(p_1-p_{2,p}), \tag{36}$$

and

$$p_{2,s}-p_3=(p_1-p_3)-(p_1-p_{2,s}). \tag{37}$$

These changes were evaluated, and the results are plotted in figure 5, d. For this chamber the loss in static pressure from station 2 to 3 does not change greatly with T_4/T_1.

Mixing of the primary and secondary streams begins at station 3, and the change of pressure that results may be calculated as before by eq 19 through 22. This is plotted in figure 5, e, and the over-all change of pressure from station 1 to 4 is plotted in figure 5, f. Loss of total pressure may also be evaluated as before (see eq 23), and is plotted in figure 5, g. In this equivalent chamber the total loss is about $6q_1$.

Observed loss of total pressure in a practical combustion chamber is also shown for comparison. These data were observed when V_1 was equal to 70 ft/sec, and displacement of the curves from each other is an indication of the relative magnitude of the loss of pressure due to friction. Loss of pressure in a combustion chamber is undesirable, because it lowers the over-all efficiency of the engine in which it is used, and from this standpoint it appears that this equivalent chamber would be superior. However, size and performance of the chambers in other respects must also be considered before an effective

mparison can be made. Combustion efficiency, bility, etc. are very important, but all the factors at influence these are not thoroughly understood. ch factors as pressure, temperature, character of e mixture of air and fuel, etc. may not have the me effects in all combustion chambers, and these e not considered in this analysis. Their influence any one chamber is determined almost exclusively experiment.

The ratio of the velocities of the primary to secdary air at station 3, $V_{3,p}/V_{3,s}$ was evaluated as fore (see eq 24) and is plotted versus T_4/T_1 in gure 5, h. It increases with T_4/T_1, and probably the ixing process will be most effective in bringing the s to a uniform state when outlet temperature is gh. Effective mixing is needed most at this conion of high temperature.

The combustion chamber described and analyzed similar to practical chambers in which over-all tio of temperature T_4/T_1 is controlled by rate of el injection into the primary zone. In the analysis is method of control is simulated by variation of mperature ratio, $T_{3,p}/T_1$, in the primary zone. It s been pointed out that this system of control has rtain undesirable effects in the combustion chamber. hen the conditions of operation deviate from the sign point, the quality of the mixture of air and el in the primary zone also deviates from the qualy that is most favorable for combustion. Hence e efficiency of combustion probably would decrease, nd at extreme conditions the mixture would become ither too rich or lean to support combustion. It is ecognized that this system has certain advantages, uch as simplicity of control, because all that is required is a control of the rate of fuel injection into e primary zone. However, the advantages of aintaining conditions for good combustion are also pparent, and some effort may well be made to nvestigate the requirements for this objective.

3. Analysis of Operation of a Chamber with a Controlled Primary Zone

As stated before, combustion is usually best when he mixture of air and fuel is near stoichiometric, nd hence $T_{3,p}/T_1$ may be selected to be equal to 25 as before. The problem then is to select a ethod and determine the conditions that are necssary to hold $T_{3,p}/T_1$ constant while T_4/T_1 is varied. Probably the first method that comes to mind is the ariation of the size of the mixing section, since this ethod was used in the first analysis. In that analsis d_2 was varied, and d_3 was changed simultaneously to hold $T_{3,p}/T_1$ constant. This method would equire an adjustable nozzle at station 3, and in servce it probably would be impractical. However, an djustable throttle, or valve, also may be inserted in he secondary zone for this purpose. Although this ethod of control introduces loss of pressure due to riction, it has certain advantages from the standoint of mechanical simplicity. A combustion chamber with such a device is represented by figure 6, here the throttle takes the form of two perforated, hin annuli. The pressure drop in the secondary

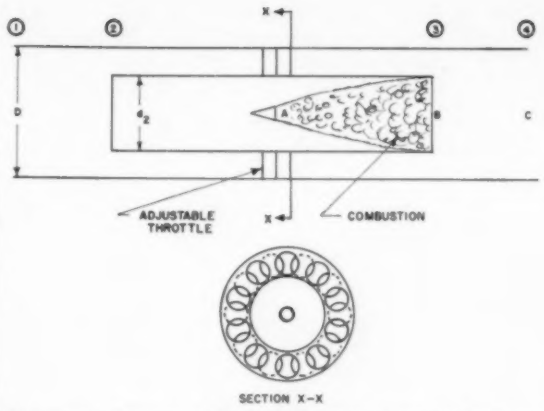

FIGURE 6. *Diagram of the chamber with the controlled primary zone.*

stream is adjusted by rotating one annulus relative to the other, thus providing larger or smaller openings as desired. This is only one of many possible schemes that might accomplish the same object. It will, however, serve for the purposes of this analysis.

The specifications for this case are (1) $T_{3,p}/T_1=7.25$; (2) $d_2^2=0.35D^2$; (3) $d_3=D$; (4) $\Delta p_p=0$; (5) $p_{3,s}=p_{3,p}$; (6) T_4/T_1 varies with $\Delta p_s/q_{2,s}$.

Stations in the chamber are shown in figure 6. It will be noted that d_2 was specified small ($0.35^{1/2}D$), and this was done for several reasons. Experimental work was planned on this chamber, and it appeared that conditions in a small primary zone would be more favorable in the proposed experiments to a well-regulated combustion process. In a large zone the velocity of the primary stream would be low, and probably the flame would seat at the fuel injector under some conditions, and under others would require a flame holder for stabilization. In a small zone, velocity would be relatively high, and combustion could be well regulated and performed in a homogeneous mixture of air and fuel with the seat of the flame at any desired position. A large primary zone would require a throttle in the primary stream, with attendant increase of mechanical problems and unknown effects on the flow conditions and combustion process. Another reason for a small zone was that a study of the mixing process of flame gas and secondary air could be made under conditions more nearly comparable with those assumed in theoretical studies of spread of free jets and of mixing of coaxial streams. The particular size chosen for the primary zone is that for which the flow of air will be undisturbed when operating at the design condition of $T_4/T_1=3.2$. At this design condition primary air is 35 percent of the total (see eq 5). With regard to the specification of no pressure loss due to friction in the primary zone, this is not a serious departure from reality because the loss can be made small when combustion is performed under the conditions mentioned. These specifications of the method of combustion and of

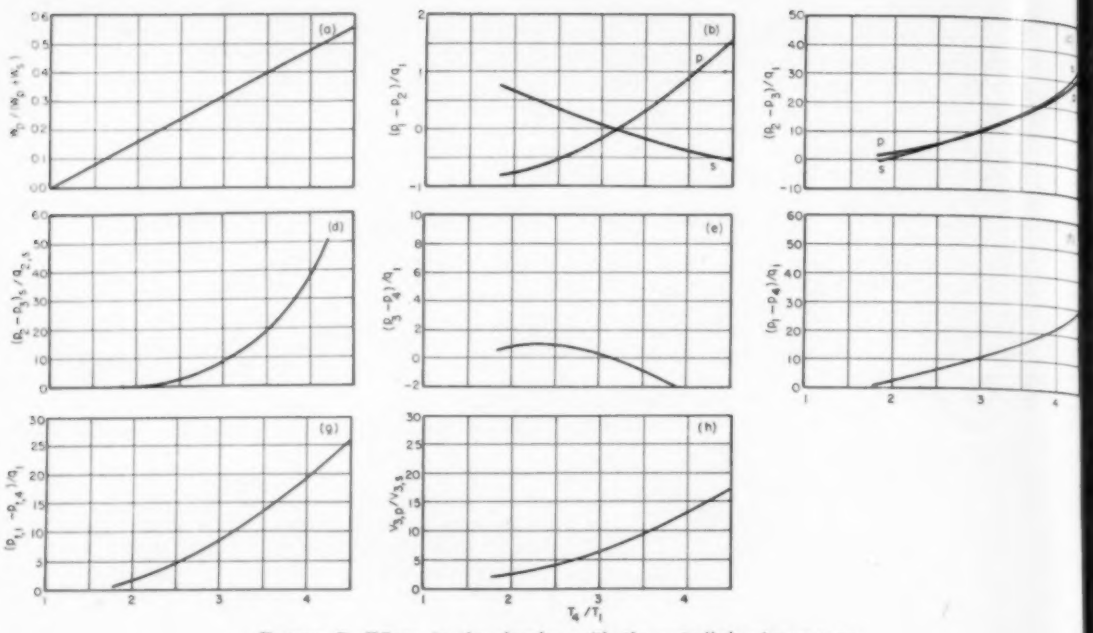

FIGURE 7. *Effects in the chamber with the controlled primary zone.*

pressure loss in the primary zone, although practical in the laboratory, probably would not be practical in actual engines where flexibility of operation is important.

The fraction of air going into the primary zone under the conditions specified may be calculated again by eq 5, using $T_{3,p}/T_1$ constant at 7.25. Results of these calculations are shown in figure 7, a. Change of pressure in the primary and secondary air between stations 1 and 2 may be calculated by using eq 10 and 11, and these changes are shown in figure 7, b.

Loss of pressure in the primary zone is

$$(p_2-p_3)_p=2\left(\frac{T_{3,p}}{T_1}-1\right)q_{2,p}, \tag{38}$$

and in order to evaluate 38 it is necessary to express $q_{2,p}$ in terms of q_1. By Bernoulli's equation, eq 1, $q_{2,p}$ may be written

$$q_{2,p}=(p_1-p_2)_p+q_1, \tag{39}$$

and since $(p_1-p_2)_p$ is determined by eq 10, eq 38 and 39 may be combined to yield:

$$(p_2-p_3)_p=2q_1\left(\frac{T_{3,p}}{T_1}-1\right)\frac{\left(\frac{W_p}{W_p+W_s}\right)^2}{\left(\frac{d_2}{D}\right)^4}. \tag{40}$$

This was evaluated and is plotted in figure 7, c.

As it is considered that the pressure is uniform across station 3, $p_{3,s}=p_{3,p}$ and $(p_2-p_3)_s$ may be determined as follows:

$$(p_2-p_3)_s=(p_1-p_2)_p+(p_2-p_3)_p-(p_1-p_2)_s. \tag{41}$$

All of the terms on the right side have been evaluated and their sum is plotted in figure 7, c.

The magnitude of this pressure change is variable over the operating range, and the variation is accomplished by changing the opening of the adjustable throttle shown in figure 6. The pressure change is expressed in terms of q_1, but it is also of interest to define the change of pressure with respect to $q_{2,s}$, as this may be of aid in the design of the throttle. Equation 9 is the relation between q_1 and $q_{2,s}$, and it may be applied for this purpose as follows:

$$\frac{\Delta p_s}{q_{2,s}}=\frac{(p_2-p_3)_s}{q_1}\,\frac{q_1}{q_{2,s}}=\frac{(p_2-p_3)_s}{q_1}\left[\frac{1-(d_2/D)^2}{1-(d_1/D)^2}\right]^2 \tag{42}$$

This relation was evaluated and $(p_2-p_3)_s/q_{2,s}$ is plotted versus T_4/T_1 in figure 7, d. When the throttle is opened, the fraction of air going into the primary zone decreases, thereby decreasing T_4/T_1. If the throttle were removed entirely ($\Delta p_s=0$), T_4/T_1 would be about 1.8. Lower values of T_4/T_1 could only be achieved by decreasing $T_{3,p}/T_1$ or by insertion of a throttle in the primary zone.

Change of pressure due to mixing of the secondary and primary streams may be calculated by eq 19 to 22. The term d_3 in these equations for this case is equal to D, and when this substitution is made, $(p_3-p_4)/q_1$ can be evaluated. Figure 7, e, is a plot of this quantity. The over-all change of pres-

ure, $(p_1 - p_4)$, which was evaluated by adding the successive changes, is plotted in figure 7, f.

Loss of total pressure may be determined by eq 23. Then q_4/q_1, expressed by eq 20, is substituted in 23 the following relation is derived:

$$\frac{\Delta p_t}{q_1} = \frac{p_1 - p_4}{q_1} - \frac{T_4}{T_1} + 1. \tag{43}$$

This was evaluated and is plotted versus T_4/T_1 in figure 7, g. Inspection of this curve reveals that the loss is substantially higher than in the previous case at the higher values of T_4/T_1. The previous case was calculated on the basis that pressure was lost due to friction in the primary zone, but in this case none was assumed. In any practical application of a chamber of this type, some means of stabilizing the flame would be necessary, and this would introduce loss of pressure in the primary zone. The magnitude of the loss of pressure required in service probably would be comparable to that in the conventional chamber. If this loss had been considered, the over-all loss of total pressure would have been higher than indicated in figure 7, g, and higher than that of the conventional chamber.

The ratio of the velocities of the primary and secondary streams at station 3, $V_{3,p}/V_{3,s}$, was evaluated and is plotted in figure 7, h. This ratio increases with T_4/T_1, and if this increase is a sign of an increase in the effectiveness of mixing, uniformity of temperature in the exhaust will be good in this chamber under conditions of maximum temperature rise.

The problem of control in combustion chambers of this type would be more difficult than that of a conventional chamber. A mechanism would be required to adjust the throttle in the secondary air in response to change of T_4 or to change of over-all air-fuel ratio. Another method, analagous to that used in reciprocating engines, would be manual control of this throttle, with fuel rate automatically controlled in accordance with throttle opening. The problems of manufacture, installation, and maintenance would be more complicated, but improved performance over a wider range might compensate for the added mechanical complications.

5. Experimental Program

The specifications for the preceding analysis were chosen with the thought that experimental work would be undertaken to check the results of the analysis. It is relatively simple to match experiment and analysis insofar as the physical size of the chamber and temperature rise therein are concerned, but deviation in other respects probably would influence the results. The mere fact that combustion occurs requires addition of mass (of fuel) to the flowing stream. Specific heat is not independent of temperature, loss of pressure due to friction cannot be localized, and exchange of heat between primary and secondary streams before mixing cannot be prevented. Although uniform velocity can be provided across the plane of the chamber entrance in the experiments, the flow will take up a nonuniform distribution at other stations. Operation of the chamber at a finite velocity of flow would also introduce some deviation due to compressibility, but not of serious magnitude if the flow Mach number is not above 0.1. Influence of compressibility on the flow relations is discussed in detail in reference [3]. Some deviation between theory and experiment is to be expected, but probably is not of serious magnitude.

5.1. Experimental Apparatus

The experimental combustion chamber was constructed of standard 6 in. pipe with a 4-ft coaxial liner, 3⅝ in. inside diameter and a wall thickness of ⅛ in. The pipe was cut and flanged as illustrated in figure 8 for accessibility to the liner. A schematic drawing of the system, in which the location of the stations is shown, is also presented in figure 8. Dimension X was 10 in. in the experiments on flow and heat release, and 8 ft in the experiments on mixing. Uniform velocity across the plane of the entrance to the chamber was provided by a nozzle of 12-in. diameter at the inlet and 6 in. at the outlet, or chamber, end. Throttles were placed in the secondary or primary zones as required to control the air distribution between zones. The throttle in the secondary zone was made of two thin annuli containing equally spaced ⅞-in. holes. Rotation of one annular plate with respect to the other controlled the opening and thereby the distribution. Throttles in the primary zone consisted of disks with various sized holes at their centers.

Flow of air to the chamber was metered by a calibrated orifice located in the system far upstream from the burner. Liquid propane flowed from a weighing tank through a rotameter to a vaporizer tube in the shape of a hairpin mounted in the system far downstream from the liner. Gaseous propane from the vaporizer flowed to the multihole fuel injector located in the liner about 6 in. downstream

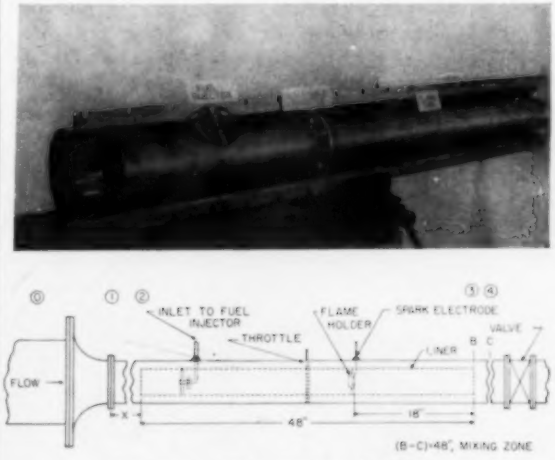

FIGURE 8. *The experimental chamber.*

from station 2. The injector was made of three concentric but not coplanar rings of tubing manifolded together and drilled with numerous small holes. The injector shown in figure 8 was used only in the preliminary experiments and was made of two concentric rings. Mixing of the fuel with primary air took place between the injector and flame holder, and the flame was initiated by a spark at the flame holder. The spark was turned off after smooth combustion was established and the flame was stabilized at the flame holder. The flame holder was a ring of triangular cross section, 2⅜-in. outside diameter and 1⅛-in. inside diameter. It was placed 18 in. upstream from the end of the liner (station 3). A water-cooled valve was placed at the outlet of the pipe system, and this was used to control the chamber pressure.

Initial attempts to operate the chamber were uniformly unsuccessful because of rough or intermittent combustion. Numerous changes in the primary zone and downstream portions of the system made no improvement whatsoever, and it was not until an orifice plate was installed 5 ft upstream from the nozzle that smooth combustion was possible. This orifice plate was replaced by one perforated with numerous smaller holes, and all experiments reported herein were made with this plate in the system. It is probable that this improvement was due to change of the effective length of the column of gas in the system.

Instrumentation was added for the measurements of temperature, pressure, and flow in the chamber. Total-pressure tubes were installed at stations 1 and 2p. A pitot-static tube was also used at station 2p. Static-pressure wall taps were located at stations 0, 1, 2p, 2s, 3s, 3p, and 4. Temperature was measured at station 0 and also at a point far downstream from station 4 by silver-shielded Chromel-Alumel thermocouples. The pipe system contained two right-angle bends beyond station 4 to insure that the gas was well mixed by the time it reached the last thermocouples. The reading of this thermocouple was considered the average temperature of the exhaust gas, T_4. Some tests were conducted with insulation around the pipe beyond station 3 to determine the magnitude of the heat loss from the system. Temperatures in the system were high, and the pipe was not insulated in the majority of tests because of possible damage to the system by the prevailing high temperature.

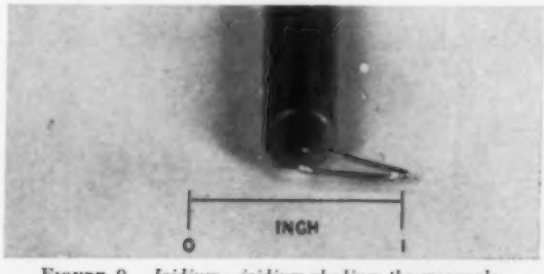

FIGURE 9. *Iridium—iridium-rhodium thermocouple.*

In the experiments in which mixing of primary and secondary streams was studied, most of the above instrumentation was removed to prevent interference with the flow distribution in the chamber. Considerable trouble with asymmetrical flow conditions in the mixing zone was experienced, and it was necessary to rebuild the system on this account. The wall thickness of the liner was increased to 3/32 in., and the liner was mounted coaxially in a 21-in. length of 6-in. pipe. Dimension X, figure 8, in these experiments was 8 ft. Elimination of flange joints in the vicinity of the liner by this means made a substantial improvement in the mixing zone. The liner of heavier construction warped less, and this also probably helped to improve the conditions for the mixing study.

Instrumentation in the mixing zone of the chamber consisted of water-cooled total-pressure tubes, bare Chromel-Alumel thermocouples of 22-gage wire, and iridium—50 percent iridium, 50 percent rhodium (Ir-IrRh) thermocouples of about 20-gage wire. Three of the Chromel-Alumel thermocouples were driven by electric motors to traverse the pipe at a speed of 2 in./min. This was equal to the chart speed of the temperature recorder, and by this means a full-scale profile of temperature was obtained. One motorized couple was located 32 in. and 2 were 48 in. from station 3 and at right angles to each other. Other Chromel-Alumel thermocouples were hand operated, and were located in the mixing zone between the motorized couples.

In order to measure the higher temperatures in the mixing zone, Ir-IrRh thermocouples [4] in water-cooled supports were used. One of these thermocouples with its support tube is shown in figure 9. In this instance the wires are bent at right angles to the tube in an effort to gain depth of immersion in the gas. Only one bent couple was used, others projected straight into the stream at least 5/8 in. These Ir-IrRh couples were operated by hand and were used in the first 32 in. of the mixing zone.

5.2. Experimental Procedure and Results

The burner was ignited at an air velocity at station 1 of about 20 ft/sec, and after smooth combustion was established, the rates of air and fuel were increased simultaneously until the velocity at station 1 was about 60 ft/sec. Measured temperature at station 4 was maintained nearly constant during this operation because this would indicate nearly constant fuel-air ratio in the primary zone (at a given throttle opening). Injection of the propane vapor through the multihole injector provided nearly homogeneous mixtures of air and fuel. Limits of smooth combustion in homogeneous mixtures are narrow, and the method of control was useful in keeping within the limits while changing conditions in the burner. After the burner was brought near the desired operating condition, final adjustments were made of fuel and air rates and burner pressure level. The fuel was adjusted until the burner sounded smoothest. This criterion did not necessarily guarantee the same fuel-air ratio in the primary

ne in all tests, but it was adopted because operation otherwise (under conditions of resonant combustion) would affect adversely the accuracy of the measurements of flow and pressures. Although resonance was not eliminated completely, the data indicate that its effects were reduced to a tolerable magnitude.

Because the primary zone was operated at nearly constant mixture ratio, the desired range of conditions of over-all temperature rise was attained through the use of throttles.

The rate of air flow was about 1.25 lb/sec in the majority of tests. Temperature of the air varied from 560° to 610° R, and pressure generally was about 1.5 atmospheres absolute. Some variation from these conditions was tried but with no effect on the results.

Dynamic pressure, q_1, at the inlet to the chamber under these conditions of flow was about 1.2 in. of water. Temperature ratio in the primary zone T_4/T_1, was calculated to be in the range of 6.6 to 7.1, for mixtures of 0.06 part of gaseous propane and 1 part of air by weight over the range of values of T_1 mentioned.

Experimental work on the chamber was divided into two parts, one in which problems of flow and heat release were studied and the other in which mixing of primary and secondary streams was studied. Results of the former will be described first.

a. Experiments in Flow and Heat Release

As mentioned before, fuel rate was adjusted in these experiments until combustion was smoothest, and consequently the fuel-air ratio in the primary zone was not constant in all tests. Tests in which the metered fuel-air ratio was $0.06 \pm .005$ were selected, and the results of these tests are reported herein. Selection by this rule reduced the spread of the data somewhat and did not change the basic relations.

Values of measured average temperature (T_4) after mixing of the gases by passage around two bends in the system indicated either low combustion efficiency (85 to 90 percent) or large heat losses. Analyses of the mixed outlet gas in three tests by a gravimetric method [5] indicated a combustion efficiency of 98 percent, while a heat balance based on T_4 and the assumption of an adiabatic system indicated efficiency of about 90 percent. When insulation was installed around the pipe beyond station 3, efficiency based on T_4 ranged between 92 and 100 percent, and it was concluded that loss of heat from the system when uninsulated was large. Prevailing temperatures in the system were high, and it appeared advisable to operate without insulation for reasons of safety. On the assumption that the low values of efficiency were caused by heat loss and not by poor combustion, data in this report are based on temperature T_4 calculated on the basis of 100-percent combustion of the mixture of total air and fuel. Cool secondary air contacted the walls of the 6-in. pipe down to and somewhat beyond station 3, and it is expected that loss of heat from the gas down to station 3 and somewhat beyond would have been negligible. The majority of the observations were made in this upper section of the burner, and this is considered a justification for ignoring the heat loss.

Results of the tests are presented graphically in figure 10, and results of the last analysis (fig. 7) are included for comparison. The portion of the air

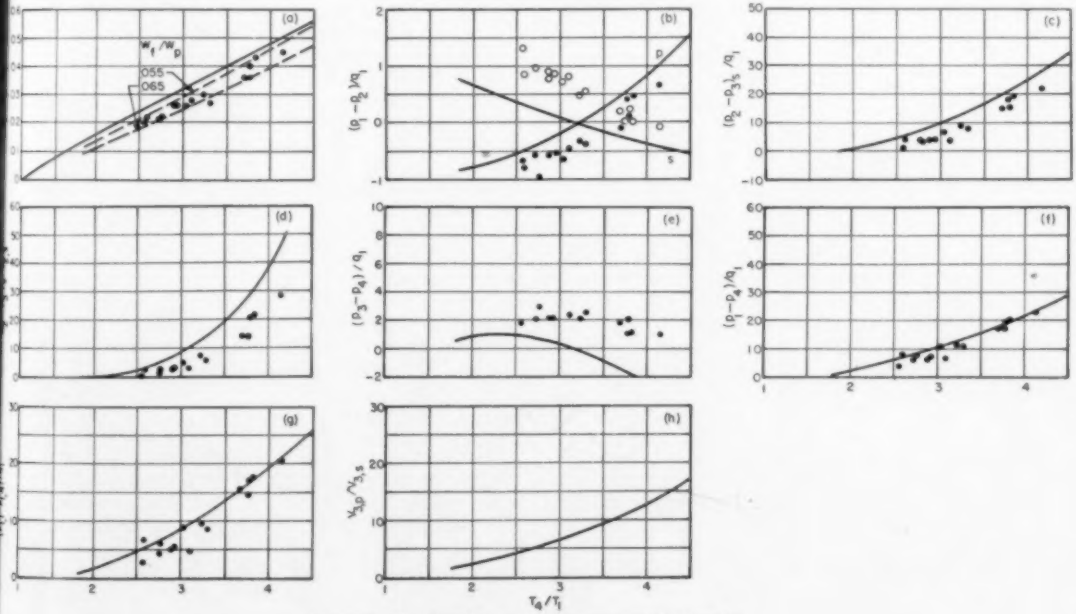

FIGURE 10. *Results in the experimental chamber*

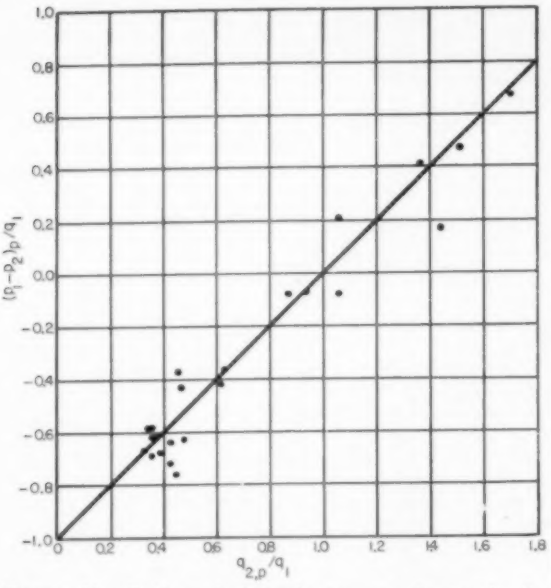

FIGURE 11. *Static and dynamic pressure changes in the primary stream.*

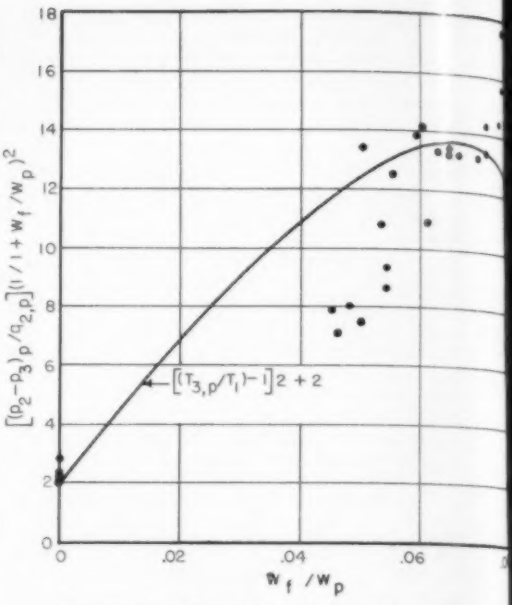

FIGURE 12. *Pressure drop in the primary zone.*

that entered the primary zone, figure 10, a, was determined from pressure $q_{2,p}$ given by a pitot-static tube at station $2p$ in the primary zone, or by the difference of pressure from a total head tube and static pressure wall tap. The data are displaced from the theoretical curve, but compare well with curves based on known combustion characteristics of propane-air mixtures. These curves were calculated for fuel-air mixtures of 0.055 and 0.065 in the primary zone, which is the range in the tests reported. These curves take into account the variation of specific heat with temperature and the added mass of fuel.

Division of the air into primary and secondary streams between stations 1 and 2 is accompanied by pressure changes, and results of measurements of these are presented in figure 10, b. The data are again displaced from the theoretical curve, but the same general relationship as predicted by Bernoulli's equation is evident. Some of the displacement is for reasons enumerated above. A comparison of the measured data for the primary stream with the curve calculated from eq 1 is presented in figure 11, where the line represents the equation. In general it appears that the equation is applicable. Because magnitudes of the pressures are small, and any effect of resonant combustion in the chamber on the measurements would be large on a percentage basis, it is difficult to decide which of the readings are correct. Several chemical analyses of the exhaust gas at station 3p were made, and the fuel-air ratios calculated from these analyses were in good agreement with those calculated from values of $q_{2,p}$ derived from eq 1 and the observed value of $(p_1-p_2)_p/q_1$. This is not regarded as conclusive evidence that measured values of $(p_1-p_2)_p$ were always correct. These chemical analyses also indicated essentially complete combustion (based on oxygen consumed across station 3p, and it was concluded that the flame holder was not too close to station 3.

Change of pressure between stations 2 and 3 in the secondary zone is plotted in figures 10, c, and 10, d, and the data, although displaced from the theoretical curves, are in good agreement with the theory. Pressures between these two stations were also measured in the primary zone, and these are compared to those predicted by the conservation of momentum equation in figure 12. In this figure observed values of $(p_2-p_3)_p/q_{2,\,p}$ were plotted versus fuel-air ratio in the primary zone, and the theoretical curve is based on calculated values of flame temperatures of propane-air mixtures. Velocity, and therefore dynamic pressure, in the primary zone is increased by the addition of fuel to the air stream, and observed $q_{2,p}$ was corrected as indicated in the figure to account for this. Observed pressures were not corrected for the momentum of the fuel, which in these experiments was injected downstream with a pressure drop in the injector of from 20 to 60 lb/in.^{2}. With no burning, observed pressure drop was about $2q_{2,p}$, which is due to friction in the primary zone. This value of $2q_{2,p}$ was added to the theoretical to account for the friction drop. In the neighborhood of fuel-air ratio of 0.06, observed pressure drop is in good agreement with the theoretical, but at lean condition the observed values are low. The reason for the low observed values is not clear, but it could be either incomplete combustion in the primary zone or an effect of resonance. If combustion were not complete in the primary zone,

did go to completion between stations 3 and 4 because observed values of T_4 indicated normal combustion efficiency.

One of the basic assumptions in the analysis of the flow in the combustion chamber was that pressure was uniform across the plane of station 3. Some deviation from this condition was observed; it was found that pressure of the secondary stream exceeded that of the primary stream by about 0.1 $q_{3,p}$ in most cases, and by as much as 0.3 $q_{3,p}$ in some. However, conditions at the static pressure wall tap may have been affected adversely by warping and scale formation caused by the high temperature of the liner. In any event it appears that the pressure differences are not large enough to detract from the value of the analysis on the basis of equal pressure. A strong flow of the secondary air into the primary jet is indicated by the surplus of pressure in the secondary stream.

Mixing of the two streams takes place beyond station 3, and the observed pressure changes between stations 3 and 4 are plotted in figure 10,e. Comparison with the theoretical indicates that the observed pressure changes are large, probably because of wall friction and turbulence caused by the velocity difference between the primary and secondary streams. Measurement of the friction drop with no burning indicated it to be about 25 percent of the dynamic pressure of the stream, which is a normal loss for this length of 6 in. pipe. During burning, average conditions of flow across the mixing section would give a dynamic pressure equal to $q_1 T_4/T_1$, and hence the wall-friction drop on this basis would be equal to $0.25\,(T_4/T_1)q_1$. If the data at the condition $T_4/T_1=4$ is used as an example, the observed $(p_3-p_4)/q_1$ was about 1, and correction by the friction drop ($\Delta p/q_1=0.25\,T_4/T_1=1$) would lead to $(p_3-p_4)/q_1=0$, which is to be compared to the theoretical value of -2. The difference is probably due to high level of turbulence in the mixing streams.

Over-all loss of pressure in the experimental chamber is plotted in figure 10, g, and compares well with the calculated values.

b. Experiments in Mixing

The combustion chamber was operated over a range of values of T_4/T_1 of from 1.5 to about 4 by changing the size of the throttle and its position. Corresponding values of the velocity ratio, $V_{3,s}/V_{3,p}$, were 1.5 to about 0.1. The mixture in the primary zone was adjusted until it was on the lean side of stoichiometric by observation of the flame temperature while decreasing the fuel rate from the condition of excessive richness. Observations of temperature were made in the mixing zone after the lean condition was established to reduce effects of reaction of the flame gas with secondary air during mixing. Only one measuring instrument was used at a time to avoid disturbance of the flow.

Accuracy of the temperature measurements of the hot gases was not of a high order, because only a rough calibration of the Ir-IrRh thermocouple was available, and because corrections to the indicated temperature were large. At high temperature, heat lost by radiation is large, and consequently the junction would be at a temperature lower than that of the gas. Corrections were calculated by a method that is based on the assumption that the heat lost from the thermocouple by radiation is equal to that gained by forced convection. The equation by which the corrections were determined is

$$T_{gas}-T_t=\frac{h_{rad.}\,\epsilon}{h_{conv.}}\,(T_t^4-T_{wall}^4). \tag{44}$$

T_t is the temperature indicated by the thermocouple, T_{wall} was assumed equal to the gas temperature next to the wall of the pipe, h_{rad} is Stefan's radiation constant (1.7×10^{-9} Btu/ft^2/°R^4 hr), $h_{conv.}$ is the coefficient of convective heat transfer. For bare thermocouples, $h_{conv.}=225\sqrt{G/6}$ Btu/ft^2/°R hr, which is an empirical relation to take into account the effect of mass rate of flow G expressed in pounds per square foot per second. A quick determination of the emissivity, ϵ, of the Ir-IrRh thermocouples indicated it to be 0.26, and ϵ for the Chromel-Alumel thermocouples was considered to be 0.9.

As an example of temperature arrived at by this means, temperature of the flame gas at station 3, $T_{3,p}$, in 13 tests averaged 4,350 °R with a root mean square deviation of 140° F. This average temperature is about 300° F greater than the calculated flame temperature of a propane and air mixture near stoichiometric condition. It is not known whether the calculated corrections were too large or whether the calibration of the thermocouple is responsible for the difference. Some of the deviation mentioned was probably caused by inability to maintain the same fuel-air ratio in all tests.

Some measurements of dynamic pressure were also made in the mixing zone, and velocity was calculated from these measurements and observed temperatures and static pressures.

In the description of the experimental results that follows, the data were correlated with the ratio of velocity of the secondary to primary stream, $V_{3,s}/V_{3,p}$. The values of this ratio reported were estimated from the observed rate of fuel injection (on the assumption of a constant fuel-air ratio of 0.062 in the primary zone) and the observed temperature and pressure in the chamber. The difference between these estimates and some measurements was not larger than 10 percent. Because the velocity measurements were not considered accurate, the estimated values were accepted as adequate for the present purpose.

1. *Axial Distribution of Temperature.* Mixing of the primary flame gas and secondary air takes place in a system bounded by the walls of the 6-in. pipe, and the gas will approach an average or mixed temperature T_4 as it travels downstream from station 3. Temperature at the axis of the burner, $T_{r=0}$, was expressed in the dimensionless form $(T_{r=0}-T_4)/(T_{3,p}-T_4)$ and correlated with distance x from station 3 by an empirical equation similar to that derived by

Pai [6] for two-dimensional jet mixing. The equation involved the probability integral, as follows:

$$\frac{T_{r=0}-T_4}{T_{3,p}-T_4}=\frac{2}{\sqrt{\pi}}\int_0^{z=f(x)} e^{-z^2}dz. \tag{45}$$

The first member of eq 45 represents experimental observations (at various values of x), and values of z were selected to make the two members of the equation equal.

In these experiments it was not possible to make accurate measurements of T_4, because both velocity and temperature gradients existed in the stream, and no bends were used in the system to mix the gas. Previous experiments in which mixed temperature, T_4, was measured, indicated relatively large heat loss from the system. These measurements were made downstream of the mixing zone, and if these were used as a guide to establish T_4 in the present experiments, T_4 by this method would probably be lower than the true value at station 4. Calculation of T_4 on the assumption of 100-percent combustion efficiency, and no heat loss would give high values. Both methods were used to establish values of T_4, and although some difference was noted, the correlation obtained was not basically changed. The wall of the pipe was relatively cool in the first half of the mixing section, and it seemed logical to conclude that T_4, based on 100-percent combustion and no heat loss, was nearer the true value, and this value of T_4 was used in the correlation to be described.

Values of z in eq 45 were determined from the observed axial temperature at various values of x, and these values of z were plotted against the corresponding values of x. It was found that plots of log z against $x/r_{3,p}$, where $r_{3,p}$ is the radius of the liner, could be represented by straight lines. Plots of this kind are shown in figure 13 for three different conditions of $V_{3,s}/V_{3,p}<1$. The three lines have the common point $z=1.5$, $x/r_{3,p}=9$, and therefore a general equation can be written

$$\ln z=-cx/r_{3,p}+k, \tag{46}$$

where k is a constant, and c is the slope of the line. When $V_{3,s}/V_{3,p}>1$, the same relationship was observed, but only two out of five tests gave plots that passed through the common point.

A Maclaurin expansion of the probability integral would indicate that $(T_{r=0}-T_4)/(T_{3,p}-T_4)=z$ to a first approximation. This approximation is good when $z\leq 0.7$, and in this range temperature can be approximated by

$$\frac{T_{r=0}-T_4}{T_{3,p}-T_4}\simeq z=ke^{-cx/r_{3,p}}, \tag{47}$$

and differentiation of this would lead to

$$\frac{d\left[\frac{T_{r=0}-T_4}{T_{3,p}-T_4}\right]}{dx}\simeq -c\,\frac{T_{r=0}-T_4}{T_{3,p}-T_4}, \tag{48}$$

and from this it appears that c is a measure of the effectiveness of the mixing in bringing the temperature at the axis to the mixed temperature T_4.

Slope c was correlated with $V_{3,s}/V_{3,p}$ in figure 14, and the data suggest a parabolic relationship, with a minimum at a velocity ratio of unity

These results have been presented thus far without reference to or comparison with the theory of mixing of jets. The mixing of streams, different in both temperature and velocity, has received very limited attention, and consequently the present results will be compared with the theory for incompressible flow presented in reference [2] and utilized in a previous

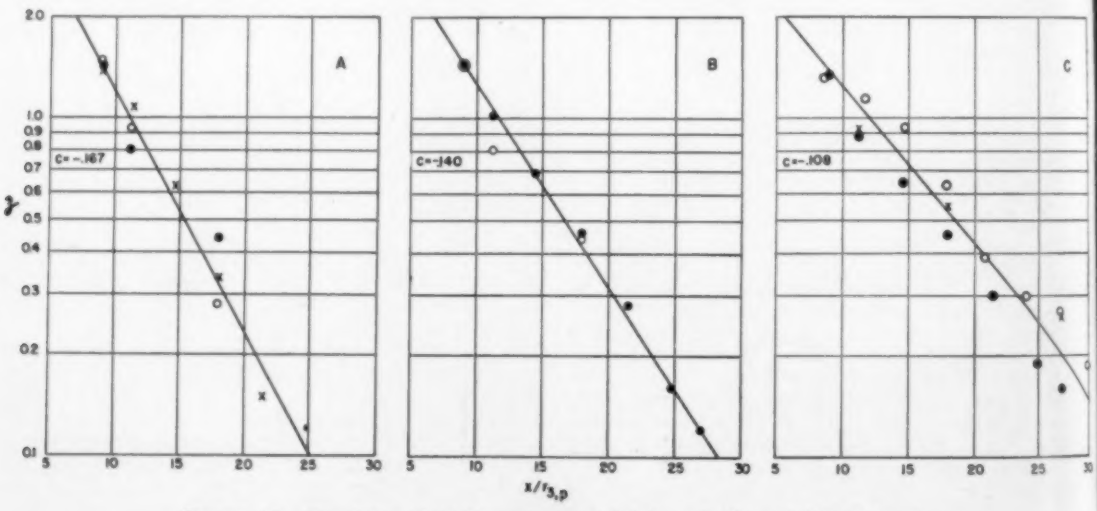

FIGURE 13. *Correlation of axial temperature with distance by the probability integral.*

(A) $V_{3,s}/V_{3,p}=0.12$; $T_4/T_1=3.8$. (B) $V_{3,s}/V_{3,p}=0.17$; $T_4/T_1=3.3$. (C) $V_{3,s}/V_{3,p}=0.38$; $T_4/T_1=2.3$.

section of this report. A comparison will be presented also with the recently presented experimental results of Forstall and Shapiro [7] obtained in the study of coaxial streams at a common temperature. It is expected that differences shown by the comparisons would be caused by the large difference of Temperature or density between the streams in the present experiments. Hereinafter, comparison with the work of Squire and Trouncer [2] is referred to as a comparison with the theory, and the results of Forstall and Shapiro are referred to as the "other experiments."

Figure 15 is a comparison of the characteristics of the mixing as observed along the axis of the burner with the theory and also with the other experiments. Because a jet in a general stream would mix and eventually approach the properties of the stream, the dimensionless fractions of temperature (and velocity) contain the temperature (and velocity) of the secondary stream in order to make the comparison. In general, it may be said that in the median range, temperature expressed this way varies inversely with axial distance, and this is in agreement with the other experiments but not with the theory.

At the condition of $V_{3,s}/V_{3,p}=0.375$, limited information about axial velocity in the mixing zone indicates that it is transferred at a slower rate than temperature. Three other tests at the condition $V_{3,s}/V_{3,p}=0.25$ also indicated this. Comparison of the data on velocity with the other experimental results indicates a somewhat slower rate of transfer in the present experiments.

When $V_{3,s}/V_{3,p}$ was 0.125, the data show that transfer of temperature in the present experiments approximates that of velocity in the other experiments. However, in the expectation that velocity would be transferred in this case also at a slower rate than temperature, it appears that the rate of transfer is less in the present experiments than in the other experiments. One set of data points in this figure was for the condition $V_{3,s}/V_{3,p}=0.18$, and this was included because it illustrates more clearly the inverse relationship of temperature and distance. In this system temperature approaches T_4 as mixing becomes complete, not T_1, and the completely mixed condition would be attained when $(T_{r=0}-T_1)/(T_{3,p}-T_1)=(T_4-T_1)/(T_{3,p}-T_1)$. The latter fraction is 0.47 when $V_{3,s}/V_{3,p}=0.125$, and the x data points show the beginning of a slower approach of temperature (at the lower values) to the mixed condition. At $V_{3,s}/V_{3,p}=0.18$, the fraction was 0.33, and the slower approach to the mixed condition occurred downstream from the place where the observations were made in this case.

It will be noted that the straight lines were extended to a value of unity for the temperature fraction, and at both conditions of $V_{3,s}/V_{3,p}<1$ the axial distance is about $11r_{3,p}$. This same value of $11r_{3,p}$ was noted when $V_{3,s}/V_{3,p}$ was 0.55, which leads to the conclusion that the burner can be assigned a characteristic length. The general inverse relationship of temperature and axial distance, and the characteristic length, would be of general utility in making an approximation of the temperature field. In the theory the extent of the potential core of velocity is variable, whereas in the present experi-

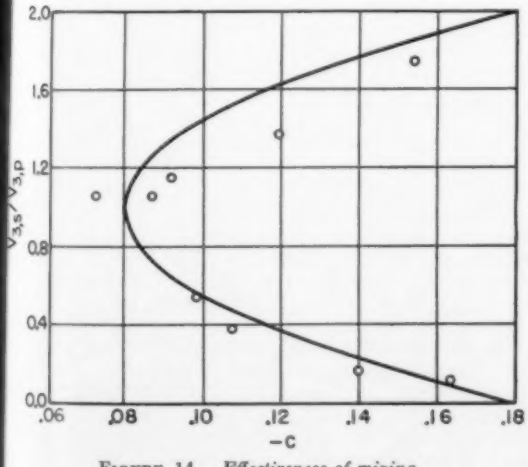

FIGURE 14. *Effectiveness of mixing.*

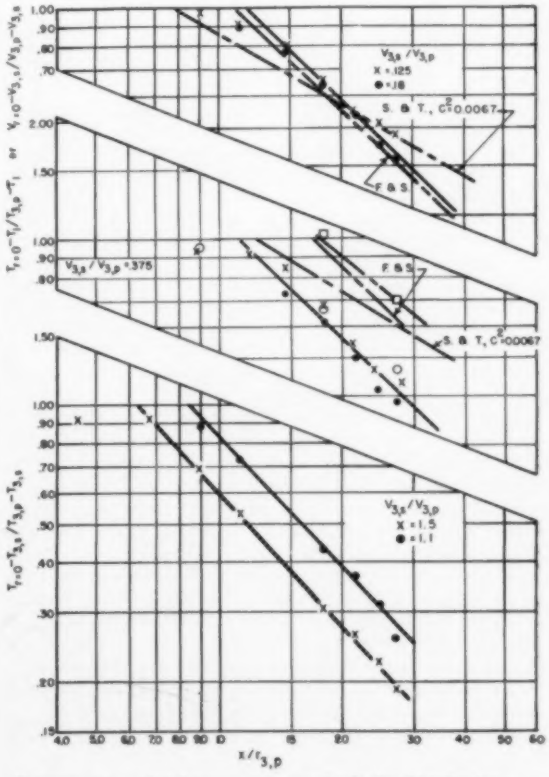

FIGURE 15. *Axial temperature and velocity distribution.*
—, Temperature; – – –, velocity.

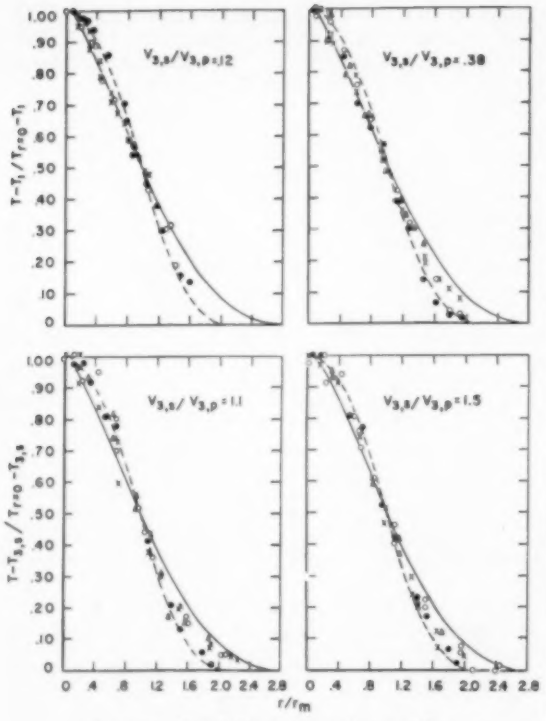

FIGURE 16. *Lateral temperature profile.*

– – – –, Cosine curve; ——, Tollmien's curve; ●, $x/r_{3,p}=9$; ×, $x/r_{3,p}=18$; ○, $x/r_{3,p}=11$; △, $x/r_{3,p}=27$.

ments it appears that the extent of the potential core of temperature (for purposes of approximation) can be regarded as constant.

Data at the conditions of $V_{3,s}/V_{3,p}>1$ are also included in figure 15, but comparison is not possible because this condition is not investigated in references [2 and 7]. The same inverse relationship is evident, but here there appears to be no evidence of a characteristic length.

2. *Lateral Distribution of Temperature.* Numerous traverses of temperature were made in the mixing zone of the chamber to investigate the lateral spread of temperature in the two coaxial streams. The generalized profiles were compared with that of the cosine curve as assumed by Squire and Trouncer in [2], and with that calculated by Tollmien [1] for a free, round, incompressible jet. Tollmien also used the momentum transfer theory and assumed that mixing length was proportional to the width of the mixing region. However, the calculations were based on the assumption of a point source, and therefore in practice similarity of profile would not be reached until axial distance became large compared to jet size.

Four profiles of temperature are presented in figure 16 to illustrate the shape over the range of operating conditions. In some of the runs, temperature of the secondary air, $T_{3,s}$, was measured just before the point of mixing, and, as expected it was somewhat higher than the inlet temperature T_3 because of heat transfer from the primary zone. Two profiles of temperature in figure 16 were calculated by using these measured values of $T_{3,s}$. Effect of this change to $T_{3,s}$ was a slight shift of the data points to lesser values of the temperature fraction and to greater values of the radius fraction.

At high relative velocity of the primary stream the edge of the mixing region intersects the wall of the 6-in. pipe in which mixing takes place at relatively small values of axial distance, and consequently the profiles are not complete. Also, the mixing downstream of the point of intersection is no longer in free streams, and the validity of comparison with mixing in free streams is questionable. However, some information can be gained by a comparison, and it is presented with this limitation in mind.

At an axial distance of 9 $r_{3,p}$, the profile of temperature is in good agreement with the cosine curve, but at greater distances there is a tendency to approach the distribution predicted by Tollmien. The experimental velocity profiles of Forstall and Shapiro were a good match with the cosine curve at all distances studied. Ratio of velocity of secondary to primary streams does not affect the shape of the temperature profile.

Although the shape of the profile tends to change with axial distance, the magnitude of the radius of half temperature r_m is a good indication of the width of the mixing region and is plotted versus axial distance in figure 17. Theoretical results of Squire and Trouncer for velocity are included for comparison. Experimental findings of Forstall and Shapiro agreed well with the theory and are therefore not included in the figure.

At the condition $V_{3,s}/V_{3,p}=.125$, r_m increases slowly in the region of the potential core, which in this case extends downstream a distance of 11 $r_{3,p}$ compared to about 8 $r_{3,p}$ in the theory. It is to be noted that at the end of the potential core of temperature r_m is 1.1 $r_{3,p}$, and therefore the width of the mixing region would be about 2.2 $r_{3,p}$ if it were not cut off by the 6-in. pipe (width=1.7 $r_{2,p}$). Beyond the potential core the experimental data are not as consistent, but it may be said that r_m grows approximately as predicted in the theory. With respect to the two points of largest r_m, these also are nominally beyond the wall of the 6-in. pipe. However, in these instances the center line of the profile was off the center of the pipe enough to measure these radii on one side of the traverse. This asymmetry has been one of the major troubles in these experiments. Unknown changes in the configuration of the burner, possibly due to high prevailing temperatures, cause asymmetry and shifts of the center lines of the traverse. If the curve as drawn represents the data, then the constant of proportionality C in the analysis would have to be less than 0.0067 by about one-third to bring the theoretical results in agreement with the present experiments. The rate of mixing on this basis is correspondingly lower than in the theory and in the other experiments.

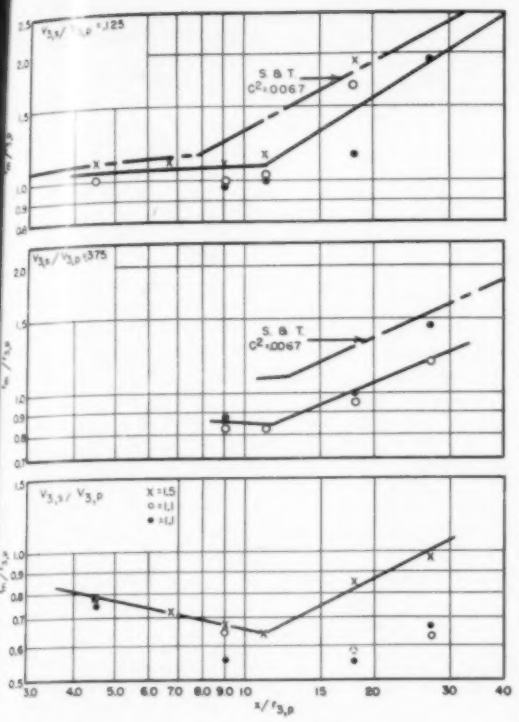

FIGURE 17. *Half-boundary of mixing.*
——, Temperature; — – —, velocity.

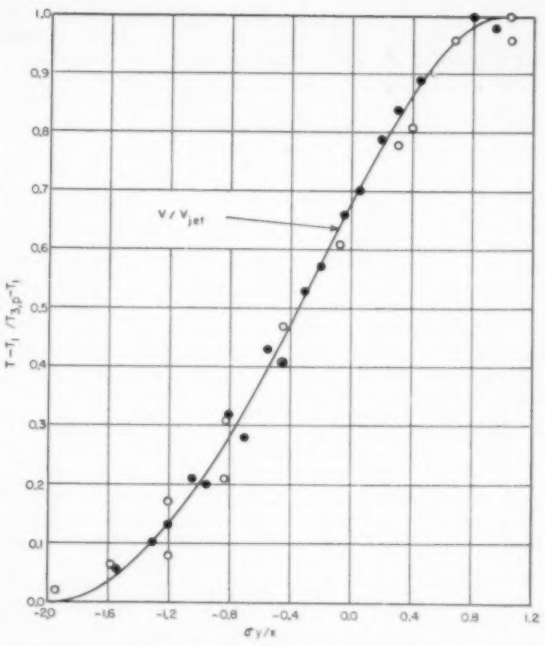

FIGURE 18. *Free jet boundary.*
○, $x/r_{1,p}=4.50$; ●, $x/r_{1,p}=6.75$; $\sigma=12$.

At the condition $V_{3,s}/V_{3,p}=.375$, the extent of the potential core is also about $11r_{3,p}$, but r_m converges to a value of about $0.85\ r_{3,p}$. At this point the mixing region extends to the wall of the pipe ($1.7\ r_{3,p}$) and therefore mixing downstream is influenced by the pipe. In this downstream region, r_m diverges approximately as predicted by theory but again at greater values of axial distance. Radius of half maximum velocity was compared to that of temperature in three runs and was less by about 5 percent, which confirms the conclusion that temperature is transferred at a greater rate than velocity.

Data are also included in figure 17 on the radius of half maximum temperature when velocity of the primary stream was low compared to the secondary stream ($V_{3,s}/V_{3,p}=1.1$ and 1.5). Convergence in the region of the potential core is pronounced, and divergence begins again at an axial distance of about $11\ r_{3,p}$. In all three cases in figure 17, divergence begins at an axial distance of about $11\ r_{3,p}$, and this is considered additional evidence that the chamber has a characteristic length.

Two runs in which $V_{3,s}/V_{3,p}$ was 1.1 were made to show the effect of velocity difference between the primary and secondary streams, and data from these tests are also included in figure 17. Curves were not drawn through the data points in these two runs in which the mass rate of flow differed by 65 percent. Because the rate of flow differed by 65 percent, $(V_{3,s}-V_{3,p})$ also differed by this amount. Three out of four comparisons of r_m show that the magnitude of $V_{3,s}-V_{3,p}$ has little affect on the field. At an axial distance of $18\ r_{3,p}$, the maximum temperature was beyond the range of the temperature recorder in one of the runs, and consequently the radius plotted (broken circle) is somewhat greater than the true value. It is expected that agreement would be better than indicated in figure 17 at this axial distance. On the basis that r_m is not affected, it is concluded that velocity ratio, rather than velocity difference, determines the mixing field. This same effect was evident in another comparison in which $V_{3,s}$ was about $0.1\ V_{3,p}$. Forstall and Shapiro reached this same conclusion.

In the region of the potential core, it may be said that the mixing region approximates that of a two-dimensional region between semiinfinite moving streams differing in both temperature and velocity. In recent years the problem of mixing in the two-dimensional case, with the mixing region bounded on one side by a quiet body of gas, has received considerable attention. Tollmien [1] presented a calculation of the velocity profile for incompressible flow, and much of the experimental work has been based on the determination of a scale factor σ to match the experimental with the theoretical profile. The magniture of σ may be regarded as an inverse measure of the rate of mixing.

A comparison of the temperature profile in the region of the potential core with Tollmien's profile

of velocity in a free jet boundary is presented in figure 18. A test in which $V_{3,s}/V_{3,p}$ was 0.12 was selected as it was the nearest approach in the present series of experiments to the condition of still gas on one side of the mixing region. The other important difference is, of course, the large difference of temperature and density between the streams in these experiments. It appears that a value of $\sigma=12$ brings a fair correspondence between the data and the curve. Liepmann and Laufer [8] report a value of 12 based on their own and other measurements of velocity in a subsonic jet. However, the conditions differ in several respects as mentioned, and no firm conclusions can therefore be drawn about the relative mixing rate, and these data are presented merely as information. Values of σ were also determined when $V_{3,s}/V_{3,p}$ was larger than unity, and these ranged as high as 18.

6. Conclusion

The problems of flow, heat release, and mixing in an equivalent gas turbine combustion chamber have been examined analytically. A large primary zone is advantageous, but the area is limited to about 60 percent of the total cross-sectional area. Practical experience has also led to the use of chambers of about this size relationship. Method of control currently used, although no doubt simple, leads to poor mixture quality in the primary zone and therefore puts a burden on the combustion process, which experience shows it cannot always overcome. Requirements for and effects of a possible means of mixture control are determined analytically. Experimental work demonstrates that the analytical method gives a good description of the flow, heat release, and mixing in the controlled combustion chamber. Although the control described would complicate the structure of the chamber, improvements in combustion could be a compensation.

Study of the mixing of primary flame gas and secondary air, and comparison with other studies of mixing reveals a general similarity. Ratio of velocity of the streams, not the velocity difference, determines the field of mixing, but the shape of the generalized profile of lateral spread of the mixing region is not affected by velocity. Temperature is transferred at a greater rate than velocity, and this conclusion also appears to be general in other studies. Some difference is noted, in that the combustion chamber has a characteristic length that may be regarded as the extent of the undisturbed potential core of temperature of the primary stream. In the incompressible case the extent of the core of velocity is variable with velocity ratio. In the region of the potential core a convergence of the radius of half maximum temperature is noted, while under similar conditions in the incompressible case there is a divergence. Beyond this region, the radius of half maximum temperature appears to have the normal divergence. Axial distribution of temperature is similar to distribution of velocity, and when expressed with reference to the temparature of the secondary stream, an inverse relationship with axial distance is obtained. This inverse relationship, which holds without regard to velocity ratio, is of general utility in the determination of the temperature field, especially when it is noted that the chamber has a characteristic length. On the basis of rate of approach of axial temperature to average or "mixed" outlet temperature, the mixing process is least effective when the velocities of the streams are equal. Comparison of the field in this with that in the incompressible case leads to the conclusion that the effect of the large difference of temperature or density between the streams is to retard mixing.

7. References

[1] W. Tollmien, Calculation of turbulent expansion processes, translation, Natl. Advisory Comm. Aeronaut. Tech. Mem. 1085 (1945).

[2] H. B. Squire and J. Trouncer, Round jets in general stream, ARC (Gt. Brit.) Report 1974 (Jan. 1944).

[3] F. R. Caldwell, F. W. Ruegg, and L. O. Olsen, Combustion in moving air, SAE Quarterly Transactions 3, 327 (1949).

[4] Wright Field Central Air Documents Office, An experimental Ir-IrRh thermocouple with cooled support, July 1949, Air Technical Index No. 58661.

[5] F. W. Ruegg and C. Halpern, Gravimetric analysis of exhaust gas from gas turbine combustion chambers, J. Research NBS **45**, 113 (1950) RP2117.

[6] S. I. Pai, Two-dimensional jet mixing of a compressible fluid, J. Aeronaut. Sci. **16**, 463 (1949).

[7] W. Forstall and A. H. Shapiro, Momentum and mass transfer in coaxial gas jets, J. Applied Mech. **17**, 399 (1950).

[8] H. W. Liepman and J. Laufer, California Institute of Technology, Investigations of free turbulent mixing, Natl. Advisory Comm. Aeronaut. Tech. Note 1257 (1947).

WASHINGTON, July 2, 1952.

Journal of Research of the National Bureau of Standards Vol. 49, No. 5, November 1952 Research Paper 2366

Corrosion of Galvanized Steel in Soils

Irving A. Denison and Melvin Romanoff

The results of measurements of the corrosion of galvanized steel and of bare steel and zinc as reference materials after exposure to different soil conditions for a maximum of 13 years are reported. The magnitude and progress of corrosion of galvanized steel as determined by weight loss and pitting is interpreted in terms of the environmental conditions to which the specimens were exposed. From analysis of data on the corrosion of galvanized specimens having different weights of coating, minimum coating requirements for different environmental conditions are suggested.

1. Introduction

In order to evaluate the effectiveness of zinc coatings in protecting iron and steel from corrosion underground, test specimens of iron and steel coated with different thicknesses of zinc, applied by the hot-dip process, were included in the extensive field-exposure tests undertaken by the National Bureau of Standards in 1924. The thinner coatings did not prevent corrosion in the more corrosive soils, but coatings having a nominal weight of 3 oz/ft² of exposed surface prevented the development of measurable pits on the specimens at all but one of the 47 test sites for the entire period of exposure [1, 2].[1] Although the sites represented a wide range of soil conditions, it was considered desirable to expose specimens with the heavier zinc coatings to additional soil environments in which some dominant corrosive factor, such as chloride content, acidity, etc., was the apparent cause of corrosion. Accordingly, specimens having the same nominal weight of coating, namely, 3 oz/ft² of surface were buried at 15 additional sites in 1937. A sufficient number of specimens of galvanized steel and of the reference materials, steel and zinc, were buried to provide for removal of two specimens of each material after each of five periods of exposure. This paper deals with the condition of the specimens of the three materials exposed for different periods up to 13 yr.

2. Properties of the Soils at the Test Sites

The test sites represent a wide range of environmental conditions with respect to both the chemical and physical properties of the soils (table 1). For example, the hydrogen-ion concentration of the soils ranges from pH 2.6 to 9.4, and the resistivity from 62 to 17,800 ohm-cm. At several of the test sites the soils are highly oxidized to considerable depths, whereas in others the permanent water table is close to the surface. The environmental conditions at several of the test sites are illustrated in figure 1.

3. Materials

The galvanized and bare steel specimens were 14-in. (35-cm) lengths of pipe 1.5 in. (3.8 cm) in diameter cut from the same lots of commercial materials. The nominal weight of the zinc coating on the galvanized specimens was 3.08 oz/ft².[2] The impurities in the spelter in percent were: Al, 0.008; Fe, 0.07; and Pb, 0.78. The steel, both galvanized and bare, was AISI No. B1010, with the nominal composition in percent as follows: C, 0.13 max; Mn, 0.30 to 0.60; P, 0.07 to 0.12; S, 0.06 max. The interior of the specimens was coated with heavy grease, and the ends were closed in order to prevent internal corrosion.

The zinc specimens were plates having the dimensions 12 in. (30.5 cm) by 2.3 in. (5.8 cm) by 0.15 in. (0.4 cm). The impurities determined in the zinc in percent were: Fe, 0.009; Pb, 0.095; Cd, 0.0038.

4. Distribution of the Coating on the Galvanized Specimens

The distribution of the coating on the galvanized specimens was measured by a magnetic method [3]. The measurements were made on one 14-in. (35 cm) length of galvanized pipe selected at random from the lot of specimens before burial, and on a 6-in. (15 cm) section cut from a second specimen from the same lot. A total of 389 measurements of thickness were made on the 14-in. length of pipe (identified as specimen A), and 162 measurements were made on the 6-in. section (identified as specimen B).

The measurements of coating thickness are shown as frequency distribution curves in figure 2. These curves indicate not only that the specimens differed widely in coating thickness, but that the distribution of the coating on the individual specimens was highly variable as well. The variation did not fall in any particular pattern.

5. Thickness of the Outer Zinc Coating and of the Alloy Layer

The thickness of the outer zinc coating and of the alloy layer was measured by modifications of the electrolytic stripping methods described by Britton [4] and by Anderson and Manuel [5].

The electrolytic cell consisted of a 4-oz (120-ml) plastic bottle from which the bottom had been re-

[1] Figures in brackets indicate the literature references at the end of this paper.

[2] This is the weight of coating on one side of the pipe. Each ounce per square foot of coating is equivalent to 0.00172 in. in thickness.

UNIVERSITY OF MICHIGAN LIBRARIES

TABLE 1. *Properties of the soils at the test sites*

Test sites			Aeration	Moisture equivalent	Apparent specific gravity	Resistivity at 60° F (15.6° C)	pH	Total acidity [a] (milligram equivalent per 100 g of soil)	Composition of water extract (milligram equivalent per 100 g of soil)						
Environment and soil type	Soil number	Location							Na+K as Na	Ca	Mg	CO_3	HCO_3	Cl	SO_4
INORGANIC OXIDIZING-ACID SOILS															
				Percent		*Ohm-cm*									
Cecil clay loam	53	Atlanta, Ga	Good	33.7	1.60	17,800	4.8	5.1	.....	.....	.....	.....	.....	.....	.....
Hagerstown loam	55	Loch Raven, Md	do	32.0	1.49	5,210	5.8	10.9	.....	.....	.....	.....	.....	.....	.....
Susquehanna clay	62	Meridian, Miss	Fair	34.6	1.79	6,920	4.5	12.0	.....	.....	.....	.....	.....	.....	.....
INORGANIC OXIDIZING-ALKALINE SOILS															
Chino silt loam	65	Wilmington, Calif	Good	26.4	1.41	148	8.0	A	7.65	12.40	2.29	0.00	1.30	6.05	16.90
Mohave fine gravelly loam	66	Phoenix, Ariz	Fair	16.5	1.79	232	8.0	A	6.55	0.51	0.18	.00	0.73	2.77	2.97
INORGANIC REDUCING-ACID SOILS															
Acadia clay	51	Spindletop, Tex	Poor	47.1	2.07	190	6.2	13.2	10.27	15.55	5.03	0.00	0.56	5.75	22.00
Sharkey clay	61	New Orleans, La	do	30.8	1.78	943	6.8	4.9	0.73	0.68	0.33	.00	.71	0.10	0.91
INORGANIC REDUCING-ALKALINE SOILS															
Docas clay	64	Cholame, Calif	Fair	41.1	1.88	62	7.5	A	28.10	2.29	0.76	0.00	0.89	28.80	0.26
Lake Charles clay	56	El Vista, Tex	Very poor	28.7	2.03	406	7.1	5.1	3.12	0.69	.47	.00	.80	1.59	3.04
Merced silt loam	70	Buttonwillow, Calif	Fair	24.7	1.69	278	9.4	A	8.38	.38	.22	.02	1.87	1.12	5.57
ORGANIC REDUCING-ACID SOILS															
Carlisle muck	59	Kalamazoo, Mich	Very poor	43.6	.....	1,660	5.6	12.6	1.03	3.08	2.70	0.00	0.00	3.47	1.04
Muck	58	New Orleans, La	Poor	57.8	1.43	712	4.8	15.0	2.03	2.23	1.29	.00	.00	0.47	2.54
Rifle peat	60	Plymouth, Ohio	do	43.4	1.28	218	2.6	297.4	2.91	10.95	2.86	.00	.00	.00	56.70
Tidal marsh	63	Charleston, S. C	Very poor	46.7	1.47	84	6.9	14.6	33.60	6.85	4.00	.00	.00	12.70	36.60
CINDERS															
Cinders	67	Milwaukee, Wis	Very poor	.....	.....	455	7.6	A	0.77	3.03	0.53	.00	.55	0.08	2.89

[a] A, alkaline reaction.

moved. The cathode was a strip of zinc 1.5 in. (38 mm) in width formed so as to fit tightly around the inner periphery of the bottle. Contact with the coating was made by means of a hole 0.19 in. (5 mm) in diameter in a No. 8 rubber stopper. A larger hole bored partly through one end of the stopper permitted the stopper to be placed over the mouth of the bottle. The electrolyte was a solution containing 20 g of NaCl, 10 g of $ZnSO_4$, and 100 g of H_2O.

In operation, the bottle was inverted and the test piece placed in contact with the hole in the stopper with sufficient pressure to prevent leakage of the electrolyte. By means of a 6-v storage battery shunted by a variable voltage divider, an initial current of 25 ma was passed through the cell with the test piece as the anode, the current being read on a recording milliammeter. As the outer zinc coating was removed by electrolysis and different phases of zinc-iron alloy and finally steel were exposed, the changes in potential associated with each phase produced corresponding changes in the recorded current.

The interpretation of the current-time curves in terms of coating thickness is illustrated by figure 3. The minimum thickness of the zinc layer is measured by the horizontal part of the curve at point A. On exposure of an alloy layer locally, the counter emf increases, and the current proportionally decreases until the zinc is completely removed and a uniform layer of the first phase of the alloy layer is exposed (point B). The current then remains unchanged until a second phase of the alloy layer is exposed and so on through the various phases until the underlying steel is completely exposed. The minimum thickness of the alloy layer, including the intermediate phases, is represented by the distance *BC*, and the maximum thickness by the distance *AD*. The reported thicknesses were computed from the areas under the curve. For the present investigation the thickness of the zinc coating was taken as the maximum thickness, that is, to point *B*, and the thickness of the alloy layer was taken as being represented by the distance *BD*.

The maximum thickness of the outer zinc coating and of the alloy layer at several points on two specimens are recorded in table 2. These data indicate that a large part of the zinc applied to the steel pipe was converted to alloy layer.

TABLE 2. *Thickness of the outer zinc coating, of the alloy layer, and of the total coating on galvanized specimens*

[In mils]

Specimen	Zinc layer	Alloy layer	Total coating
A	1.8	2.3	4.1
A	0.9	3.4	4.3
A	2.0	2.3	4.3
A	2.0	3.0	5.0
B	2.7	3.2	5.9
B	2.8	3.2	6.0

6. Condition of Coating, Weight Loss, and Pitting of Galvanized Steel, Bare Steel, and Zinc

After each exposure period, one set of specimens was removed, returned to the laboratory, and cleaned free of corrosion products by previously described methods [2]. Photographs of the specimens of galvanized steel, bare steel, and zinc removed from the different sites after exposure for 13 yr are shown in figure 4.

The losses in weight and the depths of the deepest pits on the specimens, together with the percentage of the area of the galvanized specimens on which coating remained, are recorded in table 3 for the different periods of exposure. Except as indicated, each value is the average of measurements made on two specimens.

The data of table 3 reveal that in nearly one-half of the total number of soils (53, 55, 61, 62, 64, 65, 66, and 70) the coating remained virtually intact and consequently provided complete protection to the underlying steel for the maximum period of exposure. However, in the highly reducing soils (51, 56, 58, and 60) and in cinders (67) little, if any, of the coating remained at the conclusion of the test.

In certain soils, such as 58 and 60, failure of the coating during the first few years of exposure resulted in a rate of corrosion of the galvanized specimens comparable to that of bare steel. But in other soils, contrary to expectations, destruction of the coating was not accompanied by rapid corrosion of the underlying steel. For example, the galvanized specimens in soils 51 and 56 corroded relatively slowly during the greater part of the exposure period in spite of the fact that the coating was almost completely removed by corrosion during the first few years of exposure. Even in the highly corrosive cinders, soil 67, the galvanized specimens corroded much more slowly than the specimens of bare steel.

The progress of corrosion of galvanized steel, bare steel, and zinc in the different soils is shown by the weight loss and pit depth-time curves of figure 5. The values for weight loss and pitting of the galvanized specimens on which the coating remained intact naturally apply to the coating and not to the basis metal.

The weight loss and pit-depth—time curves for the galvanized specimens in soils 64, 65, 66, and 70 are of particular interest in indicating that zinc coatings were effective in protecting steel against corrosion in soils that are highly corrosive to steel. For example, in spite of the fact that the steel specimens in soil 66 were perforated by corrosion after exposure for a few years, the coating on the galvanized specimens in this soil remained perfectly continuous throughout the entire period of the test. In soil 70, the specimens of both zinc and steel were severely corroded, but the coating on the galvanized specimens provided complete protection to the underlying steel.

UNIVERSITY OF MICHIGAN LIBRARIES

TABLE 3. *Loss in weight and maximum penetration of galvanized [a] and bare steel pipe and zinc plate*

[Average of two specimens]

Soil No.	Soil type	Exposure	Galvanized steel						Bare steel		Zinc	
			Condition of surface				Loss in weight	Maximum penetration	Loss in weight	Maximum penetration	Loss in weight	Maximum penetration
			Coated with zinc and alloy layer	Coated with zinc	Coated with alloy layer	Bare steel exposed						
	INORGANIC OXIDIZING-ACID SOILS											
		Years	*Percent*	*Percent*	*Percent*	*Percent*	*oz/ft²*	*Mils*	*oz/ft²*	*Mils*	*oz/ft²*	*Mils*
53	Cecil clay loam	2.1	85 to 100	60 to 100	0 to 40	0	0.3	9	1.8	42	0.2	10
		4.0	100	20 to 40	60 to 80	0	1.4	6	2.9	98	.6	10
		8.9	100	20 to 40	60 to 80	0	0.6	<6	3.4	74	1.1	13
		11.2	100	30	70	0	1.0	<6	3.4	78	1.6	16
		12.7	100	20	80	0	0.6	<6	3.9	68	2.2	17
55	Hagerstown loam	1.9	100	60 to 100	0 to 40	0	.3	<6	1.8	33	0.4	13
		3.9	100	20 to 40	60 to 80	0	1.2	8	2.6	50	.6	8
		9.0	95	20 to 40	55 to 75	<5	0.7	6	4.1	92	.7	8
		11.0	100	70	30	0	1.0	<6	3.9	84	1.3	10
		12.6	100	70	30	0	0.6	<6	3.4	73	1.2	9
62	Susquehanna clay	2.1	100	50 to 100	0 to 50	0	1.0	12	3.2	40	0.6	9
		4.0	100	20 to 40	60 to 80	0	2.3	9	4.3	56	1.2	9
		8.9	100	0 to 20	80 to 100	0	0.9	<6	5.3	68	1.3	12
		11.2	100	80	20	0	1.1	<6	6.0	72	1.3	11
		12.7	100	75	25	0	0.8	<6	6.8	79	1.7	9
	INORGANIC OXIDIZING-ALKALINE SOILS											
65	Chino silt loam	2.1	100	20 to 40	60 to 80	0	1.1	<6	4.3	50	0.5	30
		4.0	100	0 to 20	80 to 100	0	2.3	6	4.6	59	.8	36
		9.0	95	50 to 75	25 to 50	<5	1.6	<6	7.0	65	1.4	56
		11.2	95	0	95	<5	1.7	<6	6.2	84	1.1	40
		12.7	100	0	100	0	1.1	<6	7.2	98	1.8	56
66	Mohave fine gravelly loam	2.1	100	60 to 100	0 to 40	0	1.6	6	9.2	[d] 145+	1.7	25
		4.0	100	20 to 40	60 to 80	0	3.3	8	12.3	145+	[b] 2.6	28
		9.0	95	20 to 40	60 to 80	5	1.1	<6	8.1	78	0.9	44
		11.2	95	0	95	5	2.7	<6	16.3	145+	4.4	56
		12.7	100	0	100	0	1.1	<6	[b] 20.3	145+	5.5	34
	INORGANIC REDUCING-ACID SOILS											
61	Sharkey clay	2.1	100	60 to 100	0 to 40	0	0.6	6	2.2	40	0.5	12
		4.0	100	20 to 40	60 to 80	0	1.5	12	5.0	45	1.0	8
		8.9	95	75 to 95	5 to 20	<5	0.7	<6	4.2	48	1.1	14
		11.2	95	0	95	<5	2.2	6	6.9	58	2.1	17
		12.7	100	0	100	0	1.1	6	7.5	64	2.0	14
51	Acadia clay	2.1	15	0	15	85	3.3	6	7.5	52	2.0	30
		[c] 9.0	<5	0	<5	95	4.8	8	17.4	128+	4.8	28

		INORGANIC REDUCING-ALKALINE SOILS										
64	Docas clay	2.1	100	0 to 20	80 to 100	0	3.2	8	8.7	80	0.7	16
		4.0	100	20 to 50	50 to 100	0	1.6	9	6.0	67	6	18
		9.0	95	75 to 95	5 to 20	<5	1.6	10	4.7	80	1.4	79
		11.2	95	0	95	5	2.4	<6	12.7	118	1.6	35
		12.8	95	0	95	<5	1.6	<6	[a] 17.2	122	[illegible]	[illegible]
70	Merced silt loam	2.1	100	60 to 100	0 to 40	0	2.1	8	4.9	50	1.7	56
		4.0	100	0 to 20	80 to 100	0	4.5	12	[b] 9.7	118+	[c] 1.6	102+
		9.0	100	20 to 40	60 to 80	0	0.1	6	13.4	122	3.6	84
		11.2	85	0	85	15	2.6	8	24.5	145+	D	150+
		12.8	90	0	90	10	1.3	8	21.3	145+	D	150+
56	Lake Charles clay	2.1	5 to 15	0	5 to 15	85 to 95	3.7	5	13.8	77	1.1	10
		4.0	5 to 15	0	5 to 15	85 to 95	3.9	7	16.0	104	3.4	26
		8.9	<5	0	<5	95	5.5	13	27.8	145+	4.5	29
		11.1	<5	0	<5	95	14.3	26	[f] D	145+	6.6	42
		12.7	<5	0	<5	95	13.8	66	D	145+	[b] 9.0	[b] 53
		ORGANIC REDUCING-ACID SOILS										
59	Carlisle muck	2.1	30 to 50	0	0	50 to 70	1.2	8	1.5	12	0.7	66
		4.0	30 to 50	0	0	50 to 70	3.4	11	3.3	20	1.7	10
		9.1	50	0	20 to 50	50	3.0	8	7.5	101	4.6	22
		11.1	50	0	50	50	4.0	8	9.6	76	3.9	28
		12.7	40	0	40	60	3.4	<6	9.6	72	4.6	18
63	Tidal marsh	2.1	100	50 to 100	0 to 50	0	1.2	<6	2.7	24	1.2	26
		4.0	100	50 to 100	0 to 50	0	2.1	10	9.2	38	[b] 2.3	34
		8.9	95	0	95	5	2.0	8	10.7	80	[e] 2.0	25
		11.2	75	0	75	25	2.9	8	12.2	94	3.8	30
		12.6	60	0	60	40	[b] 4.8	[b] 52	18.5	126	4.1	43
58	Muck	2.1	5 to 15	0	5 to 15	85 to 95	4.3	13	5.1	29	3.3	38
		4.0	0	0	0	100	5.4	[b] 21	8.8	46	5.1	66
		9.1	0	0	0	100	9.0	64	17.3	98	7.4	58
		11.1	0	0	0	100	8.3	66	16.3	110	7.6	75
		12.7	0	0	0	100	10.7	76	17.6	124	7.5	59
60	Rifle peat	2.1	0	0	0	100	4.3	10	4.0	15	4.6	53
		4.0	0	0	0	100	7.2	12	8.1	[b] 38	10.4	100
		9.1	0	0	0	100	19.8	83+	17.6	58	D	150+
		11.1	0	0	0	100	17.9	66	19.6	89	D	150+
		12.7	0	0	0	100	19.5	88	21.0	118	D	150+
		CINDERS										
67	Cinders	2.1	0	0	0	100	6.7	62	40.5	145+	[e] 4.6	107+
		4.0	0	0	0	100	5.4	45	[e] 37.0	145+	[e] 12.2	118+
		9.0	<5	0	<5	95	5.6	21	31.7	145+	D	150+
		11.1	0	0	0	100	17.2	62	D	145+	12.0	78
		12.7	<5	0	<5	95	[b] 11.9	[b] 48	D	145+	D	150+

[a] Nominal weight of coating, 3.08 oz/ft².
[b] Data for the individual specimens differed from the average by more than 50 percent.
[c] Data for 8 specimens.
[d] The plus sign indicates that 1 or more specimens contained holes because of corrosion.
[e] Data for 1 specimen. The other specimens were destroyed by corrosion.
[f] D, both specimens destroyed by corrosion.
[g] Data for 1 specimen. The other specimen was missing.

The weight loss and pit depth-time curves for the galvanized specimens (fig. 5) show that the zinc coatings provided good protection in all of the 10 inorganic soils with the exception of the highly reducing soil 56. However, in only one of the four organic soils (59) could protection be considered adequate. In two of these soils, 58 and 60, the effectiveness of the zinc coating was negligible. Although it is not surprising that severe corrosion of galvanized steel occurred in these organic soils because of their corrosiveness toward zinc, it is evident from the curves in figure 5 that a high rate of corrosion of zinc in a soil does not indicate necessarily that galvanized steel would also be subject to corrosion.

The data presented on the condition of the coating on the specimens (table 3) indicate that the specimens removed from sites 64, 65, 66, and 70 after exposures for 11 and for 13 yr contained no zinc whatever. Because these specimens were covered with zinc-iron alloy layer, it might be assumed that the alloy layer protected the steel pipe electrochemically or otherwise, but unpublished results of measurements of the potentials and of the polarizing characteristics of these materials, supplemented by measurements of weight loss, indicate that the zinc-iron alloy layer cannot protect steel cathodically in soils, nor is it more resistant to corrosion than steel.

Additional evidence that galvanic action between zinc and steel does not fully account for the behavior of the galvanized specimens is provided by the data on weight loss and pitting of the specimens removed from sites 51 and 67 (table 3). Although both the outer zinc coating and the alloy layer were completely removed from the specimens during the initial period of exposure, the weight losses and pitting of the galvanized specimens during the remaining periods of exposure were considerably less than they were on the bare steel specimens. There are some indications that the relatively high resistance to corrosion of the galvanized specimens is due to an inorganic film or coating deposited by galvanic action between the outer zinc coating and the alloy layer or steel. The composition and properties of this film, which is presumably silicious in nature, are currently under study.

Reference has previously been made to an earlier series of field tests in which were included galvanized specimens having the same nominal weight of coating as those in the present test, namely, 3 oz/ft^2 [1, 2]. In comparing the behavior of these two sets of specimens, Blum and Brenner [6] concluded that the specimens in the later test corroded as a group as much in 4 yr as did the specimens in the earlier test in 10 yr. A further examination of these data, however, indicates that this observation is not entirely correct. The data for the 1924 specimens removed after 10 yr are reported as an average rate of loss of weight in ounces per square foot (or penetration) per year, whereas those for the 1937 specimens are reported as total loss of weight (or total penetration) after 4 yr exposure. Comparison of the two sets of specimens on this basis is difficult because most corrosion occurs during the first few years of exposure and the rate decreases considerably after this initial rapid corrosion.

A better comparison may be made of the two sets of specimens after each had been exposed for 10 yr. Seven of the soil sites either were common to the two series of tests or were located in soils of the same type, differing only in geographical location, making possible a comparison of the two sets under the same soil conditions. The weight losses and the maximum penetration of these specimens, both bare and galvanized, exposed to the same soil conditions are given in table 4. Because the specimens buried in 1937 were not removed after exposure for 10 yr as were the earlier specimens, it was necessary to interpolate the weight loss and pit depth-time curves for these specimens (fig. 5) between the points for 9 and

TABLE 4. *Comparison between different lots of 3-oz galvanized samples exposed to the same soil conditions for 2 different 10 yr periods*

Site number		Galvanized steel				Bare steel, weight loss	
		Weight loss		Maximum penetration			
1924	1937	1924	1937	1924	1937	1924	1937
		oz/ft²	*oz/ft²*	*Mils*	*Mils*	*oz/ft²*	*oz/ft²*
3	53	0.4	0.8	<6	<6	4.0	4.0
11	55	.9	1.0	<6	9	1.8	4.0
23	70	9.6	1.5	68	7	25.7	18.5
29	58	6.0	8.5	<6	63	14.8	16.8
40	61	0.9	1.5	<6	<6	7.5	5.5
42	62	0.7	1.0	<6	<6	10.6	5.5
*43	63	1.4	2.5	<6	8	12.7	11.5

* Site 45 is not identical with site 63 geographically, but the soil environment, tidal marsh, is the same.

13 yr. In 5 of the soils, 3 (53), 11 (55), 40 (61), 42 (62), and 43 (63) there is no significant difference in corrosion. In two soils, 23 (70) and 29 (58) real differences, particularly in penetration, are found. In the case of soil 23 (70) the penetration was greater in the 1924 specimens, but in the other, 29 (58), the penetration was greater in the 1937 specimens.

As pointed out previously there is a wide range in coating thickness of the specimens buried in 1937 (fig. 2) and a similar but somewhat smaller range in the 1924 specimens. The excellent agreement in results of the tests of the two sets of specimens in five soils indicate that these thickness differences were of little significance and that the difference in corrosion of the specimens in the other two soils must have been due to local environmental changes, such as drainage, aeration, etc. over the two periods of time.

7. Effect of Weight of Coating

Logan and Ewing [1] studied the effect of weight of coating on the loss in weight of galvanized specimens exposed to corrosion in six soils, representing a wide range of conditions, for periods of 6, 8, and 10 yr. Their results showed that the weight loss decreased with increase in weight of coating to a

certain limiting value beyond which it was constant. On the basis of this relation and other considerations, the conclusion was drawn that galvanized coatings for underground use should have a weight of not less than 2 oz/ft² of exposed surface. Although Logan and Ewing showed a rough correlation between weight loss and pitting, no attempt was made to relate the rate of pitting of the specimens directly to coating weight.

In order to obtain a direct relation between the pitting of galvanized steel specimens and weight of coating, the depths of the deepest pits after 10-yr exposure on the specimens studied by Logan and Ewing were averaged for the same six soils and plotted against the corresponding weights of coating. In obtaining the values shown in figure 6, the pit depths on specimens having coating weights within the ranges 0.8 to 0.9, 0.9 to 1.0, etc. oz/ft² were averaged. These average values also include data for specimens of different basis metals, namely, open-hearth iron, wrought iron and copper bearing steel, no specific effect of the basis metal on weight loss having been observed. Each point shown in figure 6 is the average of measurements made on from 12 to 36 specimens, usually the latter. The values for the standard deviation of the pit depths for the different coating thicknesses are seen to decrease markedly with increase in coating thickness. For the soil conditions represented, a zinc coating having a nominal weight of 2 oz/ft² of exposed surface would prevent appreciable pitting of steel for at least 10 yr, assuming reasonably uniform distribution of the coating.

As the pit depth data shown in figure 6 apply to specimens of galvanized steel which were exposed to a variety of soil environments, an optimum weight of coating that might be selected on the basis of these data might be excessive in some specific environment but insufficient in others. In table 5 are shown the depths of the deepest pits on the specimens exposed in the earlier series of tests [1], from which can be determined the minimum weight of coating required to protect steel for 10 yr in specific soil environments. Data for the specimens buried in 1937 are also included in the table.

TABLE 5. *Condition or maximum penetration of galvanized pipe and 16-gage steel sheet*

[Maximum penetration, in mils]

Z, Zinc continuous over specimen; A, zinc-iron alloy layer exposed over at least a part of the specimen; R, rusted; M, shallow metal attack.

Soil number	Coating weight (oz/ft²) on—					
	Sheet *			Pipe		
	0.81	0.99	1.07	1.81	2.82	3.08
INORGANIC OXIDIZING—ACID SOILS						
3	R	R	Z	M	Z	.....
53	.....	.....	.....	.....	.....	A
4	16	22	13	R	R	.....
6	A	A	Z	.....	Z	.....
10	24	16	12	A	R	.....
11	21	16	13	.....	A	.....
55	.....	.....	.....	.....	.....	A
12	M	A	A	A	.....	.....
16	15	20	18	Z	M	.....
19	20	27	22	A	Z	.....
22	32	56	29	.....	R	.....
24	A	A	Z	Z	Z	.....
25	R	10	R	.....	Z	.....
26	6	11	8	A	A	.....
31	A	Z	Z	.....	Z	.....
32	R	A	A	R	R	.....
35	R	A	A	A	A	.....
36	4	A	A	.....	Z	.....
38	A	A	A	.....	Z	.....
41	A	A	A	M	A	.....
42	.....	21	23	.....	R	.....
62	.....	.....	.....	.....	.....	A
46	Z	Z	Z	A	Z	.....
INORGANIC OXIDIZING—ALKALINE SOILS						
13	R	15	8	.....	R	.....
65	.....	.....	.....	.....	.....	A
66	.....	.....	.....	.....	.....	A
INORGANIC REDUCING—ACID SOILS						
1	30	30	33	29	R	.....
2	R	A	Z	M	Z	.....
5	22	12	12	.....	R	.....
7	17	17	22	R	R	.....
9	19	29	23	R	A	.....
14	A	A	R	A	Z	.....
17	27	22	19	R	R	.....
27	10	12	9	.....	A	.....
28	63	33	22	.....	R	.....
30	13	20	11	12	A	.....
37	17	20	14	.....	R	.....
40	48	47	38	R	R	.....
61	.....	.....	.....	.....	.....	M
44	A	A	A	.....	.....	.....
51	.....	.....	.....	.....	.....	15
INORGANIC REDUCING—ALKALINE SOILS						
8	R	A	A	R	Z	.....
15	A	Z	Z	.....	Z	.....
20	21	17	13	R	R	.....
23	21	37	41	.....	68	.....
70	.....	.....	.....	.....	.....	7
45	5	19	16	38	R	.....
47	R	R	R	A	A	.....
56	.....	.....	.....	.....	.....	17
64	.....	.....	.....	.....	.....	7
ORGANIC REDUCING—ACID SOILS						
29	26	32	28	30	R	.....
58	.....	.....	.....	.....	.....	65
33	29	17	14	.....	R	.....
43	63	R	R	25	A	.....
63	.....	.....	.....	.....	.....	8
59	.....	.....	.....	.....	.....	8
60	.....	.....	.....	.....	.....	75
CINDERS						
67	.....	.....	.....	.....	.....	40

* Weights of the coating on one side. This is half the nominal weight of the coating on sheets.

It will be observed that in the group of oxidizing, inorganic soils, pitting occurred on the specimens having a weight of coating of 1.07 oz/ft² or less, but no pits developed on the specimens having a coating of 1.81 oz/ft². Hence it is reasonable to conclude that a nominal 2-oz coating is probably adequate for oxidizing soils for at least 10 yr. A 3-oz coating would provide adequate protection in the group of reducing inorganic soils except for highly reducing soils high in soluble salts, for example, 51 and 56. These latter soils and the group of reducing organic soils and cinders would require a coating in excess of 3 oz/ft².

8. Summary

This report contains the results of measurements of corrosion made on specimens of galvanized steel, bare steel and zinc exposed to different soil conditions for periods up to 13 yr. The nominal weight of the zinc coating was 3 oz/ft², but the actual thickness varied over a wide range. In approximately one-half of the 15 soils to which the specimens were exposed, the coating on the galvanized specimens remained virtually intact throughout the entire duration of the field test. The galvanized specimens were especially resistant to corrosion in alkaline soils that were highly corrosive to bare steel. In only two soils, both organic, failure of the zinc coating after relatively short exposures was accompanied by marked corrosion of the steel. The high corrosion resistance shown by most of the galvanized specimens after the outer zinc coating had been virtually removed corrosion is tentatively attributed to a film or co ing, probably silicious in nature, that was deposit cathodically by galvanic action between the out zinc coating and the alloy layer or the underly steel.

The results of these tests show that the minim weight of zinc coating required to protect steel fr corrosion for a minimum of 10 yr depends on t nature of the soil environment. In these expos tests, a 2-oz coating was sufficient to protect steel inorganic oxidizing soils, but for inorganic moderat reducing soils a 3-oz coating was required. High reducing, inorganic and organic soils require coatin in excess of 3 oz/ft².

The field tests described were initiated and i stalled, and until 1946 were conducted under th supervision of K. H. Logan.

9. References

[1] Kirk H. Logan and Scott P. Ewing, J. Research NBS 1 361 (1937) RP 982.
[2] Kirk H. Logan, NBS Circular C450 (1945).
[3] A. Brenner, J. Research NBS **20,** 357 (1938) RP1081.
[4] S. C. Britton, J. Inst. Metals **58,** 211 (1936).
[5] Stanley Anderson and R. W. Manuel, Trans. Electroche Soc. **78,** 373 (1940).
[6] William Blum and Abner Brenner, Corrosion Handbo p. 814. John Wiley & Sons, Inc., New York 1, N. (1948).

FIGURE 1. *Environmental conditions at typical test sites.*

A, site 56, Lake Charles clay at El Vista, Texas; B, site 70, Merced silt loam at Buttonwillow, Calif.; C, site 63, tidal marsh at Charleston, S. C.; D, site 55, Hagerstown loam at Loch Raven, Md.

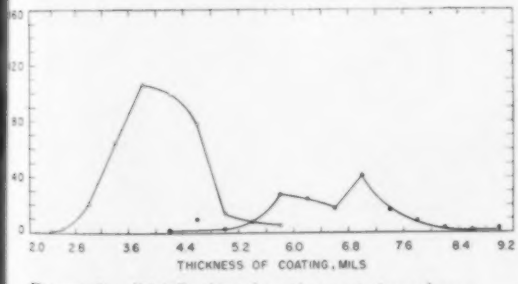

FIGURE 2. *Distribution of coating on test specimens.*

○ Specimen A; length, 14 in.; number of observations, 389. ● Specimen B; length, 6 in.; number of observations, 162.

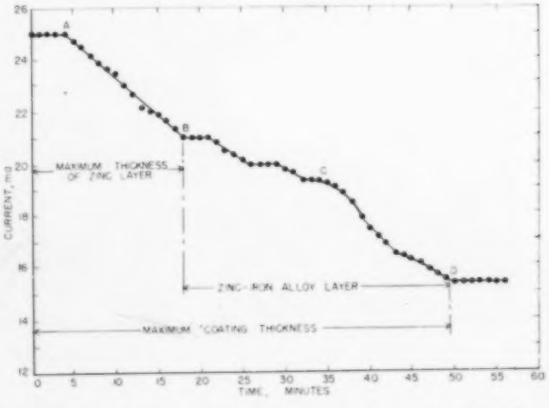

FIGURE 3. *Thickness of the outer zinc coating and of the alloy layer.*

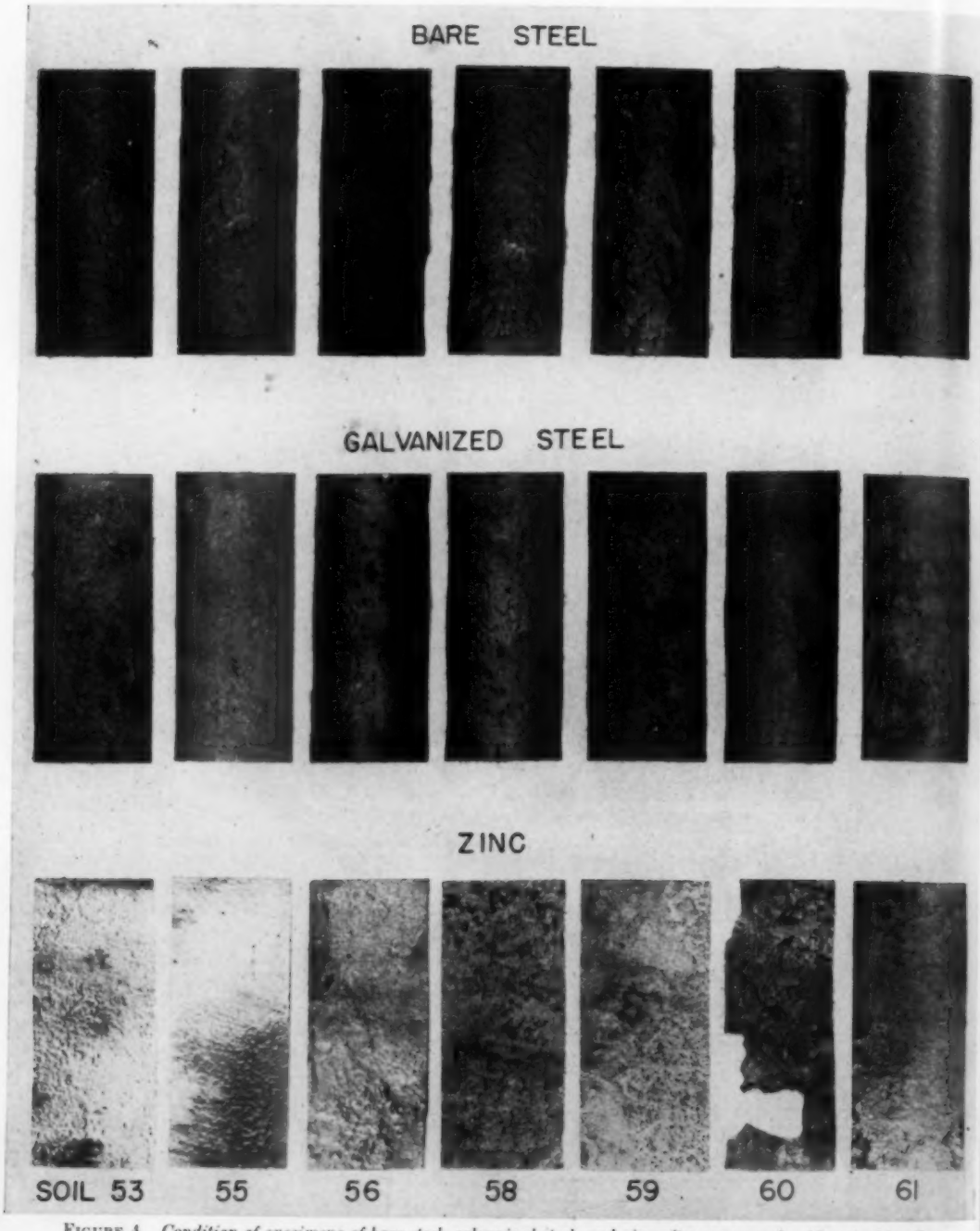

FIGURE 4. *Condition of specimens of bare steel, galvanized steel, and zinc after exposure for 13 yr to 14 soils.*

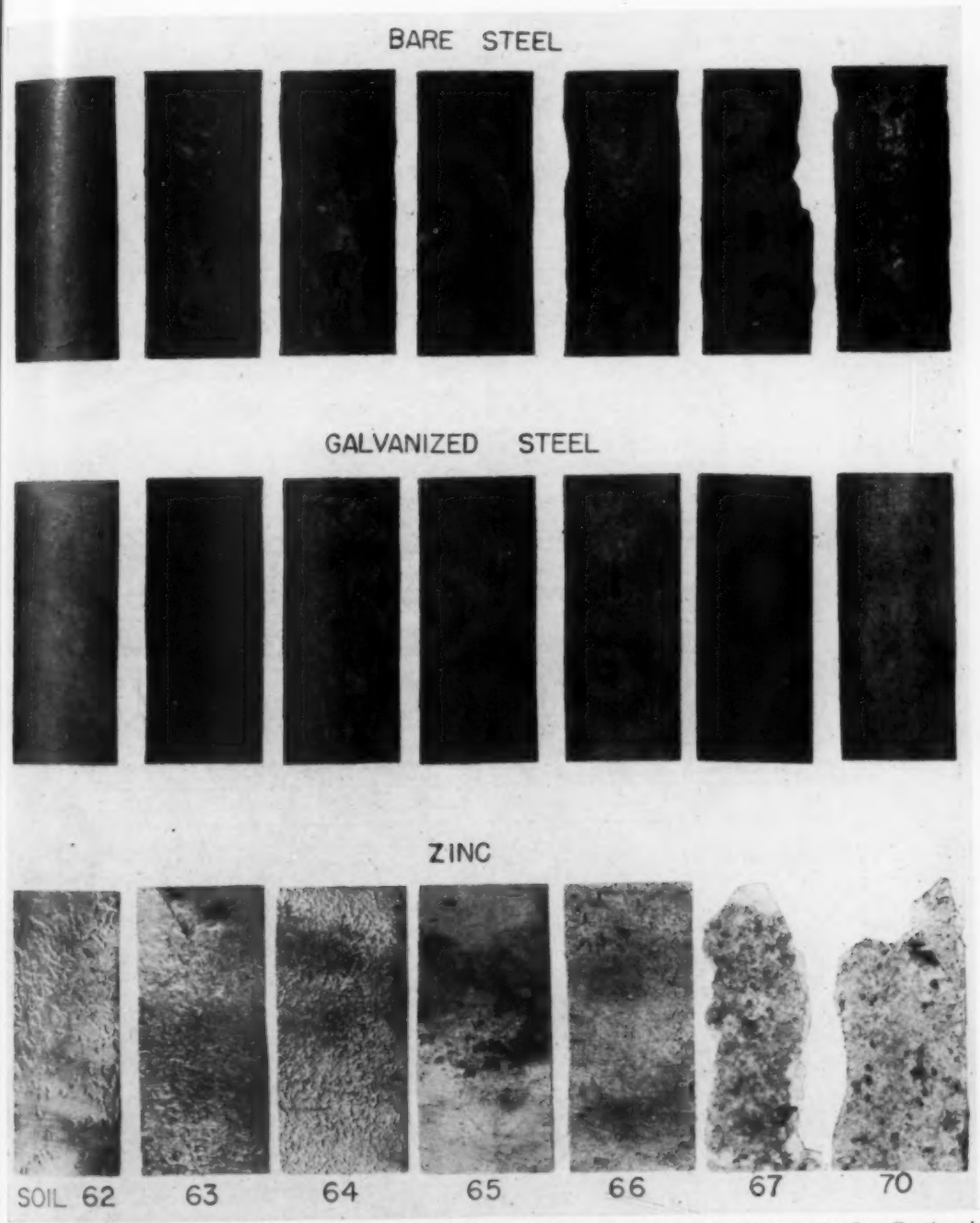

FIGURE 4. *Condition of specimens of bare steel, galvanized steel, and zinc after exposure for 13 yr to 14 soils.*—Continued

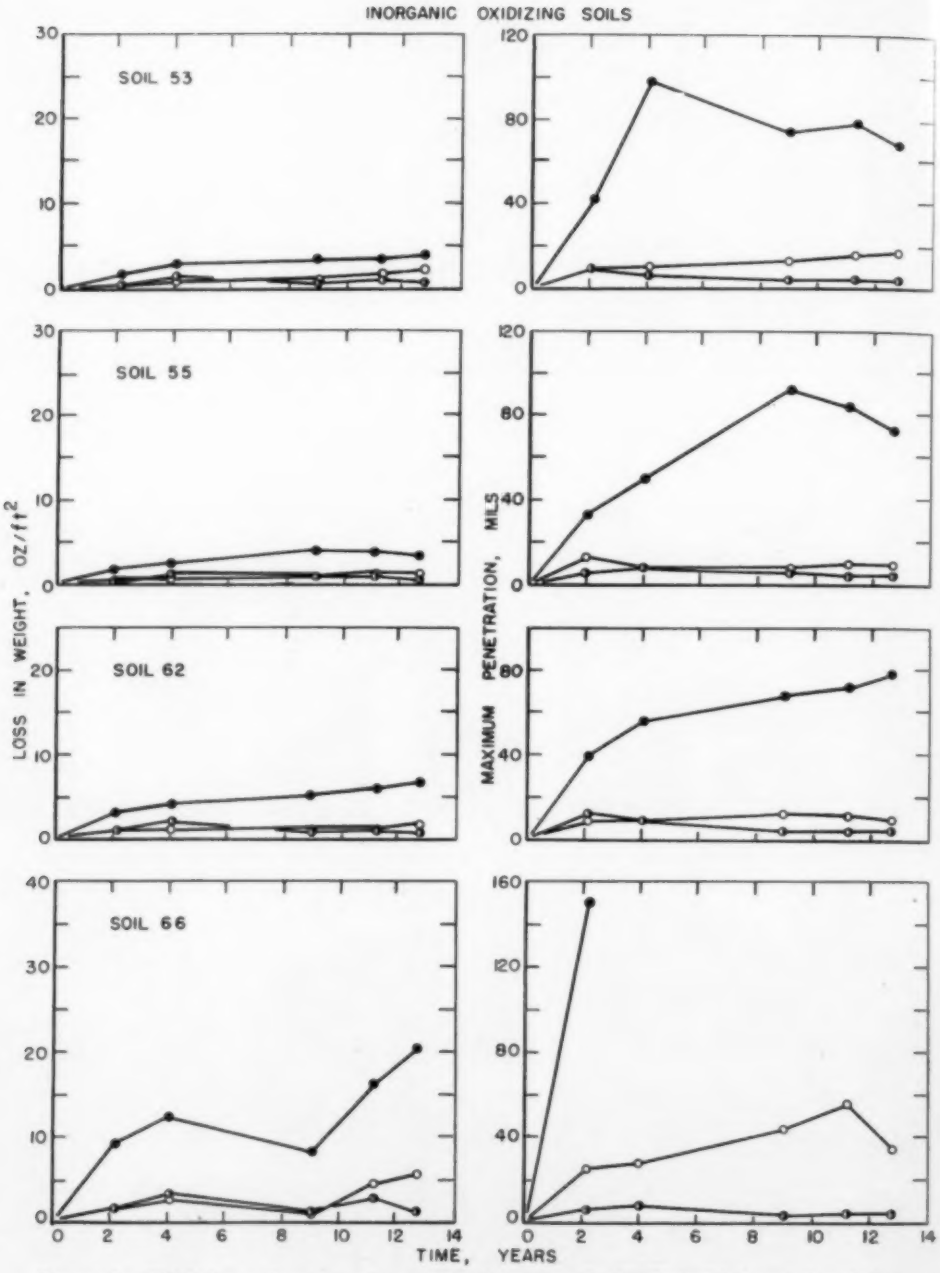

FIGURE 5. *Weight-loss and maximum-penetration–time curves of galvanized steel, bare steel, and zinc.*

● Bare steel, ○ zinc, ◑ Galvanized steel.

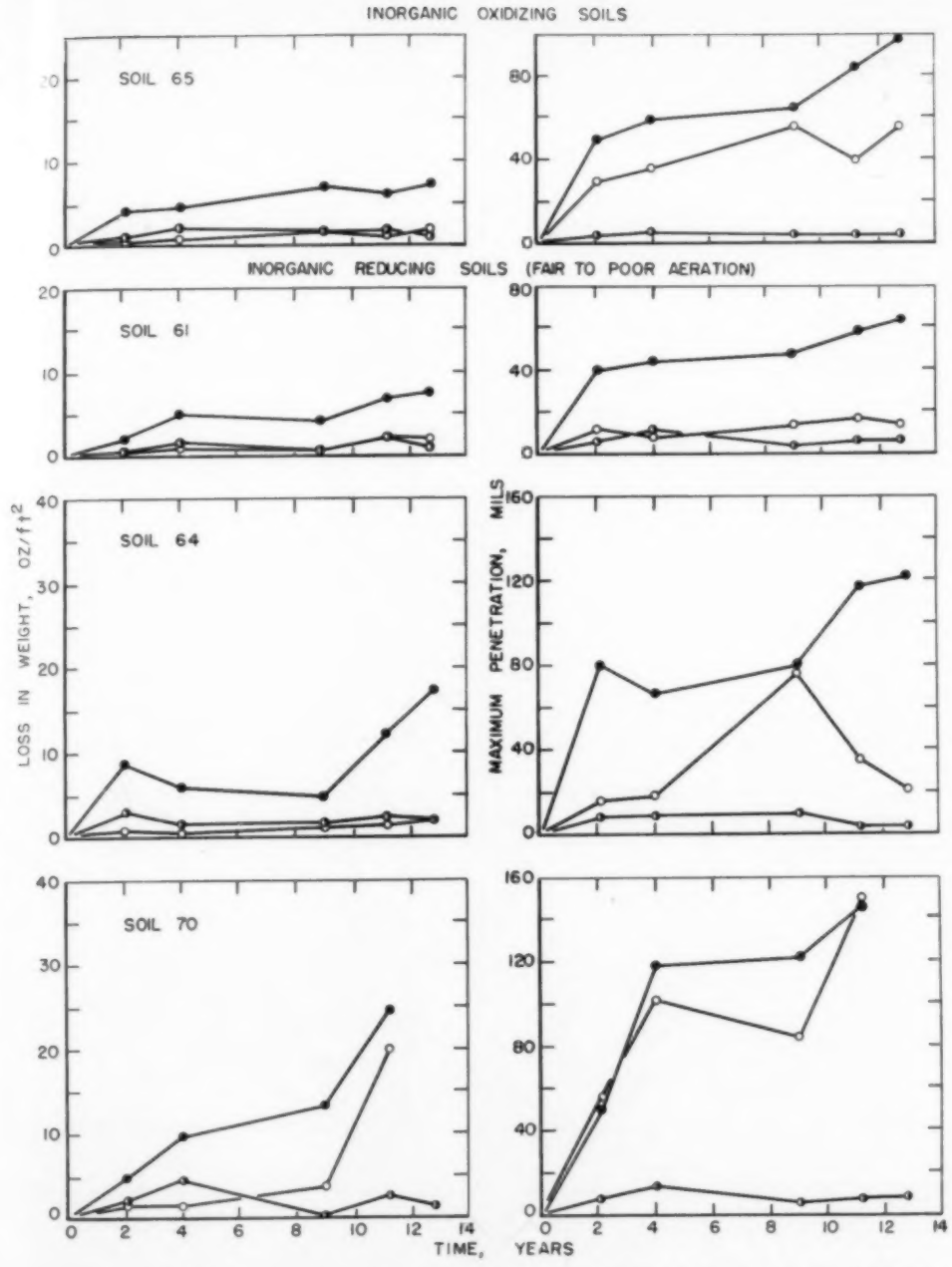

FIGURE 5. *Weight-loss and maximum-penetration–time curves of galvanized steel, bare steel, and zinc*—Continued

● Bare steel, ○ zinc, ◑ Galvanized steel.

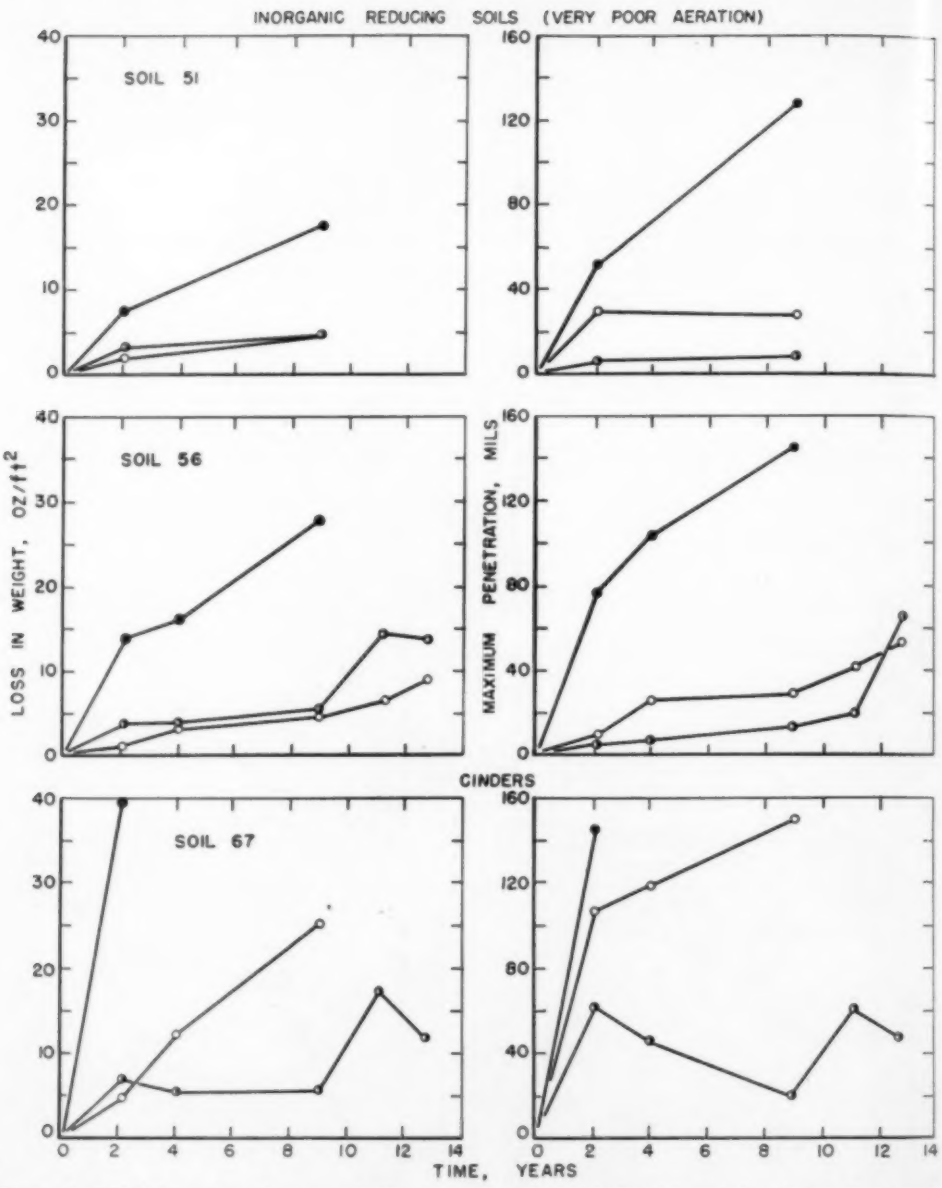

FIGURE 5. *Weight-loss and maximum-penetration–time curves of galvanized steel, bare steel, and zinc*—Continued

● Bare steel, ○ zinc, ◑ galvanized steel.

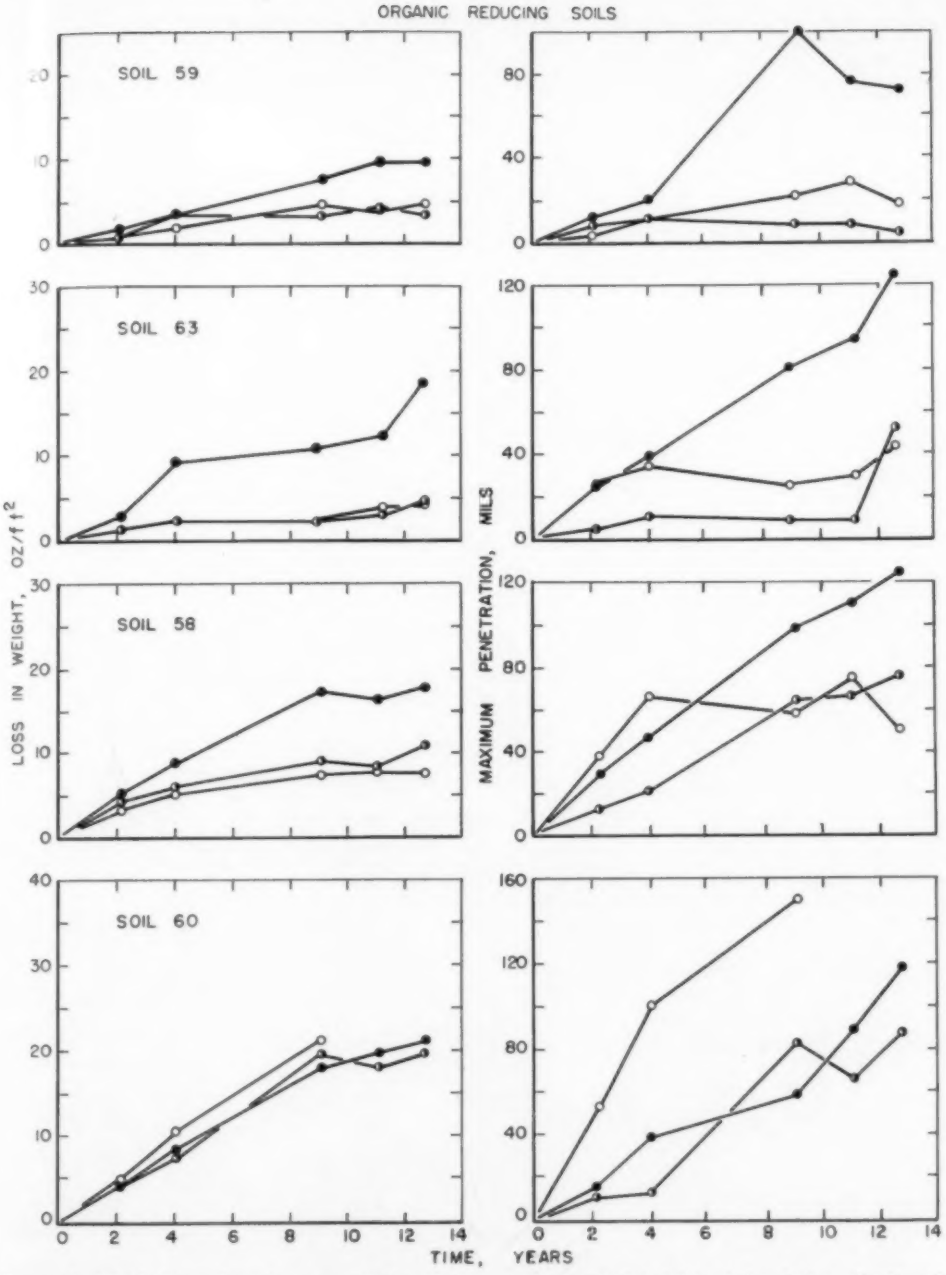

FIGURE 5. *Weight-loss and maximum-penetration–time curves of galvanized steel, bare steel, and zinc*—Continued

● Bare steel, ○ zinc, ◑ galvanized steel.

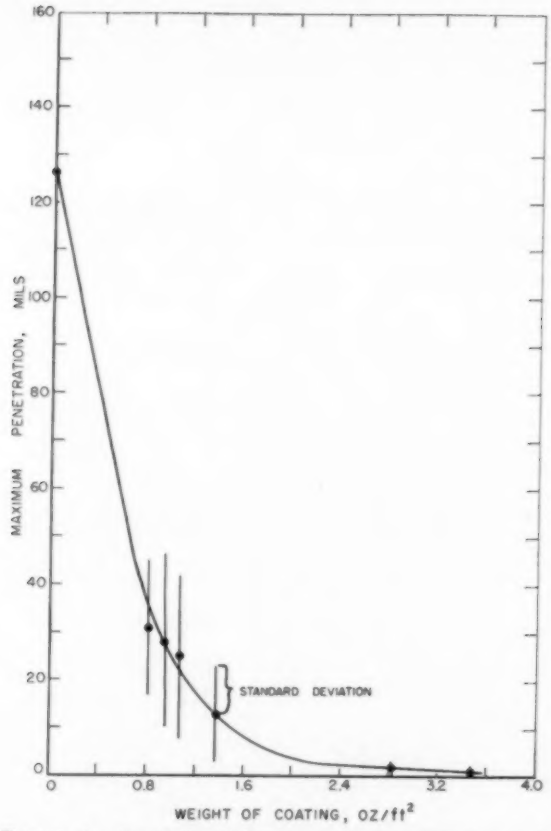

FIGURE 6. *Correlation between maximum penetration and weight of coating on galvanized pipe and sheet exposed 10 yr in 6 soils.*

(Data of Logan and Ewing.)

WASHINGTON, August 18, 1952.

Corrosion of Low-Alloy Irons and Steels in Soils

Irving A. Denison and Melvin Romanoff

The results of measurements of the corrosion of 10 low-alloy irons and steels exposed to 14 soils for periods up to 13 years are given. The magnitude and progress of corrosion as determined by weight-loss and pit-depth measurements are correlated with the composition of the materials and the nature of the environmental conditions to which the test specimens were exposed.

1. Introduction

n 1932 the National Bureau of Standards in peration with a number of manufacturers and sumers of pipe materials initiated an extensive estigation of the corrosion of certain materials d in underground construction. Examination the test specimens removed during the early iods of exposure indicated that certain alloy steels improved corrosion resistance over ordinary s and steels. Consequently, specimens repre- ting a greater variety of alloy irons and steels e installed at the sites at intervals during the rse of the exposure tests. The condition of the imens removed from the various sites after essively longer periods of exposure has been ribed in a series of progress reports, and in 0 a final report on the specimens buried in 1932 s published [1].[1] The present report contains results of measurements of weight loss and pitting samples of 10 varieties of irons and steels that e exposed in 1937 and removed from the test s after five periods of exposure, ranging from to 13-yr duration. The properties of the soils the test sites, the installation of the specimens the sites, and the methods used in cleaning the imens removed prior to 1946 are described in lier papers [1, 2]. Specimens subsequently re- ved were cleaned by immersion in fused sodium ride [3].

2. Description of the Materials

The specimens were in the form of plates 12 in. g and 25 in. wide, ranging in thickness from 0.175 to 0.265 in. The compositions of the materials are given in table 1.

3. Results of the Exposure Tests

The corrosion of the different materials in typical soils is illustrated in figures 1 and 2. Each of the four environmental groups based on aeration is represented as follows: good aeration, soil 55; fair aeration, soil 66; poor aeration, soil 61; and very poor aeration, soil 56.

The extent of corrosion damage was determined from the loss in weight of the specimens as a result of the exposure, and from the depths of the deepest pits. The results of these measurements for the different periods of exposure are given in tables 2 and 3. Unless indicated otherwise, these values are the averages of measurements on two specimens. The exposure periods did not differ from the average values given in the tables by more than 5 percent.

A number of the specimens exposed for the longer periods in the more corrosive soils were perforated by pitting. Because the depths of the pits producing these perforations would obviously have been greater after successively longer periods of exposure if thicker specimens had been used, some adjustment of the values for pitting of the perforated specimens was desirable. An approximate adjustment was made by multiplying the average penetration of the perforated specimens by the pitting factor, defined as the ratio of the maximum to the average penetration. Denison and Hobbs [4] showed that the pitting factor of plain irons and steels decreased with time during the early periods of exposure underground but became approximately constant after exposures for 6 to 8 yr. The value of the pitting factor was con-

TABLE 1. *Composition of the materials*

Material	Identification	C	Si	Mn	S	P	Cr	Ni	Cu	Mo	Other elements
		%	%	%	%	%	%	%	%	%	%
Open-hearth steel	A	0.033	0.002	0.029	0.017	0.006	0.049	0.034	0.052	.....	
Copper-molybdenum open-hearth iron	O	.03	.003	.16	.032	.007	.02	.15	.45	0.07	
Do	N	.06	.001	.098	.029	.069	.02	.14	.54	.13	
Copper-nickel steel	[a] J	.06	.047	.49	.025	.095	.....	.52	.95	.....	
Nickel-copper steel	[b] B	.07	.14	.44	.022	.010	.....	1.96	1.01	.....	
Chromium-silicon-copper-phosphorus steel	C	.075	.84	.20	.018	.124	1.02	0.022	0.428	.....	
2% chromium steel with molybdenum	KK	.082	.51	.46	.015	.017	2.01	.07	.004	.57	
4 to 6% chromium steel	D	.077	.43	.37	.005	.015	5.02	.09	.008	.....	
4 to 6% chromium steel with molybdenum	E	.074	.41	.32	.006	.013	4.67	.09	.004	.51	Al 0.030, Ti 0.022.
Do	H	.060	.39	.40	.014	.021	5.76	.17	.004	.43	Al 0.27.

[a] Some mill scale on the specimens at time of burial.
[b] Specimens completely covered with a hard, black mill scale at the time of burial.

[1] Figures in brackets indicate the literature references at the end of this paper.

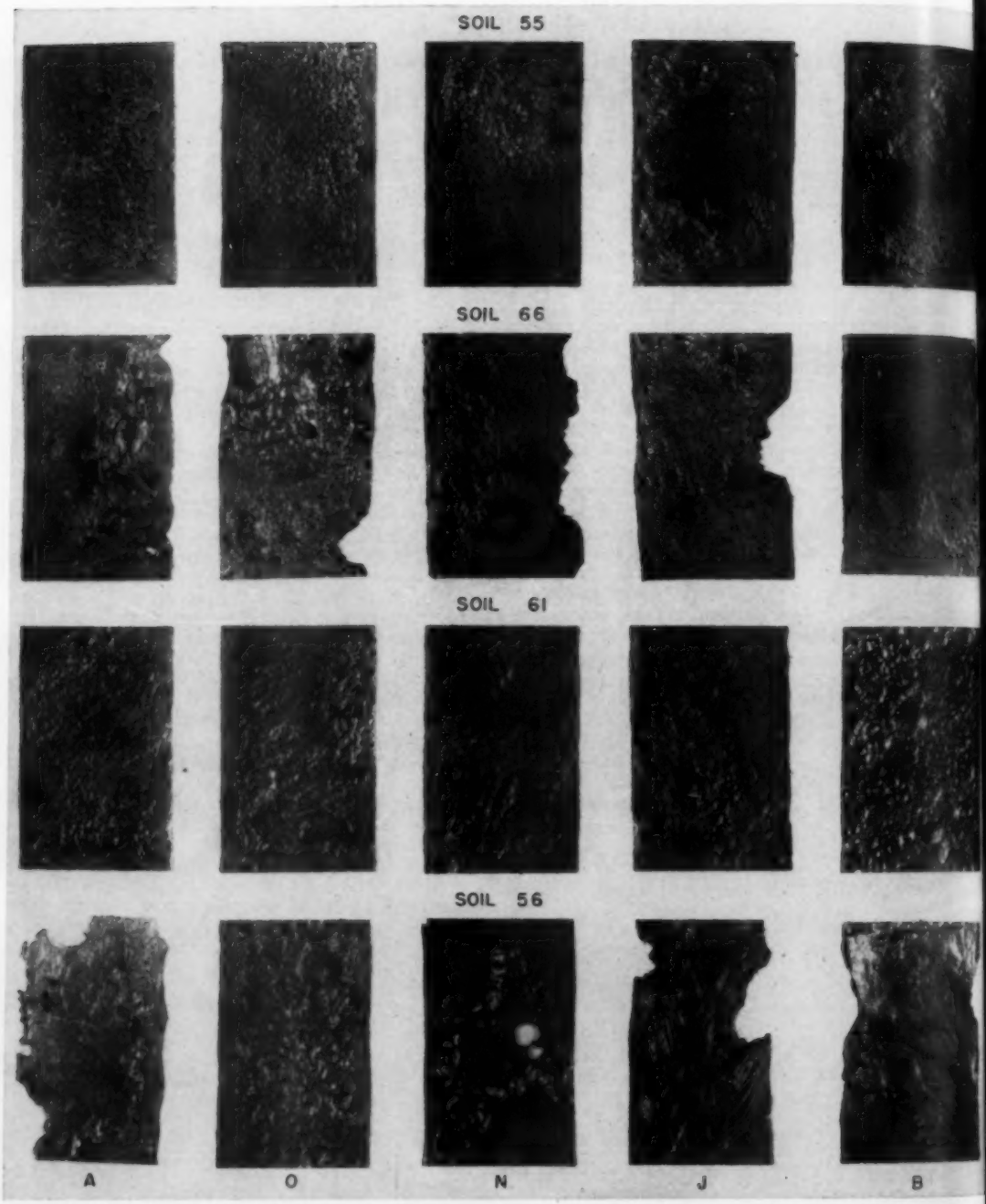

FIGURE 1. *Corrosion of plain steel, copper-molybdenum open-hearth irons and nickel-copper steels in several soil environments*

A, open-hearth steel; O, open-hearth iron, 0.45 Cu, 0.07 Mo; N, open-hearth iron, 0.54 Cu, 0.13 Mo; J, steel, 0.95 Cu, 0.52 Ni; B, steel, 1.96 Ni, 1.01 Cu. Soil 55, well-oxidized acid silt loam deficient in soluble salts; soil 66, fairly well aerated alkaline loam containing a high concentration of soluble material; soil 61, poorly aerated clay containing a moderate amount of soluble material; soil 56, very poorly aerated heavy clay containing a high concentration of soluble salts.

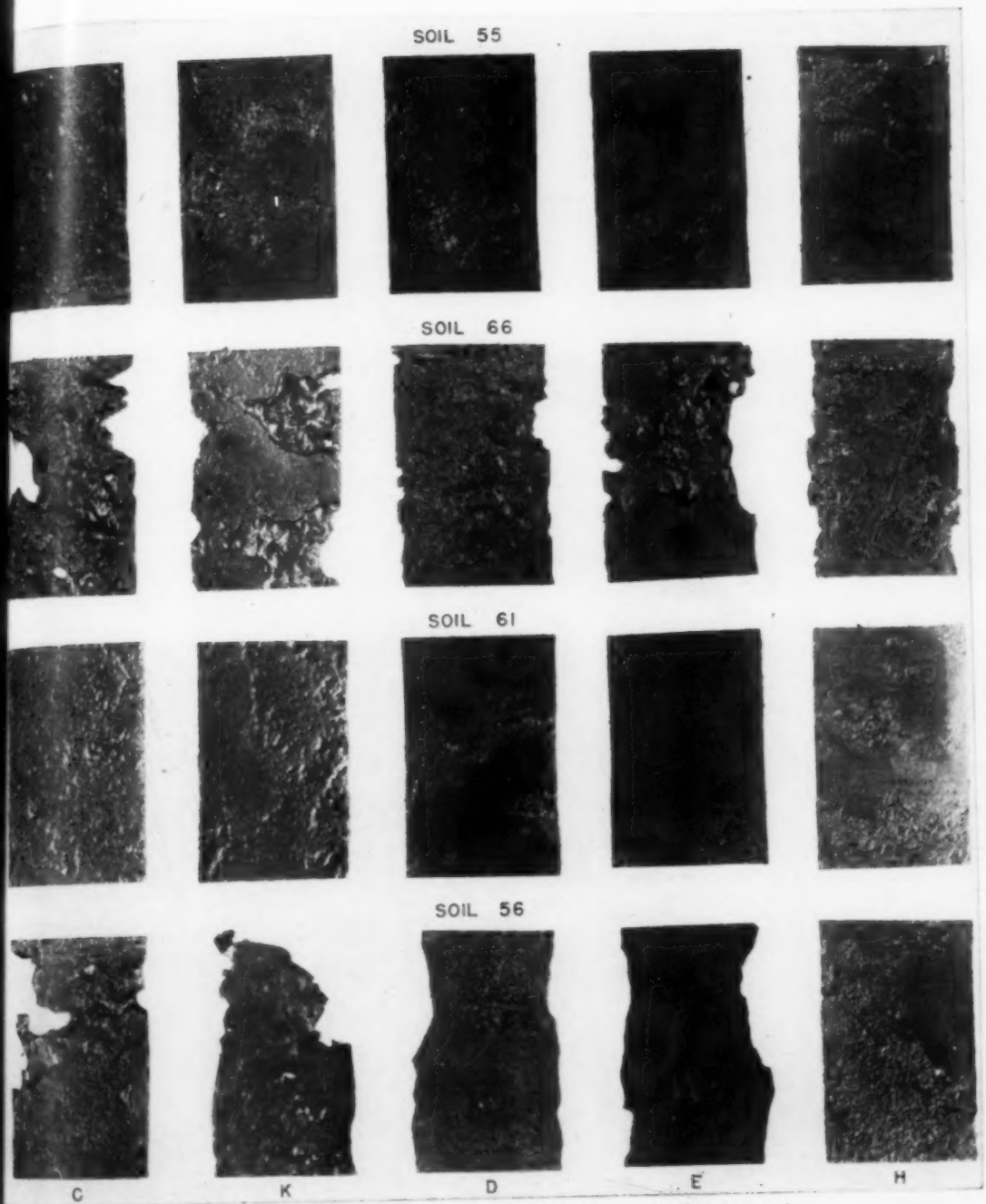

FIGURE 2. *Corrosion of chromium-containing steels in several soil environments.*

C, Cr-Si-Cu-P steel, 1.02 Cr, 0.42 Cu; KK, steel, 2.01 Cr, 0.57 Mo; D, steel, 5.02 Cr; E, steel, 4.67 Cr, 0.51 Mo; H, steel, 5.76 Cr, 0.43 Cr. Soil 55, well oxidized gray silt loam deficient in soluble salts; soil 66, fairly well aerated loam containing a high concentration of soluble material; soil 61, poorly aerated clay containing a moderate amount of soluble material; soil 56, very poorly aerated heavy clay containing a high concentration of soluble salts.

TABLE 2. *Loss in weight of alloy irons and steels in different soils*

[Average of two specimens, in ounces per square foot]

Identification	Material [a]	Average exposure	Aeration, test site number and soil type [b]														
			Good aeration				Fair aeration			Poor aeration			Very poor aeration				
			53 Cecil clay loam	55 Hagerstown loam	62 Susquehanna clay	65 Chino silt loam	64 Docas clay	60 Mohave fine gravelly loam	70 Merced silt loam	58 Muck	60 Rifle peat	61 Sharkey clay	51 Acadia clay	56 Lake Charles clay	59 Carlisle muck	63 Tidal marsh	67 Cinders
		yr															
A	Open-hearth steel	2.1	1.8	2.0	2.8	4.6	7.1	8.3	5.0	5.7	6.3	2.6	11.6	14.4	1.5	3.6	12.0
		4.0	3.2	2.6	3.7	5.3	7.4	16.8	10.6	9.9	9.5	5.4	------	18.4	4.2	[c] 6.2	34.3
		9.0	3.9	3.8	4.2	7.2	7.5	4.6	17.9	16.9	22.0	4.3	[d] 19.1	28.0	9.9	[c] 8.9	[e] D(36)
		11.1	3.4	3.3	5.0	6.1	[f] 19.0	[f] 17.7	24.0	17.2	15.8	7.3	------	48.1	9.5	16.9	37.8
		12.7	4.0	4.0	5.9	8.2	18.6	19.9	25.7	18.1	21.7	8.1	------	D(53)	11.1	16.5	D(42)
O	Open-hearth iron; 0.45 Cu, 0.07 Mo	2.1	2.1	2.0	3.0	5.0	8.0	9.1	5.4	5.8	4.1	3.0	7.5	12.4	1.3	2.5	33.8
		4.0	2.9	2.8	3.6	5.0	8.0	11.6	[f] 11.0	9.9	7.4	5.6	------	13.8	2.9	4.7	33.2
		9.0	3.4	4.7	4.6	6.4	6.4	5.9	13.6	17.3	16.4	4.8	[d] 19.0	28.4	7.8	7.1	25.1
		11.1	3.7	3.7	5.0	5.3	13.3	16.4	22.9	17.0	21.1	7.9	------	48.2	8.3	11.6	29.3
		12.7	3.7	3.3	5.2	8.9	18.5	15.2	21.8	17.5	17.9	8.6	------	D(53)	10.1	15.9	30.5
N	Open-hearth iron; 0.54 Cu, 0.13 Mo	2.1	2.0	1.9	3.0	4.6	8.0	7.4	4.8	5.5	4.8	2.7	7.2	13.0	1.4	3.0	20.9
		4.0	3.0	2.7	3.7	5.0	6.6	12.0	[f] 10.2	9.4	8.2	5.6	------	17.4	2.9	4.7	27.7
		9.0	3.3	4.6	4.7	6.7	5.8	[f] 6.9	15.0	17.0	14.5	4.6	[d] 18.8	33.7	7.6	7.2	21.9
		11.1	3.5	3.5	5.2	5.5	14.7	[f] 20.5	20.3	17.1	20.0	7.5	------	45.2	7.9	9.1	27.5
		12.7	3.8	3.4	5.3	8.1	18.0	15.1	20.0	17.0	20.8	8.6	------	D(50)	7.4	11.7	29.5
J	Copper-nickel steel; 0.95 Cu, 0.52 Ni	2.1	0.8	1.2	2.4	3.4	9.0	7.3	4.2	5.2	5.3	2.3	7.0	14.0	1.6	[c] 2.5	20.3
		4.0	1.3	1.8	3.3	5.0	6.0	10.4	[f] 7.6	10.6	8.6	4.8	------	19.2	2.6	3.5	35.1
		9.0	2.4	3.5	4.0	6.2	4.7	8.2	17.3	16.0	18.8	3.9	[d] 18.1	34.6	5.5	7.0	30.4
		11.1	2.8	2.6	5.4	4.7	17.7	17.8	22.7	17.6	20.1	6.7	------	49.5	8.2	7.8	28.2
		12.7	3.0	2.6	5.5	8.8	23.2	25.5	20.0	18.7	14.3	7.9	------	53.9	8.5	9.3	[c] 17.4
B [g]	Nickel-copper steel; 1.96 Ni, 1.01 Cu	2.1	0.6	0.8	2.1	4.9	6.6	8.9	3.9	6.2	6.4	2.0	7.4	13.0	1.4	2.3	23.0
		4.0	1.1	1.2	2.9	5.0	4.9	11.4	7.8	11.0	9.6	3.9	------	19.5	2.4	3.4	44.3
		9.0	2.8	2.6	2.9	7.6	7.1	3.1	18.4	17.7	24.1	3.2	[d] 20.2	31.2	7.2	8.9	D(49)
		11.1	2.4	2.4	5.1	5.4	[f] 21.2	[f] 17.4	26.8	18.8	17.0	6.8	------	45.9	7.8	7.3	31.9
		12.7	3.2	3.1	8.2	10.8	14.4	19.8	29.6	20.8	21.0	7.6	------	D(50)	9.4	11.7	39.0
C	Cr-Si-Cu-P steel; 1.02 Cr, 0.42 Cu	2.1	1.5	1.3	1.9	4.4	4.9	6.9	5.4	4.4	5.8	2.4	9.2	12.5	1.1	2.4	17.7
		4.0	2.4	2.3	3.0	5.4	5.1	13.6	9.8	9.0	10.2	4.6	------	20.8	2.5	4.1	13.9
		9.0	3.3	3.0	3.8	11.0	5.7	3.9	15.8	16.7	24.9	3.6	[d] 19.6	28.1	7.8	[c] 5.8	26.3
		11.1	2.9	2.7	4.7	9.9	10.6	[f] 12.3	28.1	18.0	18.5	7.1	------	44.0	7.5	7.9	25.2
		12.7	3.6	3.3	5.5	11.4	7.6	17.6	D(33)	18.7	18.0	7.1	------	D(49)	8.5	7.8	D(31)
KK	2.01% chromium steel with 0.57 Mo	2.1	1.6	1.6	2.4	4.2	4.9	7.2	5.4	3.3	3.8	2.4	7.9	9.0	1.2	1.8	[f] 18.1
		4.0	2.2	2.4	3.0	4.5	5.4	12.3	9.7	8.4	6.0	4.7	------	14.5	2.5	3.1	16.4
		9.0	2.9	4.7	4.3	7.7	4.6	[f] 6.0	13.5	12.9	13.8	4.1	[d] 17.9	28.9	4.8	4.9	15.0
		11.1	3.0	2.8	3.8	7.3	8.5	[f] 18.9	26.2	13.6	18.5	6.4	------	34.3	7.9	5.3	20.4
		12.7	3.5	2.5	4.7	9.1	8.8	14.0	20.6	14.0	15.3	6.6	------	34.2	7.3	6.7	13.7
D	5.02% chromium steel	2.1	0.9	0.7	0.7	2.3	4.5	5.8	4.9	4.1	4.5	0.6	6.6	9.4	0.4	1.8	17.1
		4.0	1.3	1.1	1.2	2.2	4.4	12.1	[f] 10.0	5.9	6.6	1.6	------	17.9	.9	3.8	18.1
		9.0	2.0	1.7	1.8	3.6	4.4	[f] 3.5	19.1	7.5	14.8	1.1	[d] 17.6	28.8	3.0	5.6	12.2
		11.1	2.1	1.7	2.2	2.8	10.0	[f] 13.5	29.5	7.2	14.6	2.2	------	43.1	4.8	6.0	7.9
		12.7	2.8	1.6	2.5	3.5	7.2	14.7	[c] 22.8	7.8	17.2	1.9	------	D(48)	3.1	9.2	10.3
E	4.67% chromium steel with 0.51 Mo	2.1	0.9	0.6	0.7	2.5	4.2	7.9	5.2	3.9	4.1	0.9	7.1	9.6	0.4	1.7	12.2
		4.0	1.6	1.2	1.1	2.1	5.2	12.0	9.9	7.2	6.2	1.8	------	16.3	.8	5.2	[f] 11.7
		9.0	2.0	1.7	2.0	3.3	4.2	[f] 5.2	19.5	6.4	13.2	1.4	[d] 16.2	28.2	2.5	5.3	11.2
		11.1	2.3	1.6	2.3	2.1	10.2	[f] 13.9	26.0	8.1	14.9	2.4	------	36.8	4.9	5.4	5.7
		12.7	2.9	1.7	2.4	3.8	6.4	14.6	[c] 18.1	9.5	15.0	2.6	------	D(41)	3.4	9.0	8.3
H	5.76% chromium steel with 0.43 Mo	2.1	[c] 0.8	0.7	0.7	2.5	5.9	8.4	5.0	3.5	4.6	0.8	[c] 8.3	[c] 11.4	0.2	[c] 1.7	12.6
		4.0	1.4	1.1	1.3	2.2	5.0	14.5	10.2	[c] 6.8	6.2	1.6	------	14.3	.7	5.4	[f] 12.9
		9.0	1.9	2.0	1.9	3.7	4.0	[f] 5.0	17.6	6.1	14.2	[c] 1.0	[d] 16.7	------	2.2	6.4	8.9
		11.1	2.0	1.8	2.4	2.1	9.0	12.2	29.1	------	19.0	1.9	------	[c] 14.8	4.4	6.4	7.8
		12.7	2.7	1.8	[c] 2.1	3.6	8.5	15.2	[c] 31.0	[c] 7.1	14.4	1.8	------	[c] D(49)	2.4	8.0	10.2

[a] See table 1 for composition of materials.
[b] See reference [1] for properties of soils.
[c] Data for 1 specimen.
[d] Average of 8 specimens.
[e] D, Both specimens destroyed by corrosion. The number in parentheses is the observed loss in weight.
[f] Data for the individual specimens differed from the average by more than 30%.

TABLE 3. *Maximum depth of pits in alloy irons and steels in different soils*

[Average of two specimens, in mils]

[Average of two specimens, in mils]

Identification	Material [a]	Average exposure	Aeration, test site number and soil type [b]: Good aeration				Fair aeration			Poor aeration			Very poor aeration				
			53 Cecil clay loam	55 Hagerstown loam	62 Susquehanna clay	65 Chino silt loam	64 Docas clay	66 Mohave fine gravelly loam	70 Merced silt loam	58 Muck	60 Rifle peat	61 Sharkey clay	51 Acadia clay	56 Lake Charles clay	59 Carlisle muck	63 Tidal marsh	67 Cinders
		yr															
A	Open-hearth steel	2.1	40	42	34	47	44	86	56	31	30	34	54	80	6	18	46
		4.0	76	54	47	51	78	[c] 188+	77	61	40	50		100	22	[d] 26	[e] 132+
		9.0	57	99	59	75	87	66	136+	89	56	90	[f] 138+	126+	98	[d] 56	188+
		11.1	72	77	77	79	156+	[e] (202+)	188+	161+	63	103		188+	96	48	188+
		12.7	78	66	84	91	188+	[e] (228+)	[e] (196+)	188+	60	85		[e] (206+)	99	44	188+
O	Open-hearth iron; 0.45 Cu, 0.07 Mo	2.1	38	31	36	44	70	105	48	30	21	33	54	100	6	[d] 20	70
		4.0	74	44	38	65	75	84	[c] 97	48	28	66		116	20	[c] 48	55
		9.0	72	85	66	102	102	63	89	97	38	64	[f] 242+	174	66	74	80
		11.1	68	81	59	97	125	154	205+	106	55	74		243+	70	65	118
		12.7	64	76	51	116	143	145	224+	114	50	64		243+	58	60	140
N	Open-hearth iron; 0.54 Cu, 0.13 Mo	2.1	38	29	36	32	72	132	51	32	20	32	66	77	6	33	50
		4.0	[c] 72	51	49	[c] 57	76	98	[c] 122	44	[c] 26	54		100	16	47	74
		9.0	53	92	56	52	70	62	92	102	35	70	[f] 171+	162+	68	50	58
		11.1	61	84	65	41	118	137	214+	118	43	78		250+	74	66	139
		12.7	59	67	68	44	129	141	179+	71	44	88		[e] (268+)	54	78	152
J	Copper-nickel steel; 0.95 Cu, 0.52 Ni	2.1	38	34	38	49	60	108	48	26	25	53	63	82	6	14	58
		4.0	57	50	60	60	84	85	82	64	40	63		96	15	28	90
		9.0	38	77	69	58	76	67	136	72	57	84	[f] 148+	140+	33	40	102
		11.1	63	76	87	67	109	149	180	127	66	112		205+	39	48	218+
		12.7	68	72	93	79	132	172+	192	173	60	100		[e] (280+)	47	50	[d] 133
B [g]	Nickel-copper steel; 1.96 Ni, 1.01 Cu	2.1	26	34	51	45	66	38	50	36	20	62	54	100	6	22	64
		4.0	56	52	69	84	88	73	78	52	28	56		139	12	25	84
		9.0	45	88	70	75	80	51	142	97	73	80	[f] 161+	135	32	37	248+
		11.1	72	70	93	79	[c] 128	[c] 93	165	107	58	97		198+	41	46	164
		12.7	94	74	115	124	102	109	159	98	63	108		248+	56	55	138
C	Cr-Si-Cu-P steel; 1.02 Cr, 0.42 Cu	2.1	40	40	36	50	42	56	66	71	23	30	58	52	14	31	58
		4.0	64	51	44	44	70	80	94	52	67	41		77	42	41	47
		9.0	45	77	56	86	60	58	148+	98	112+	76	[f] 92	84	56	[d] 50	58
		11.1	68	79	83	94	86	[c] 119+	[e] (237+)	110	118	67		170+	53	61	147+
		12.7	[c] 78	92	88	105	62	128+	[e] (278+)	106	107	56		188+	64	58	138+
KK	2.01% chromium steel with 0.57 Mo	2.1	40	26	26	56	56	78	102	29	19	31	35	38	22	20	58
		4.0	52	52	56	55	70	130+	94	42	26	35		60	27	24	47
		9.0	69	84	58	76	70	80	110	67	57	76	[f] 110+	96+	34	41	58
		11.1	66	89	67	67	73	157+	175+	76	67	75		175+	48	54	[c] 146+
		12.7	48	114	72	70	66	146+	175+	74	71	65		[e] (183+)	43	56	139+
D	5.02% chromium steel	2.1	43	34	32	37	48	59	87	48	32	30	62	66	18	62	53
		4.0	57	48	52	46	60	99	14	44	51	36		95	39	70	68
		9.0	66	70	74	63	62	92	194	64	64	42	[f] 114	104	66	108	[c] 78+
		11.1	74	66	94	54	87	[c] 115	208	60	60	55		188	71	118	[c] 109+
		12.7	84	56	113	66	154	126	[d] 158	68	69	42		245+	55	136	81
E	4.67% chromium steel with 0.51 Mo	2.1	36	34	26	39	46	81	79	39	26	26	50	62	20	46	46
		4.0	50	47	46	48	66	88	106	46	36	36		80	26	73	57
		9.0	66	51	54	52	46	57	154	56	72	30	[f] 86	108+	55	88	48
		11.1	75	49	63	50	76	[c] 109+	172+	79	77	35		165+	51	86	51
		12.7	98	54	74	70	74	[c] 124+	[d] 188+	88	74	38		188+	46	98	60
H	5.76% chromium steel with 0.43 Mo	2.1	[d] 32	30	32	50	46	72	88	48	26	24	64	[d] 60	18	[d] 42	56
		4.0	57	39	58	56	72	117	94	[d] 44	32	32		90	33	72	52
		9.0	71	58	56	63	70	76	132+	52	76	[d] 38	[f] 109		64	78	52
		11.1	77	51	65	56	78	141+	196+		87	49		203+	63	72	48
		12.7	82	54	[d] 70	68	90	152+	[d] 203+	[d] 60	100	44		[e] (212+)	55	108	55

[a] See table 1 for composition of materials.
[b] See reference [1] for properties of soils.
[c] The plus sign indicates 1 or more specimens contained holes because of corrosion.
[d] Data for 1 specimen.
[e] Data for the individual specimens differed from the average by more than 50%.
[f] Average of 8 specimens.
[g] Numbers in parentheses are pit depths adjusted for perforation by multiplying the average penetration by the pitting factor (see text).
[h] The mill scale was not removed from these specimens.

sidered by Denison and Hobbs to be characteristic of soils and Logan [2] showed that it varied directly with the aeration. Adjusted values of pit depths recorded in table 3 are enclosed in parentheses.

The over-all behavior of materials and the effect of the various alloying constituents on the corrosion of iron and steel in the soils is indicated by the weight loss and pit depth-time curves shown in figures 3 and 4. In preparing these curves, the values for weight loss and pit depth for each material in all of the soils, except 51,[2] were averaged for each period of exposure. The logarithms of these average values were then plotted against the logarithms of the periods of exposure.

The curves shown in figure 3 and 4 conform to the equations

$$P=kT^n \tag{1}$$

$$W=k'T^u \tag{2}$$

where P is the depth of the deepest pit at the time T and W is the weight loss at the time T.

Converting to logarithms,

$$\log P=n \log T+\log k \tag{3}$$

$$\log W=u \log T+\log k'. \tag{4}$$

Hence $n(u)$ is the slope of the line and $k(k')$ is the intercept on the log $P(W)$ axis.

Equations 1 and 2 were derived originally by Logan, Ewing, and Denison [5], and by Martin [6], respectively.

The constants of the equations, expressing the initial corrosion rate of the materials and the change in the rate with time, were calculated by the method of least squares for each material in each soil. By means of these constants, values of the average weight loss and pitting of each material in all of the soils were calculated for the maximum periods of exposure. These values, together with the constants of the equations and their standard errors, are tabulated in table 4.

In order to estimate the probability that the weight loss or pitting of each material was significantly different from the corresponding values for plain steel, taken as the reference material, the standard t-test was applied, and from the calculated values of t, the probability of the differences being due to chance was obtained [7].

The weight loss and pitting data for the copper-molybdenum open-hearth irons O and N and for the nickel-copper steels J and B, presented in figure 3 and in table 4 show that these alloys corroded slightly less than the plain steel A. However, the probability is high that several of the observed differences are due to chance. Because mill scale was not removed from the specimens of steel B before burial, the data recorded for this steel cannot be taken as truly representing the effect of additions of 2 percent of nickel and 1 percent of copper on the corrosion of steel in these soils.

[2] The data for the specimens in soil 51 were omitted because data were available for two periods only.

The average depths of the deepest pits on the materials, given by the values of the constant (y-intercept), indicate that the low-alloy steels had greater initial pitting rate than the plain steel. However, as the exposure increased, the rate of pitting of the alloy steels diminished more rapidly than the rate for the plain steel so that after 13 the order of the materials was reversed.

The weight loss and pit depth data for the group chromium and chromium-molybdenum steels, KK, D, E, and H, (fig. 4 and table 4) exhibit similar but somewhat greater effects of the alloying constituents than the copper-molybdenum and copper nickel irons and steels. Chromium reduced the weight losses in a fairly regular manner, but increased the initial pitting rates of the steels. However, the rates of pitting of the alloy steels decreased more rapidly with time than the rate for plain steel.

The separate effects of chromium and molybdenum on the pitting of steel are difficult to determine because the chromium steels also generally contain molybdenum. It will be observed that steels C and D, containing 1 and 5 percent of chromium, respectively, had pits of about the same depth. Within this range chromium alone in excess of 1 or 2 percent does not appreciably increase the resistance of the material to pitting. On the other hand, the influence of molybdenum in reducing pitting is quite definite because all of the chromium steels containing molybdenum, KK, E, and H, had shallower pits than the straight chromium steel D.

The pit-depth–time curves, figures 3 and 4, indicate that the change in the rate of pitting with time depends on the composition of the steel. In general the greater the amount of nickel, chromium and molybdenum in the steels, the greater was the change in the rate of pitting of the steels with time. It may be assumed that the alloying constituents induced the formation of corrosion products, which were effective in diminishing the rates of pitting of the alloy steels with time. The results of a previous study of the effect of corrosion products on the rate of pitting of steel [8] suggests a probable explanation for the observed differences in corrosion rate. In that study it was observed that in soils in which the corrosion products of ferrous metals diffused outward into the soil, the rate of pitting changed relatively little with time, but in soils in which the corrosion products remained in close contact with the corroding surface, the rate of pitting diminished with time, often becoming negligible after relatively short periods of exposure.

The conclusions that can be drawn from the data in table 4 and in figures 3, 4, and 5 are necessarily limited because these data indicate only the average behavior of the materials under a wide variety of environmental conditions. Whether a particular alloy is more resistant to corrosion than plain steel in a specific soil environment obviously cannot be predicted from these average values. Although the average rates of pitting of the alloy steels decrease more rapidly than the pitting rate of plain steel, it should be recalled that this effect is a consequence

the environment as well as of the material. For example, in a very poorly aerated soil, corrosion products would tend to diffuse and migrate outward to the soil rather than to form protective layers enclosing pits. Under such conditions, the higher initial rate of pitting of the alloy steels would tend to be maintained.

For comparison of the behavior of the materials under different environmental conditions, the corrosion data for the soils classified according to aeration (tables 2 and 3) were calculated on a relative basis for each material for all periods of exposure, the weight losses and pit depths of the reference steel A being taken as 100 percent. The averages of these values for all periods and for all soils in the same environmental groups are given in table 5. Because the data for soil 51 are incomplete, they were not included in calculating the relative values.

The relative corrodibility of the low-alloy irons and steels as measured by weight loss was not affected appreciably by differences in the aeration of the soils. However, the 4- to 6-percent chromium steels were deeply pitted in all of the very poorly aerated soils, except cinders. These steels had higher initial rates of pitting than plain steel, but the rates decreased considerably with time in most of the soils. In the poorly aerated soils, however, this high rate of pitting continued throughout the exposure period, probably because conditions were not favorable to the formation of tubercles, which would have diminished the pitting rate. In contrast is the behavior of these steels in cinders (table 3 and fig. 5), where the initial pitting of all the steels was about the same. The pitting of the plain steel continued at a high rate for the entire exposure period, but most of the pitting of the 4- to 6-percent chromium steels occurred during the first 4 yr of the test, there being only slight increases in pit depth of these steels after that time. This is even more marked in the case of the steels containing molybdenum in addition to chromium (E and H), in which there was practically no additional pitting after the first 4 yr.

Steels containing copper and molybdenum also show more resistance to pitting in cinders after 4 yr of exposure than the plain steel, although to a lesser extent than the 4- to 6-percent-chromium steels.

4. Summary

This report contains the results of measurements of corrosion made on several low-alloy irons and steels after exposure to different soils for periods up to 13 yr. Empirical equations fitted to weight loss and pit-depth–time curves permitted the initial rates of weight loss and pitting and the change in these rates with time to be evaluated. The general effect of the alloying elements was to reduce the initial rate of corrosion of the alloys as measured by weight loss but to increase the initial rate of pitting. Except in very poorly aerated soils, the rate of pitting of the alloy steels diminished more rapidly with time than the rate of pitting of plain steel, with the result that the maximum depths of pits after the maximum period of exposure were less on the alloy steels than on the plain steels. Chromium was observed to have the most pronounced effect on weight loss, but for maximum reduction in pitting, molybdenum also was necessary. Chromium and molybdenum were particularly effective in reducing the corrosion of alloy steels exposed to cinders.

The field tests described in this paper were planned and installed, and until 1946 were conducted under the supervision of K. H. Logan.

The writers gratefully acknowledge the cooperation of O. B. Ellis, Research Laboratory, Armco Steel Co. and of C. P. Larrabee, Research Laboratory, United States Steel Co. in making available their equipment for cleaning the specimens by the sodium hydride process.

The authors also gratefully acknowledge the assistance received from the following organizations that cooperated in the project by providing the test sites and the labor required during the installation and removal of the test specimens: Water Department, Charleston, S. C.; Department of Water Works, Atlanta, Ga.; City of Meridian, Meridian, Miss.; New Orleans Public Service Co., New Orleans, La.; Sewerage and Water Board, New Orleans, La.; Gulf Oil Corp., Houston, Tex.; Water Department, Phoenix, Ariz.; Shell Oil Co., Inc., Wilmington, Calif.; Pacific Gas & Electric Co., Bakersfield, Calif.; Union Oil Company of California, San Luis Obispo, Calif.; Milwaukee Gas & Electric Co., Milwaukee, Wis.; City Light & Water Utilities, Kalamazoo, Mich.; Columbia Engineering Corp., Columbus, Ohio; Sinclair Refining Co., Fort Worth, Tex.; Bureau of Water Supply, Baltimore, Md.

5. References

[1] Irving A. Denison and Melvin Romanoff, J. Research NBS **44,** 47 (1950) RP2057.
[2] Kirk H. Logan, Underground corrosion, NBS Circular 450 (1945).
[3] H. L. Alexander, Iron & Steel Eng. **24,** 5, 44 (May 1947).
[4] I. A. Denison and R. B. Hobbs, J. Research NBS **13,** 125 (1934) RP696.
[5] K. H. Logan, S. P. Ewing and I. A. Denison, Symposium on corrosion testing procedures, Am. Soc. Testing Mtls., Philadelphia, Pa. (1937).
[6] L. M. Martin, NBS Soil Corrosion Conference 1937 (unpublished).
[7] G. S. Eldredge, Section on statistical methods, p. 1083, Corrosion Handbook, (John Wiley & Sons, New York, N. Y., 1948).
[8] I. A. Denison, Chemical aspects of underground corrosion and corrosion prevention, Monograph, Technical Section, Am. Gas Assn. (1948).

TABLE 4. *Calculated average values of weight loss and pit depth after 13 years of exposure and constants of the weight-loss and pit-depth equations* [a]

Identification	Material	Weight loss										Maximum penetration									
		Mean, $\overline{X}$ ($W_{T=13yr}$)	Standard error, σ ($W_{T=13yr}$)	Reduction in weight loss as compared with control A		t [b]	Probability of the difference being due to chance	k'	$\sigma_{k'}$	n	σ_n	Mean, $\overline{X}$ ($P_{T=13yr}$)	Standard error, σ ($P_{T=13yr}$)	Reduction in maximum pit depth as compared with control A		t [b]	Probability of the difference being due to chance	k	σ_k	n	σ_n
				$\overline{X}_1-\overline{X}_2$	Relative basis									$\overline{X}_1-\overline{X}_2$	Relative basis						
		oz/ft²	oz/ft²	oz/ft²	Percent		Percent	oz/ft³	oz/ft³			Mils	Mils	Mils	Percent		Percent	Mils	Mils		
A	Open-hearth steel	17.7	1.2					3.78	0.52	0.60	0.07	127	9.3					28.8	4.2	0.58	0.07
O	Open-hearth iron; 0.45 Cu, 0.07 Mo.	15.2	1.2	2.5	14	1.47	16	4.79	.75	.45	.08	110	5.0	17.3	14	1.64	12	31.4	2.9	.49	.05
N	Open-hearth iron; 0.54 Cu, 0.13 Mo.	15.2	0.8	2.5	14	1.74	10	4.02	.45	.52	.05	102	7.7	25.1	20	2.09	2	33.2	5.0	.44	.08
J	Copper-nickel steel; 0.95 Cu, 0.52 Ni.	15.6	.8	2.1	12	1.46	16	3.87	.37	.54	.05	112	10.4	15.3	12	1.09	29	30.8	5.8	.50	.10
B	Nickel-copper steel; 1.96 Ni, 1.01 Cu.	17.3	.6	0.4	2	0.30	77	3.93	.25	.58	.03	110	3.6	17.1	13	1.72	10	31.1	2.0	.49	.03
C	Cr-Si-Cu-P steel; 1.02 Cr, 0.42 Cu.	15.3	.6	2.4	14	1.79	10	3.30	.23	.60	.04	107	7.0	20.2	16	1.74	10	29.3	3.9	.50	.07
KK	2.01% chromium steel with 0.57 Mo.	12.0	.7	5.7	32	4.10	<1	3.27	.02	.51	.05	93	5.5	33.4	26	3.10	<1	30.3	3.6	.44	.05
D	5.02% chromium steel	10.7	.6	7.0	40	5.22	<1	2.85	.34	.52	.05	100	3.0	24.4	19	2.50	2	33.5	1.9	.44	.03
E	4.67% chromium steel with 0.51 Mo.	10.0	.5	7.7	44	5.92	<1	2.76	.28	.50	.05	85	4.2	41.1	32	4.03	<1	33.0	0.1	.37	.05
H	5.76% chromium steel with 0.43 Mo.	10.1	1.6	7.6	43	3.80	<1	2.86	.29	.49	.16	92	6.3	35.0	28	3.15	<1	33.5	4.6	.39	.07

[a] $W=k'T^n$, $P=kT^n$, where W is the weight loss at the time T, and P is the depth of the deepest pit at the time T.

[b] $t=\dfrac{\overline{X}_1-\overline{X}_2}{\sqrt{\sigma_{\overline{X}_1}^2+\sigma_{\overline{X}_2}^2}}$.

TABLE 5. *Effect of composition on the corrosion of low-alloy iron and steel specimens in soils classified according to aeration (maximum exposure 13 yrs.)*

Identification	Composition of steel (percent)				Aeration									
	Cr	Ni	Cu	Mo	Good	Fair	Poor	Very poor	Very poor cinders	Good	Fair	Poor	Very poor	Very poor cinders
					Average loss in weight [a]					Average maximum penetration [a]				
A	0.049	0.034	0.052	----	100	100	100	100	100	100	100	100	100	100
O	.02	.15	.45	0.07	100	95	98	84	120	100	95	82	120	75
N	.02	.14	.54	.13	100	93	97	83	92	87	96	80	119	63
J	------	.52	.95	----	79	98	94	81	94	96	92	102	93	72
B	------	1.96	1.01	----	79	91	99	81	127	110	81	100	95	72
C	1.02	0.22	0.428	----	94	83	95	76	80	101	84	116	115	64
KK	2.01	.07	.004	.57	90	82	80	63	66	97	91	78	103	60
D	5.02	.09	.008	----	45	77	51	58	55	96	94	83	176	64
E	4.67	.09	.004	.51	46	79	53	56	40	84	83	78	149	54
H	5.76	.17	.004	.43	46	85	52	56	43	88	100	84	149	59

[a] Average for 5 periods of exposure, relative to open-hearth steel (A) = 100.

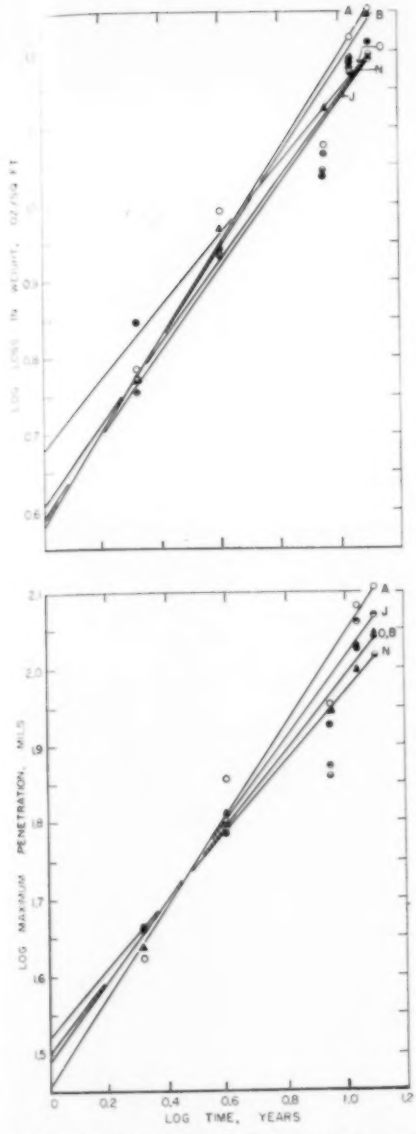

FIGURE 3. *Average loss in weight and maximum penetration-time curves for copper-molybdenum open-hearth irons and nickel-copper steels in 13 soils.*

A, open-hearth steel; O, open-hearth iron, 0.45 Cu, 0.07 Mo; N, open-hearth iron, 0.54 Cu, 0.13 Mo; J, steel 0.85 Cu, 0.52 Ni; B, steel, 1.96 Ni, 1.01 Cu.

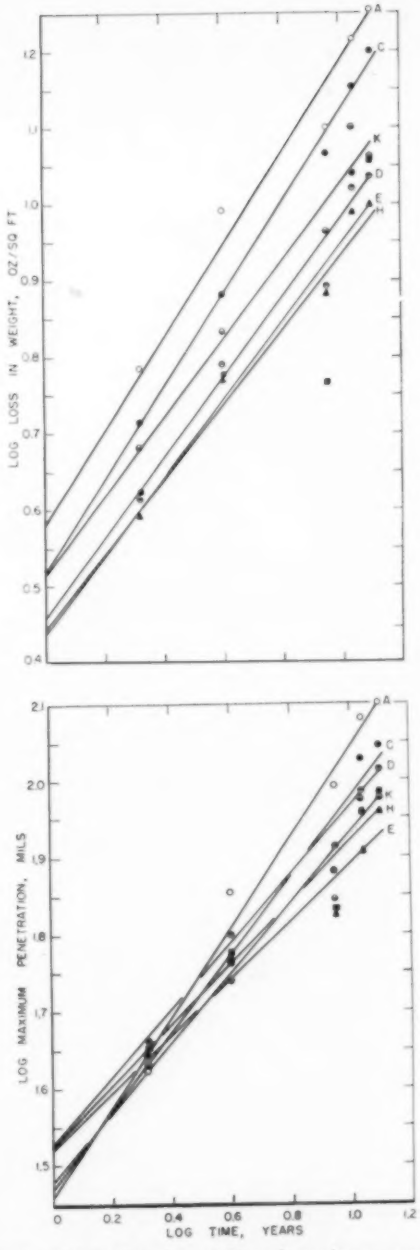

FIGURE 4. *Average loss in weight and maximum penetration-time curves for chromium and chromium-molybdenum steels in 13 soils.*

A, open-hearth steel; C, Cr-Si-Cu-P steel, 1.02 Cr, 0.42 Cu; KK, steel, 2.01 Cr, 0.57 Mo; D, steel, 5.02 Cr; E, steel, 4.67 Cr, 0.51 Mo; H, steel, 5.76 Cr, 0.43 Mo.

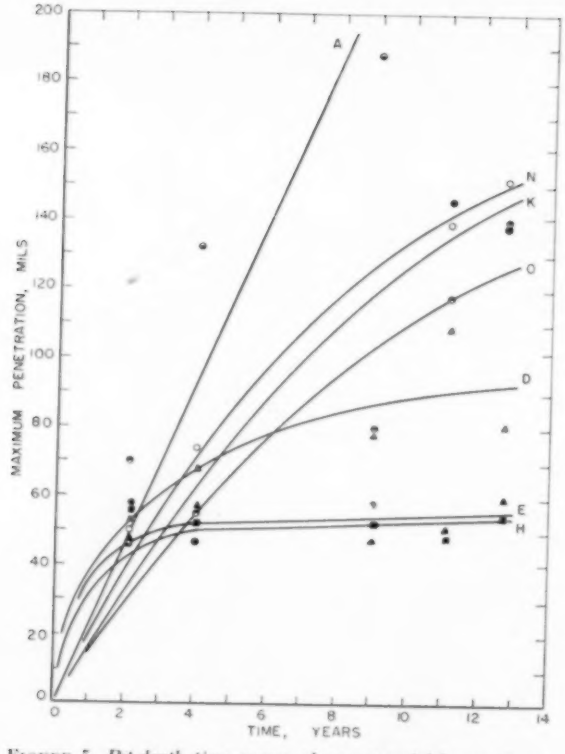

FIGURE 5. *Pit-depth–time curves of copper-molybdenum open-hearth irons, chromium and chromium molybdenum steels in cinders.*

A, open-hearth steel; N, open-hearth iron, 0.54 Cu, 0.13 Mo; K, 2 percent Cr-steel with Mo; D, 5.02 percent Cr-steel; E, 4.67 percent Cr-steel with Mo; H, 5.76 percent Cr-steel with Mo.

WASHINGTON, August 22, 1952.

Journal of Research of the National Bureau of Standards Vol. 49, No. 5, November 1952 Research Paper 2368

Loading of Quartz Oscillator Plates

Leland T. Sogn and Philip A. Simpson

The effects of physically loading the surface of two types of piezoelectric quartz oscillator plates have been experimentally investigated. Various amounts of Wood's metal were applied to different parts of the crystal surfaces. Thickness-shear-mode plates were benefited only when the metal was applied on or near the active central area of the plate, but X-cut crystals employing an extensional mode of vibration responded favorably only when the metal was applied near the periphery of the plate.

In both types of oscillator plates loading increased the crystal unit Q several fold. Activity-frequency characteristics over a temperature range —60° to +90°C were greatly improved.

1. Introduction

Piezoelectric quartz crystal units are extensively employed as frequency controlling and filtering devices in electronic circuits because of their extremely constant equivalent electrical parameters and high Q. However, coupled with the fundamental vibrational mode there are secondary modes of vibration that, under conditions favorable to them, often become so active that they affect both the activity and frequency of the fundamental controlling mode as well as other critical parameters of the crystal equivalent circuit. Various methods, such as face contouring and edge dimensioning, have been used to minimize the effects of this coupling. Experiments recently concluded at the Bureau indicate that selective physical loading on the piezoelectric quartz-plate surface gives approximately equivalent results.

2. Preliminary Experiments

Observations made on 0.5- by 0.6-in. hand-finished quartz plates a few years ago yielded many interesting data that provided the basis for the present investigation. When the electrodes coupling the crystal to the oscillator circuit were placed on the thicker portion of a wedge-shaped plate, not only was the frequency lower but the activity was higher than when they were placed on the thinner portion of the plate. In order to investigate this phenomenon more effectively, a small brass electrode ¼ in. in diameter at the base was constructed. This electrode made it possible to couple much smaller portions of the quartz plate to the oscillator circuit and to study the effect of coupling to local irregularities in the crystal surface that resulted from the application of nonuniform finger pressure during grinding. As expected, it was possible to excite a large number of frequencies by coupling areas of different thickness to the oscillator circuit. The previously mentioned inverse frequency-activity relationship was apparent and was found to be very consistent as the electrode was moved about on the surface of the plate. It was noted that whenever a certain frequency was excited by coupling to different areas of the crystal plate the activity was the same. It was also noted that the lowest frequency was associated with the highest activity.

Similar studies were made later on machine-lapped, slightly convex quartz plates. Results were much the same, except that random distribution of frequencies was replaced by orderly progression as the electrode was moved from the center along a diagonal toward a corner of the plate. Areas to which the oscillator circuit could be coupled in order to excite a certain frequency were arranged in the form of concentric rings about the center, with the lowest frequencies near the center and the highest at the corners.

The frequency associated with the highest activity was not the lowest frequency obtained by coupling to the exact center of the plate, but was a slightly higher one excited by coupling to an area immediately surrounding the center. In a plate whose frequency increased 25 kc between center and corner, the frequency with the highest activity was 4 or 5 kc higher than that of the center. It was this fact that suggested the hypothesis that for each crystal plate there is one frequency and electrode position that will give the highest activity, and that physical loading of the plate would be beneficial through causing it to oscillate nearer this optimum frequency.

3. Detailed Experiments

3.1. Concave Crystals

The first crystals loaded were a group of 10-Mc plates, 0.6 by 0.5 in., with their centers approximately 0.00005 in. thinner than the corners. The activities (rectified oscillator grid current) of these plates unloaded varied between 0.0 and 0.2 ma over the range—60° to +90°C. The frequency curves also were very poor, showing many irregularities.

The plates were then etched 3 to 5 kc and loaded back the same amount so as to maintain the same relationship between their fundamental and secondary modes. The load was Wood's metal arranged in a ring concentric with the center of the plate and

approximately ¼ in. in diameter. It was applied with several light strokes rather than one heavy one.

The activity of these plates increased to 0.7 ma or more, and subsequent temperature tests revealed that the frequency curves, as well as the activity curves, were much smoother.

In order to investigate further the effect of loading, several 10-Mc crystals were etched and loaded in approximately 1-kc steps. The crystals showed immediate improvement and continued to improve until lowered 6 kc by loading, after which further loading resulted in a slight loss in activity (fig. 1). Moreover, the crystals, which in the unloaded condition worked intermittently, oscillated throughout the temperature range; the fluctuations decreased in number and in size (fig. 2).

3.2. Flat Crystals

AT-cut plates, 0.6 by 0.5 in., of a lower frequency also were prepared and showed a favorable response to loading. The plates, whose frequencies were around 3,700 and 5,500 kc, had a very slight convex contour, less than 0.00001 in. They were etched in 5-kc steps and loaded back to the original frequency. The activity began to increase at once, and best results were attained with a load reducing the frequency 35 to 45 kc (fig. 3). Further loading resulted in a decrease in activity. Evidently the load had the same effect as contouring, that is, it created an area of low frequency in the center of the plate.

Several different patterns of loading were used. Best results were obtained when the major length of the load was parallel to the X-direction, although a circular pattern did give good results with concave crystals. Besides the circular pattern, an elliptical load, wide-band load, narrow-band load, and pinhead load were used (fig. 4). A narrow band applied parallel to the Z′-direction appeared to have a deleterious effect on the performance. The most favorable pattern appeared to be the elliptical one, although the wide-band load also improved the crystal to a large degree. The narrow-band load in the X-direction produced only a slight improvement, which never approached that of the elliptical or wide band. In general, it appeared that a load was most beneficial when its shape conformed to that of the active central area of the oscillator plate.

Interesting results were obtained with a pinhead size load. Initial application of load decreased the frequency as expected. However, after the crystal fundamental had been reduced about 0.2 percent, the frequency suddenly jumped to many kilocycles above the fundamental of the unloaded crystal. Explorations with a small probe electrode revealed that the plate was inert along a line through the center parallel to the X-axis, and that each half of the plate was oscillating. Lycopodium powder patterns further confirmed this.

Measurements were made on 0.6- by 0.5-in. AT-cut plates with the X-direction parallel to the long dimension. Their frequency was approximately 6,702 kc. Elliptical loads differing in length, but not width, were used. The plates were etched and then loaded back to their original frequency so as to maintain as closely as possible the original relationship between primary and secondary modes.

Associated with the general improvement of crystal unit there is, as expected, an increase in its Q, or quality factor. A crystal unit may be represented as a tuned circuit as shown in figure 5, where C_1 is the equivalent series (motional) capacity, R_s the series resistance, L_1 the equivalent series inductance, and C_t the total effective capacity shunting the series resonant circuit. The Q of this circuit may then be determined by the formula

$$Q \approx \frac{1}{4\pi \Delta f R_s C_t},$$

where $\Delta f = f_a - f_r$, the difference between the antiresonance and resonance of the crystal unit.

The loading of the crystal plate affected Δf and R_s very much but produced, at most, a negligible change in C_t. Both Δf and R_s tended to decrease at first, resulting in a rise in Q. At some loads, dips in the Q occurred, probably due to coupling between the fundamental and some other mode associated with the oscillator plate. However, the crystal unit Q was still several times the original one.

When the frequency change produced by the load reached approximately 1 percent of the fundamental, R_s began to increase, resulting in a drop in activity. However, the Q continued upward because Δf was still decreasing (fig. 6). Further loading caused the frequency to jump to a value several kilocycles above that of the unloaded plate (fig. 7). It appeared that the loaded area became so far off frequency that a thinner region farther from the center became active. In other words, this was just another case of the previously mentioned "pinhead jump."

The area of the load also had a definite effect on the Q. For a load one-third the length of the X-dimension and 0.3 the width of the Z′, the Q of the 6,702-kc plate rose steeply to a high value and remained high until shifted 65 kc. Attempts to shift 70 kc resulted in a frequency jump. For loads longer in the X-direction, the Q rose less steeply but heavier loads could be applied before the frequency jumped. In all cases, the Q's reached approximately the same maximum value. An increase in the width of a given load was accompanied by an increase in Δf, but its effect on R_s was unpredictable.

3.3. Off-Center Load

In order to determine the effect of placing the load off-center, 12 BT-cut plates were prepared at approximately 4,930 kc. These crystals were 0.6 by 0.5 in., with the X-axis parallel to the short dimension, and had a slight convexity. Areas ⅛, 3/16, or ¼ in. in diameter were then plated on both sides with gold

They were located as shown in figure 8. Contact was then made with the plating, so that the gold served as an electrode as well as a load. In order to map out the active area, a pencil point under moderate pressure was then moved from the edges toward the center until all oscillations ceased. The points in figure 8 show the position of the pencil when this occurred. The region within was considered the active area.

Two definite effects were noted. Although the electrodes were not over the center of the crystal and that region was therefore apparently outside the field created by the electrode, the central portion of the plate was still approximately in the center of the active area. However, the active area was shifted in that it also encompassed some of the region under the electrode and usually extended beyond it (fig. 8). The position of the load did not shift the region of activity in the central area very much, but did elongate the active area when placed off-center.

3.4. X-cuts

X-cut oscillator plates have their best performance characteristics if their contour is concave rather than convex. This type, which vibrates in an extensional (compressional) mode, is more difficult to excite into oscillation if the contour is flat or convex, that is, the resulting crystal units have low Q.

It therefore seemed logical that to obtain a good crystal by loading, the metal should be applied near the edges of the face rather than in the center, and the results justify this reasoning.

The plates were approximately $1\frac{15}{16}$ in. square and had a contour such that the corners were 0.0002 in. thicker than the center. They were mounted in an adjustable air-gap holder, and the air gap was adjusted for maximum activity.

Because of the contour, all of the plates had fairly good characteristics before loading. One unit, X–2, had an unloaded Q of approximately 100,000, but this was increased to approximately 262,000 by the additions of a load. The loaded area was a band $\frac{1}{4}$ in. wide along the edges, and the material was Wood's metal (fig. 9). Table 1 shows the resulting improvement in this unit. The small changes in C_0 are the result of varying the air gap to keep the activity at a maximum.

TABLE 1

Load	R_s	f_r	f_a	Δf	C_0	Q
mg	*Ohms*	*c/s*	*c/s*	*c/s*	*μμf*	
0	19	3,877,455	3,878,717	1,262	33.0	100,000
3.0	18	3,877,397	3,878,592	1,195	33.1	112,000
5.8	19	3,877,630	3,878,645	1,015	33.8	124,000
6.4	17	3,877,482	3,878,495	1,013	33.0	140,000
9.6	14	3,877,512	3,878,162	650	33.4	262,000

Slightly increasing the area by widening the load had the same effect as increasing the area of the load in the case of thickness-shear-mode plates. It resulted in an increase in Δf but had no predictable effect on R_s.

4. Summary

The effects of loading vary not only with the type and condition of the oscillator plate but also with the size, position, and mass of the load. The first effect, observed in heavily loaded flat thickness-shear-mode plates, is probably due to the establishment of a large resonance frequency differential between the center and edges, causing the lower frequency vibrations originating in the central regions to be almost completely attenuated (fig. 10). Because the secondary modes coupled to the fundamental are confined to the central region and are effectively reduced in amplitude, the peripheral area of the plate is unable to oscillate and remains relatively inert. This concentration of activity in the center isolates the vibrating quartz and the mount and prevents reflections of energy from the crystal edges.

The effect of loading observable in concave thickness-shear-mode plates and X-cut plates operating in an extensional mode parallel to the thickness appears also to be one primarily of dimensioning certain areas by loading. The load here serves the purpose of slightly changing the frequency of certain regions of the plate so that the distribution of like frequency areas over the plate as a whole is more favorable for oscillation. In concave plates this is accomplished by the addition of the load to the central regions. It appears that thickness-shear-mode crystals of this contour vibrate at a frequency above the optimum frequency of the plate as a whole because the central controlling area is the thinnest. The loading of the central area makes its frequency slightly lower, thereby establishing conditions more favorable for the plate as a whole. Flat or convex X-cut plates vibrating in extensional mode in the thickness direction are improved by the application of the load to the peripheral areas of the X faces. This improvement is possibly due to the surrounding quartz having a higher natural frequency than that of the central areas of the plate. Loading the outer areas tends to correct this condition by reducing the frequency of the higher frequency peripheral areas. This loading may be accomplished by applying a foreign material to the outer portions of the plate, as illustrated in figure 9, or by hollow grinding the edges, as shown in figure 11. In the latter case, the overhanging quartz may be thought of as constituting the load. This type of loading is more effective with plates of relatively low frequency.

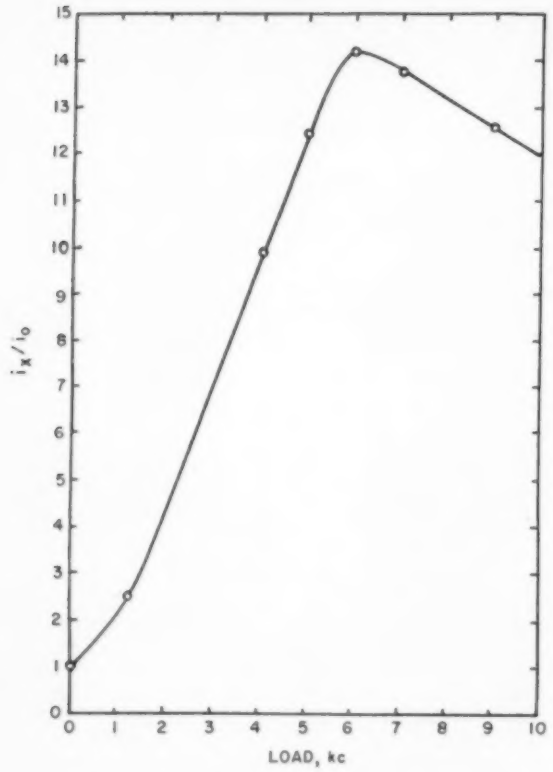

FIGURE 1. *Effect of load on the activity (rectified grid current) of a concave BT-cut oscillator plate.*

i_o is the average activity with no load, and i_x is the average activity with x-kc load.

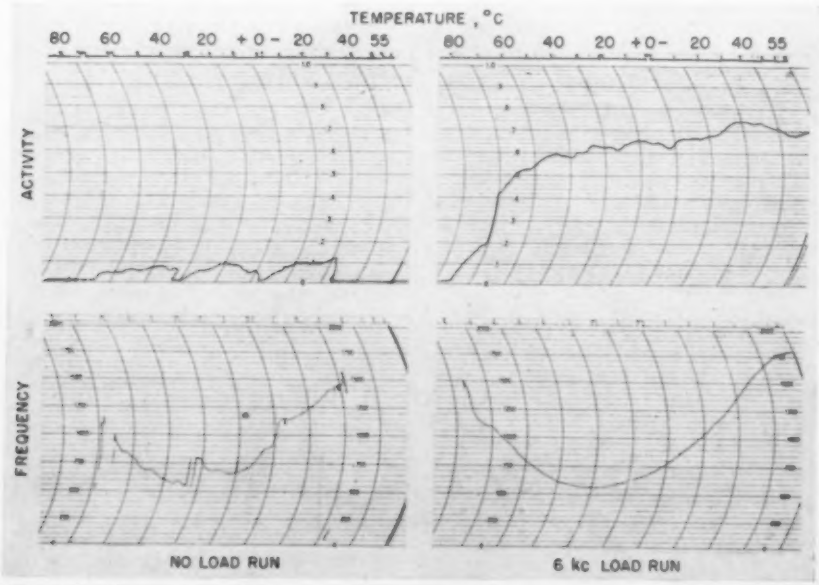

FIGURE 2. *Improvement of a concave BT-cut oscillator plate CC-8 as a result of loading.*

The dip near 70° in the loaded run is due to the melting of the Wood's metal.

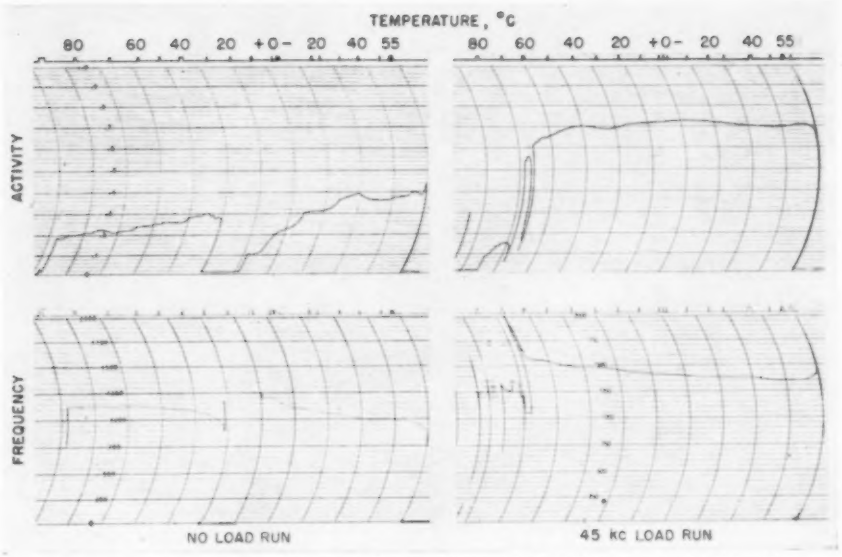

FIGURE 3. *Improvement of a flat AT-cut oscillator plate AT-2 as a result of loading.*
The dip near 70° in the loaded run is due to the melting of the Wood's metal.

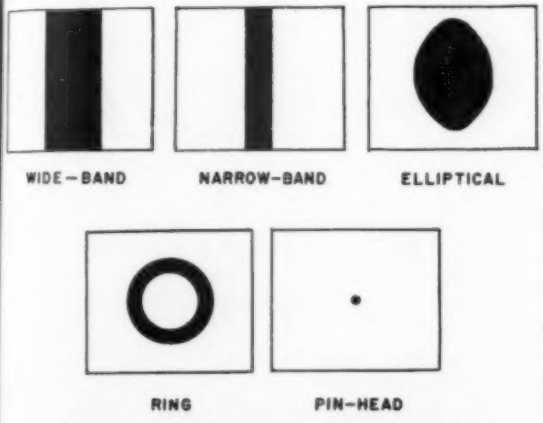

FIGURE 4. *Load patterns used in experiments.*

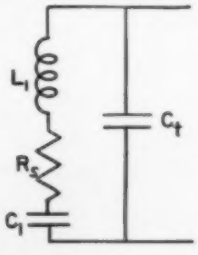

FIGURE 5. *Electrical equivalent circuit of a quartz-crystal oscillator plate.*

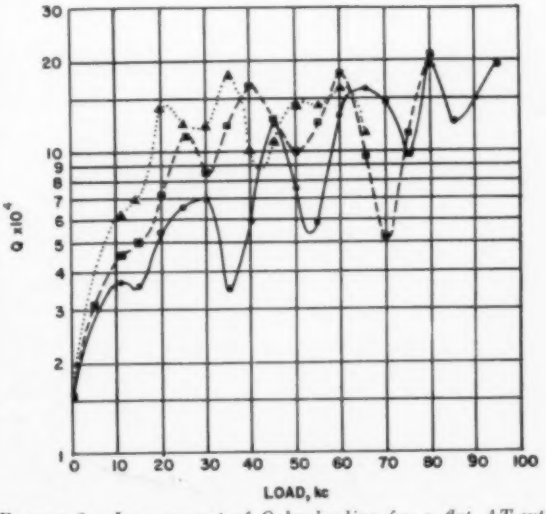

FIGURE 6. *Improvement of Q by loading for a flat AT-cut oscillator plate.*

....., Load ¼ length of X dimension.
— — —, Load ½ length of X dimension.
———, Load ¾ length of X dimension.
Width of all loads three-tenths width of oscillator plate.

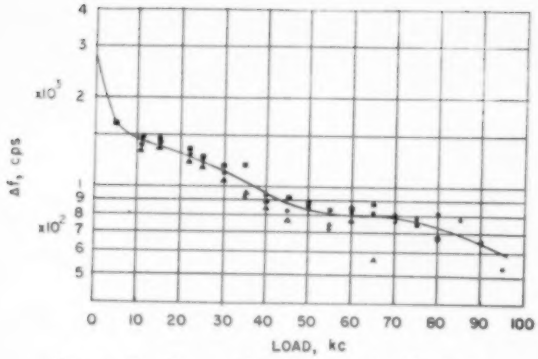

FIGURE 7. *Decrease in Δf as a result of loading.*

▲, Load ⅛ length of X dimension.
■, Load ½ length of X dimension.
●, Load ¾ length of X dimension.
Width of all loads three-tenths width of oscillator plate

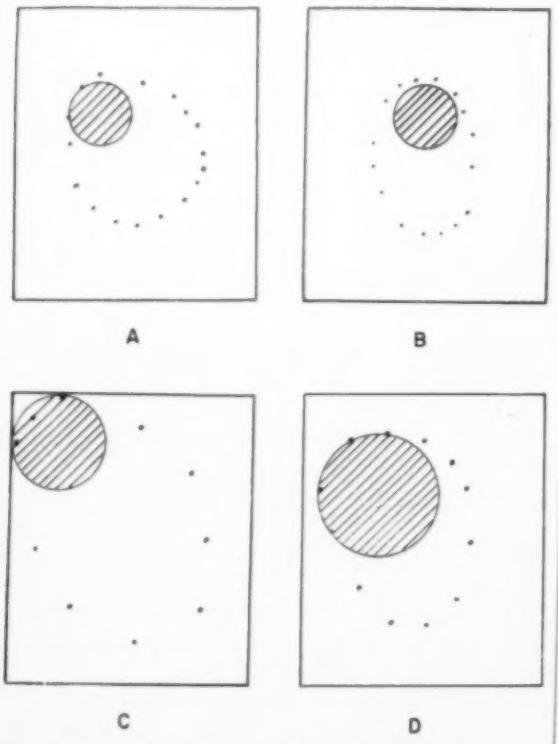

FIGURE 8. *Active area of crystal plates with off-centered electrodes.*

A, ⅛-in. electrode near to center in line with corner; B, ⅛-in. electrode tangent to center in middle of short dimension; C, 3/16-in. electrode in corner; D, ¼-in. electrode tangent to center in line with the corner.

FIGURE 9. *Load pattern used on X-cut plates.*

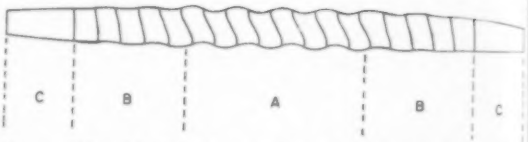

FIGURE 10. *Idealized drawing of the cross section of a convex thickness-shear plate illustrating the damping effect of contouring.*

Region A, active central area; B, damping area; C, inert quartz.

FIGURE 11. *X-cut plate with hollow-ground edges.*

WASHINGTON, June 17, 1952.

Journal of Research of the National Bureau of Standards Vol. 49, No. 5, November 1952 Research Paper 2369

Effects of Moderate Biaxial Stretch-Forming on Tensile and Crazing Properties of Acrylic Plastic Glazing[1]

B. M. Axilrod, M. A. Sherman, V. Cohen, and I. Wolock

The effects of biaxial stretch-forming to approximately 50-percent strain on the tensile and crazing properties of polymethyl methacrylate were investigated. The materials used were commercial cast polymethyl methacrylate sheets, nominally 0.15 in. thick, of both general-purpose and heat-resistant grades. Portions of the sheets were biaxially stretch-formed by means of a vacuum-forming vessel, which had been designed to produce flat uniformly stretched disks of 10-in. diameter. Specimens from the formed pieces, as well as from the unformed portions of the same sheets, were subjected to various tests, including standard tensile, stress-solvent crazing with benzene, long-time tensile loading, and accelerated weathering.

The results indicate that biaxially stretch-forming polymethyl methacrylate approximately 50 percent does not affect its tensile strength or secant modulus of elasticity in tension. However, the total elongation and the stress and strain at the onset of crazing in the short-time tests were greatly increased by the stretch-forming. The forming also increased the threshold stress of stress crazing about 40 percent for loading times up to 7 days and increased the threshold stress of stress-solvent crazing with benzene about 70 to 80 percent. It was observed in the long-time tensile tests that the crazing cracks were more closely spaced and finer on formed as compared to unformed specimens.

1. Introduction

Although polymethyl methacrylate glazing in aircraft is frequently prepared by a forming process that stretches the material, there is little information reported on the effect of this stretching on the tensile and crazing properties of the material. Some data of this type were obtained at Northrop Aircraft, Inc. [1].[2] Tensile tests were made on specimens taken from pieces of polymethyl methacrylate that had been stretched uniaxially. The pieces were stretched about 60 percent while at 129° C (265° F) and cooled while held at this elongation. It was found that at both room and subzero temperatures the specimens oriented transversely to the direction of stretch were appreciably weaker than the longitudinal specimens; also, at room temperature the latter specimens showed appreciable permanent set in contrast to the former.

The effects of hot stretch-forming on polystyrene, a material somewhat similar to polymethyl methacrylate in forming behavior, have been reported by Bailey [2]. It was found that uniaxial stretching of several hundred percent greatly increased the tensile strength, the elongation at failure, and the "crazing strength"[3] in the direction of stretch; the tensile strength was greatly reduced perpendicular to the direction of stretch. Also the tensile strength of sheets hot-stretched first longitudinally and then transversely roughly 200 percent was reported as greatly increased for both directions.

The experiments described in this report were made to gain more information on the effect of forming on the crazing and other properties of polymethyl methacrylate. The properties determined on both formed and unformed pieces of sheet material included tensile strength, total elongation, strain and stress at the onset of stress crazing, threshold stress for stress-solvent crazing, and resistance to weathering.

The major portion of the work was done on material stretched biaxially to an elongation of about 50 percent, that is, about 50 percent in all directions in the plane of the sheet. A few experiments were also made on pieces stretched slightly, about 7 to 20 percent. This work was carried out as one phase of a research program concerned with factors affecting the crazing and strength properties of laminated acrylic glazing.

2. Materials

The materials used were commercial cast polymethyl methacrylate sheets 0.12 to 0.15 in. in thickness. The samples used for all experiments except the exploratory work were obtained directly from the manufacturers and were masked on one side only, as is done for sheets used to make laminated acrylic glazing. These samples, which included both the general-purpose grade and the heat-resistant grade,[4] consisted of one 36- by 48- by 0.15-in. sheet from each of three production runs. They are referred to subsequently as "representative" samples and are identified as follows:

NBS sample	Material	Grade	Date received
L1d	Lucite HC201	General-purpose	Sept. 1949
L2d	Lucite HC202	Heat-resistant	Do.
P1a	Plexiglas I–A	General-purpose	Oct. 1949
P2a	Plexiglas II	Heat-resistant	Do.

[4] The two grades are defined in ASTM Specification D 702–46 for Cast Methacrylate Plastic Sheets, Rods, Tubes, Shapes.

[1] This investigation was conducted under the sponsorship of the National Advisory Committee for Aeronautics; this report is a condensation of NACA Technical Note TN2779.

[2] Figures in brackets indicate the literature references at the end of this paper.

[3] In reference [2] the test conditions were not indicated nor was it specified whether the "crazing strength" was a stress-crazing or a solvent-crazing threshold.

3. Apparatus and Procedure

3.1. Forming Process

a. Equipment and Procedure

A vacuum-forming apparatus that would produce flat biaxially stretched disks about 10 in. in diameter was designed according to suggestions offered by W. F. Bartoe of the Rohm & Haas Co.

A schematic diagram of the forming equipment is shown in figure 1. In this apparatus a sheet of acrylic material, A, heated to the rubbery state is clamped to the flange of the cylindrical forming vessel, B. A partial vacuum is created in the vessel by connecting the latter to an evacuated tank. The pressure differential is controlled by the plug valve, C, and the unclamped part of the sheet is drawn into the vessel. The form D, an open-ended cylindrical tube a little smaller in diameter than the forming vessel and constrained by the guide E, is inserted into the vessel. The pressure differential is then removed quickly by admitting air through the plug valve, F, so that the stretched acrylic sheet shrinks about the end of the form. The sheet cannot retract completely; the central portion remains uniformly stretched across the open end of the form. The formed acrylic sheet, shaped like a top hat, is cooled to room temperature in the vessel before removal.

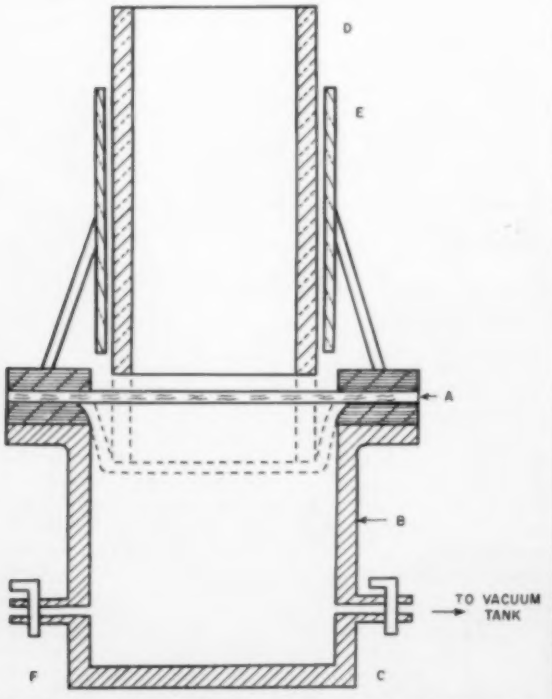

FIGURE 1. *Schematic drawing of vacuum-forming apparatus.*

A, Plastic sheet to be formed; B, forming vessel; C, valve to evacuated tank; D, form; E, guide; F, valve to atmosphere.

In practice, the forming operation is done as quickly as possible so that the acrylic sheet will still be in the rubbery state when the pressure differential is removed; the time from removal of the sheet from the oven until forming is complete is less than 1 min. The forming apparatus, assembled for the drawing of a sheet and disassembled for the removal of a drawn sheet, is shown in figures 2 and 3, respectively.

b. Uniformity of Forming and Equation for Elongation

To determine whether the amount of stretching is uniform over the face of the biaxially stretched pieces, the following experiments were made: A 10-in. disk of Lucite HC201, which had been biaxially stretched 150 percent after heating to 140° C, was marked off in 1-in. squares, then heated to 140° C and allowed to assume its original size. The lines on the resulting disk were still equidistant within ± 5 percent, the standard deviation of the measurement and marking errors, indicating that the amount of stretching was reasonably uniform over the face of the disk. Next, another piece of Lucite HC201 was marked with a square grid having a spacing of 15 mm; the piece was then biaxially hot-stretched to an elongation of 150 percent. The lines on the flat top of the stretched dome were still equidistant to within ± 5 percent, verifying that the stretching was reasonably uniform.

The formula used for calculating the amount of biaxial stretching in a formed disk is

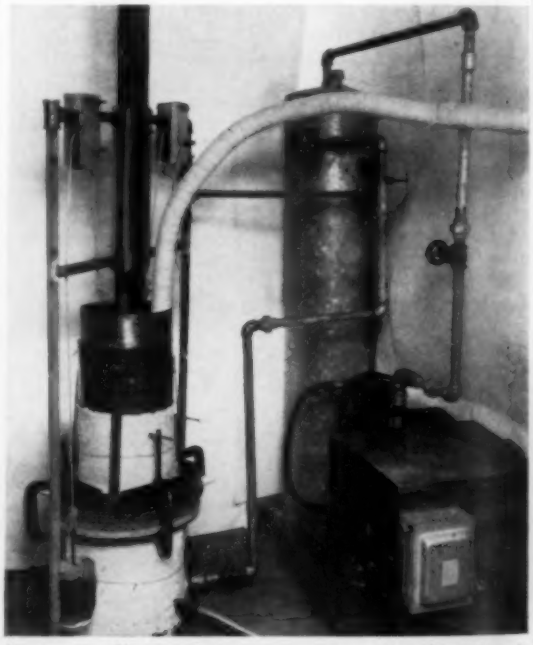

FIGURE 2. *Vacuum-forming apparatus with a sheet of acrylic plastic in place ready to be formed.*

$$e = 100(\sqrt{t_i/t_f} - 1), \quad (1)$$

where e is the elongation in percent, and t_i and t_f are the initial and final thicknesses, respectively. This formula is based on the fact that the volume of the material remains essentially constant on stretching. This property of the materials was verified by measuring the density of a small piece of both 160-percent-formed and unformed material from each of the four samples. The sample of Lucite HC201 showed a decrease in density of 0.8 percent as a result of forming to 160-percent strain. The other three samples showed density changes of less than 0.2 percent as a result of this amount of stretch-forming.

3.2. Standard Tensile Test

The standard tensile tests were made in most details in accordance with Method 1011 of Federal Specification L–P–406a. In these tests the threshold of stress crazing was noted visually by an observer who immediately applied a sudden momentary pressure to the sensitive cross head of the testing machine to cause a jog in the load-extension record drawn by the autographic recorder. The strain and the stress at this threshold could thus be readily obtained from the record. The observer viewed the crazing against a dark background, using north daylight or fluorescent light.

FIGURE 3. *Vacuum-forming apparatus partly disassembled after forming a sheet of acrylic plastic.*
The formed piece is on the end of the form which is held by the operator.

3.3. Stress-Solvent Crazing Test

In the stress-solvent crazing tests, tapered tensile specimens of the same dimensions as the long-time tensile test specimens described in section 3.4 were placed under load in a hydraulic testing machine, benzene applied, and the load maintained for 4 min. From preliminary trials on other specimens, the loads on these specimens were selected to produce crazing over a part of the tapered portion. The two specimens of each formed or control piece were tested with slightly different loads in an effort to locate the threshold at different parts of the tapered portion of the specimen.

Benzene was applied to the central ¼- by 3-in. portion of the specimen with a brush. Subsequently the solvent-crazed specimens were examined under suitable lighting and the extent of the crazing noted.

3.4. Long-Time Tensile Test

The long-time tensile-loading cabinet for testing at high relative humidity (about 95 percent) is shown in figures 4 and 5. A similar cabinet without a front cover or blower and with an interior instead of exterior light was used for tests at 50-percent relative humidity, the condition in the controlled atmosphere room in which the cabinets were located.

In each cabinet four specimens can be tested simultaneously. The load on the specimen is applied by a 300-lb-capacity weigh beam through a turnbuckle. A pair of alinement holes in each end of the specimen and an alinement hole and an alinement pin in the clamp, as shown on the specimen at the left of figure 4, facilitate alining the clamps and specimen. The specimen alinement must be done very carefully, as otherwise stress crazing occurs much sooner on one face than on the other or along one edge rather than across the width of the specimen.

The humidity cabinet (fig. 4) has a blower that directs air against cloth wicks dipping into a tray of water. The relative humidity is readily measured

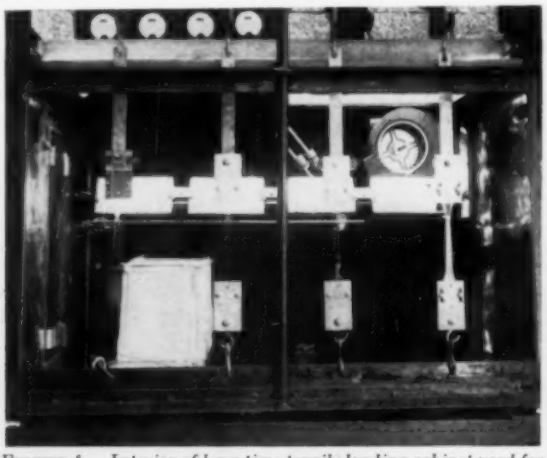

FIGURE 4. *Interior of long-time tensile loading cabinet used for testing at high relative humidity.*

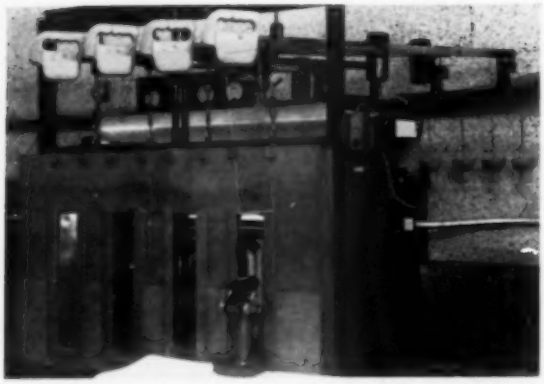

FIGURE 5. *Exterior of long-time tensile loading cabinet for testing at high relative humidity.*

The front of the cabinet is in place and a Brinell microscope on an adjustable stand is inserted in the right-hand window for examining the crazing of a specimen.

with wet- and dry-bulb thermometers placed near the exhaust part of the blower. The relative humidity is maintained at 95 ± 2 percent.

To avoid heating of the cabinet, the fluorescent lights used for observing crazing are placed just outside a window in the top of the box. Mirrors, mounted behind and slightly above the specimens, direct the light against the latter, which are viewed against a black-felt background.

The tensile specimen used for the long-time loading tests has a 3-in.-long reduced section tapering uniformly in width from 0.50 in. at the maximum cross section to 0.33 in. at the minimum. In this way the stress in the reduced section decreases from a value of S_0 at the minimum section to 2/3 S_0 at the other end. The time for the onset of crazing for different stresses is found by observing the specimen periodically and noting the extent of the crazing. Some of the details of the test procedure are as follows. The specimens being tested were observed with the unaided eye, and, in addition, in the tests on the representative samples nearly all specimens were also observed with a 20-power Brinell microscope (fig. 5). Observations of the extent and nature of crazing were made several times on the first day the load was applied, then generally daily through the fifth day, and once on the eighth day, after which the load was removed. The extent of the crazing from the minimum cross section was measured with a paper scale to the nearest millimeter; this corresponds to an accuracy of better than one percent when converted to stress. The observed data on the extent of the crazing were converted into stress values and the latter were plotted against log time.

3.5. Accelerated Weathering Test

The accelerated weathering test employed was the sunlamp-fog chamber type. This test was made in accordance with Method 6021, Federal Specification L–P–406a, except that it was carried out for 480 h instead of 240 hr, the recommended time.

Light-transmission and haze measurements were taken before and after the weathering test, using a pivotable-sphere hazemeter, following the procedure in ASTM Method D 1003–49T.

To permit the measurement of shrinkage, scratches were ruled on each specimen about 2 in. apart before the weathering. The scratches were measured with a steel rule graduated to hundredths of an inch. In measuring the distance between scratches a seven-power magnifier was used, the distance being estimated to a thousandth of an inch.

3.6. Degree of Forming of Representative Samples

Exploratory tests were made with pieces of acrylic plastic sheet biaxially stretched slightly, 7- to 20 percent elongation, and moderately, about 45 percent. The latter elongation is an amount that may be attained at some locations in formed aircraft enclosures [3,4].[5] The results of tensile and stress-solvent crazing tests indicated that the crazing properties, such as threshold of stress crazing in the standard tensile test and threshold stress for stress-solvent crazing, were unaffected or only very slightly affected by biaxial stretching 7 to 20 percent. However, for the 45-percent-stretched piece, the crazing properties were considerably changed; for example, the threshold stress for stress-solvent crazing appeared to increase about 50 percent.[6] Accordingly, it was decided to form pieces from each sheet of the representative samples to an elongation of approximately 50 percent.

One piece was formed from each sheet. The piece to be formed was heated in an oven to a temperature of 120° or 140° C, depending on whether the material was general-purpose or heat-resistant grade. Four standard tensile and four tapered tensile specimens and an accelerated weathering specimen were taken from each disk. An equal number of control specimens were cut out of each sheet from a location adjacent to the piece used for forming.

While it was desired to obtain the same amount of stretch to within about 5 percent on the three formed pieces of a sample, the actual variation in elongation between disks was greater than this amount, except for sample P1a. The values for individual disks, based on the formula, eq 1, are as follows:

NBS sample	Biaxial stretch of the three disks	NBS sample	Biaxial stretch of the three disks
	Percent		*Percent*
L1d	48, 56, 57	P1a	57, 58, 61
L2d	49, 54, 69	P2a	44, 50, 56

[5] In these references the reduction in thickness was reported, not the elongation; the elongations were calculated by using eq (1).

[6] It was interesting to note that the elongation at failure was increased to the order of about 20 percent by the slight stretching.

TABLE 1. *Tensile properties of polymethyl methacrylate formed by biaxial stretching* [a]

Material	NBS sample	Biaxial stretch [b]	Tensile strength, S_m	Elongation	Secant modulus [f]	Stress and strain at threshold of crazing		
						Stress, S_r	$\frac{S_r}{S_m}$	Strain
Unformed								
		Percent	*lb/in.²*	*Percent*	*lb/in.²*	*lb/in.²*		*Percent*
Lucite HC201	L1d	------	7,850 ±80	[c] 8.8 ±1.2	3.63 ±.05	6,780 ±140	86	2.4 ±.15
Lucite HC202	L2d	------	9,580 ±100	14 ±3	4.00 ±.03	8,380 ±180	88	2.9 ±.3
Plexiglas I-A	P1a	------	7,920 ±50	19 ±7	3.75 ±.01	7,170 ±100	91	2.6 ±.1
Plexiglas II	P2a	------	10,070 ±170	[d] 7.6 ±0.4	4.06 ±.09	9,080 ±180	90	3.2 ±.1
Formed								
Lucite HC201	L1d	54	7,830 ±130	[e] 73 ±3	3.60 ±.05	.....	--	Very light crazing; two specimens crazed at 4 and 6.5 percent, respectively, others at hand marks at >10-percent strain.
Lucite HC202	L2d	57	9,650 ±140	59 ±4	4.01 ±.05	.....	--	Three specimens did not craze. Very light crazing on two specimens at ~7 percent, on one at >10-percent strain.
Plexiglas I-A	P1a	59	8,030 ±90	67 ±4	3.73 ±.05	.....	--	Four specimens did not craze. Possible very faint crazing on two specimens.
Plexiglas II	P2a	50	9,930 ±80	49 ±3	4.04 ±.01	.....	--	Three specimens did not craze. Very light crazing on others at hand marks at >10-percent strain.

[a] The tests were made on standard tensile specimens, Federal Specification L-P-406a, Method 1011, Type I. The testing machine used was a 2,400-lb-capacity hydraulic universal testing machine. Autographic load-elongation records were obtained with a nonaveraging Southwark-Peters extensometer, model PS-6, coupled to the associated recorder on the testing machine. The testing speed was 0.05 in./min up to 10-percent strain; the strain gage was removed at this point and the speed increased to 0.25 in./min with further extension measured with dividers. The testing was done at 23° C and 50-percent relative humidity after conditioning the specimens 2 weeks in this atmosphere. All results are the average for six specimens, two specimens from each sheet, unless otherwise noted, plus or minus the standard error. The standard error was calculated taking into account the possible existence of sheet-to-sheet variations.

[b] Average for three disks.

[c] One specimen failed at knife edge, at 5.1-percent elongation.

[d] Two specimens failed at knife edges, at 4.4- and 9-percent elongation, respectively.

[e] Two specimens failed at knife-edge marks, each at 77-percent elongation.

[f] The stress range used for the calculation of the secant modulus was 0 to 4,000 lb/in.² for the Lucite HC201 and Plexiglas I-A and 0 to 5,000 lb/in.² for the Lucite HC202 and Plexiglas II.

4. Results and Discussion

4.1. Standard Tensile Tests

The results of the standard tensile tests on the formed and the unformed portions of the four representative samples are shown in table 1. Figure 6 illustrates the appearance of the fractures on broken specimens of formed and unformed material.

The tensile strength and secant modulus of elasticity of the four samples of polymethyl methacrylate were unaffected by stretch-forming to about 50-percent elongation. The elongation at failure, as in the exploratory tests, was greatly increased by forming from approximately 10 percent to about 60 percent.

The strain at the threshold of crazing also was increased greatly as a result of the forming. In fact, for samples L2d, P1a, and P2a, at least half of the specimens showed no stress-crazing up to rupture. Crazing on other specimens was very light or was observed only at accidental finger marks.

b. Discussion of Fracture Behavior

It is of interest to consider the fracture behavior and the fracture mechanism in the formed and unformed material. First it was noted that while the specimens of the unformed material commonly failed at 5- to 10-percent elongation with the fracture approximately flat and normal to the tensile load line, as shown by A in figure 6, occasionally a specimen exhibited a much greater elongation, sometimes accompanied by an oblique fracture (B in fig. 6).

Next, it was observed that the formed specimens, as shown in figure 6 (C, D, E, F), had a laminar fracture. The laminar fracture of formed material indicates that the segments of the polymer molecules have a preferred orientation in the plane of the sheet, thus favoring fracture propagation on planes nearly parallel to the plane of the sheet. In the unformed material the segments of the polymer molecule are assumed to be randomly oriented.

Although it is not readily seen from figure 6, on the fracture surface of each specimen there was a small mirror-like area oriented perpendicularly

FIGURE 6. *Effect of biaxial stretch-forming to about 50 percent elongation on the fracture of tensile specimens*

A, Sample P2a, not formed, total elongation 6 percent; B, sample P1a, not formed, total elongation 54 percent; C, sample L1d, formed 57 percent, total elongation 77 percent; D, sample P1a, formed 58 percent, total elongation 57 percent; E, sample L2d, formed 49 percent, total elongation 52 percent; F, sample P2a, formed 55 percent, total elongation 40 percent.

to the tensile load line. On specimens of unformed material, the mirror area was diffusely bounded; on the formed, the boundary was sharp. The mirror-like surface was of the order of a few square millimeters in area and was found extending inward from the boundary of a cross section.

On unformed material this area was located at the corner of the cross section for most of the specimens; in the other instances, it was found either extending inward from the cast edge or from the machined edge. At corner locations the mirror was roughly a quadrant of a circle, and at the edges it was semicircular.

On specimens of formed material the mirror area was located at a corner on almost all of the specimens. However, on the other specimens the mirrors were located only at the machined edge. At corner locations the mirror area was almost a right triangle with the hypotenuse a convex curve instead of a straight line; the area extended much farther along the cast edge than along the machined edge. When located on a machined edge, the mirror area appeared to be somewhat less than a semiellipse, with the major axis normal to the edge. In testing a formed specimen, usually some edge cracks appeared normal to the edge after the material had been strained considerably. These cracks became larger as the specimen was stretched further, and at failure the fracture appeared to go through one of them. In figure 6 two such cracks are evident on the left edge of specimen C just above the identifying letter. Such cracks reflect light similarly to large crazing cracks, indicating a mirror-like surface. Also, the large edge cracks extend farther in the direction of the cast surface than in the thickness direction, as in the cases of the mirror areas on the fracture surface. For this reason it is quite plausible to expect the fracture in specimens of the formed material to start at such edge cracks.[7]

From the fracture behavior of specimens of unformed material, discussed below, it is logical to suppose that the fracture in such material also begins in the mirror area and that in this material this area is an extension of a crazing crack.

The experimental evidence, that suggested that the fracture started at the mirror area is as follows: The fractures were examined on a large number of unformed tensile specimens which were solvent-crazed and then broken. The tensile tests were done in connection with another phase of this investigation on crazing [5]. The specimens, of the standard tensile type, were wetted with benzene while under a load; the solvent was applied to the central ¼- by 2-in. portion of one face of the reduced part of the specimen. On all the specimens inspected it was noted that a semicircular mirror-like area was present on the fracture surface; this area was located with its center at or near the solvent-crazed surface. It is plausible to suppose that this mirror area is an extension of a solvent-craze crack, and hence that fracture is initiated at such a crack. This hypothesis was strengthened by comparing the location of the fractures on a number of these specimens with photographs of the solvent-crazed specimens taken prior to breaking. In all cases, the fracture was found to pass through a crazing crack. Visual evidence to justify further this supposition was obtained in a different portion of the investigation, to be described in detail in a separate report. In the latter work, experiments were made on several different cast polymethyl methacrylate sheets of viscosity average molecular weights ranging from 90,000 to 3,000,000. In stress-solvent crazing tests on low-molecular-weight material, one or a few large crazing cracks developed, and the specimens were seen to fail by the rapid growth of one craze crack. It should be noted that solvent crazing reduces the tensile strength of the specimens [5].

Because the evidence on the solvent-crazed specimens strongly suggests fracture propagating outward from the mirror area that originates at a crazing crack, and because similar mirror areas extending in from the edge are found in standard tensile specimens that are not solvent-crazed, it seems reasonable to conclude, as previously noted, that failure begins at the surface of the specimen and that the mechanisms of fracture and crazing are closely related. Indeed, one might go further and say that in the specimens of unformed material that are not solvent-crazed the fracture first starts at a stress-crazing crack. In the formed specimens, which frequently do not exhibit stress crazing, the fracture of the specimens is delayed, that is, occurs at a much higher strain than in the unformed material. Furthermore, the true stress is probably higher at or near failure in the formed material than in the unformed as was actually found in a few tests.[8]

The difference in appearance between the mirror part of the fracture surface and the rougher portion may be associated with a low velocity of fracture propagation at the former and a higher velocity in the rougher portion. Such an explanation of the fracture behavior of glass is discussed by Morey [6] in his monograph on glass.

The fact that on the broken specimens of formed material the mirror area had a smaller dimension in the direction perpendicular to than parallel to the plane of the sheet, or laminas, suggests that the rate of crack growth, and perhaps the subsequent high-speed fracture, too, is slower across the laminas than parallel to them.

Hsiao and Sauer [7], who studied crazing in specimens of polystyrene, present a different picture of the relation between crazing and fracture. They conclude that "the fracture cracks of the material are not the same as crazing cracks and that the

[7] In this report these edge cracks have somewhat arbitrarily been considered as distinct from crazing cracks; also any fine crazing on machined edges was disregarded. The reason is that such edge cracks and crazing are dependent on the machining of the specimens, and could possibly be minimized or caused to begin at higher strains by varying the machining technique or by properly annealing the specimens.

[8] In the exploratory work with specimens of a disk biaxially stretched to 45-percent elongation, the load-elongation graph was taken out to 50-percent strain with a low-magnification recording strain gage. After the maximum load was attained, at about 4-percent strain, the load declined with increasing strain to about four-fifths of its maximum value and then remained almost constant out to 50-percent strain, the limit of elongation of the strain gage; at this point the load was increasing slowly. As the volume of the material remains practically constant in the plastic range, the reduced cross-sectional area can be calculated from the strain and the true stress then derived. It was found that the true stress at 50-percent strain was about 10 percent greater than at the maximum load.

source of fracture is usually some flaw in the material and not one of the crazing openings." However, it would seem reasonable to expect that, since the crazing crack produces a stress concentration at its apex, the subsequent fracture would be initiated at the apex of the crack. A microscopic examination of the fracture surfaces, such as carried out by Kies and coworkers [8] on several materials, is planned; this study may clarify the situation.

4.2. Stress-Solvent Crazing Tests

The threshold stress data for the stress-solvent crazing tests on the 50-percent biaxially stretched disks are shown in table 2. Typical specimens are shown in figure 7. The threshold was determined visually, using two criteria. For the first, called criterion A, the threshold was taken as the maximum stress below which there was no regular distribution of crazing cracks visible to the unaided eye, the isolated cracks being disregarded. This was the same criterion used in the exploratory tests. For the second, criterion B, the threshold stress was taken as the maximum stress below which no crazing cracks were visible to the unaided eye.

As might be expected, the average threshold crazing stress obtained by criterion B is slightly less than by criterion A. The principal results as obtained by the two methods are in agreement, however, and are as follows:

The average threshold crazing stress for general-purpose grade polymethyl methacrylate, crazed with benzene by the procedure described previously, is about 2,000 lb/in.^{2} for unformed, and about 3,400 to 3,800 lb/in.^{2} for the 50-percent biaxially stretched sheets. The corresponding values for the heat-resistant grade are about 3,000 lb/in.^{2} and 5,000 to 6,000 lb/in.^{2}, respectively. This represents an improvement of from 70 to 80 percent for each grade.

Not only did the formed specimens exhibit higher threshold stresses than the unformed, but also there was a tendency for the crazing cracks to be somewhat finer and more closely spaced on the formed specimens.

4.3. Long-Time Tensile Test

a. Threshold stress-crazing data

Values of threshold stress for stress crazing at 1, 10, and 100 hr, derived from plots of threshold stress versus log time, are given in table 3.

The plots of threshold-crazing stress versus log time were in general approximately linear. For most specimens the extent of crazing was recorded separately for each face of the specimen, because the crazing often progressed more rapidly on one face than on the other. An examination of the plotted data showed no consistent behavior of the masked relative to the unmasked face.[9] Any consistent difference in the extent of crazing on the two faces was accordingly assumed to be caused by a slight misalinement of the specimen. In such cases a single straight line was fitted to the data for the two faces, and the values in table 3 were taken from this line.

The slopes of the threshold stress versus log time plots appeared to be about the same for all materials and test conditions. The effect of such factors as forming, relative humidity, sample, and grade on the threshold stress is indicated best by examining the 100-hr unaided-eye values, as these are the most numerous and precise. These values, taken from table 3, together with values of the ratio of the threshold stresses, S_c, for the formed and unformed specimens of each sample are listed in table 4. These data indicate that forming to a biaxial strain of about 50 percent increases the threshold-crazing

[9] In the experiments described in [5], in which the loss of strength was determined as a result of stress-solvent crazing, no effect of the masking paper was detected.

TABLE 2. *Threshold crazing stresses for stress-solvent crazed specimens of polymethyl methacrylate formed by biaxial stretching* [a]

NBS sample	Material	Biaxial stretch [b]	Threshold crazing stress [c], S_c		Range of S_s, the maximum stress applied, for the set of specimens
			Criterion A [d]	Criterion B [d]	
Unformed					
		Percent	*lb/in.*^{2}	*lb/in.*^{2}	*lb/in.*^{2}
L1d	Lucite HC201		2,110± 40	2,000± 50	2,700 to 3,000
L2d	Lucite HC202		[e] >3,020± 40	[e] >2,820±190	3,000 to 3,600
P1a	Plexiglas I–A		2,300±150	2,120±120	2,400 to 3,000
P2a	Plexiglas II		3,270±140	3,120±160	3,900 to 4,500
Formed					
L1d	Lucite HC201	54	[f] >3,390±150	[f] >3,310±130	3,000 to 4,500
L2d	Lucite HC202	57	[e] >5,550±280	[e] >5,130±380	5,600 to 6,900
P1a	Plexiglas I–A	59	3,890±310	3,690±310	4,200 to 5,400
P2a	Plexiglas II	50	[e] >5,720± 90	[e] >5,590±110	6,000 to 7,200

[a] A controlled amount of benzene, 0.03 to 0.04 g, was applied to a No. 1 camel's hair brush (about 0.1 in. in diameter and 0.5 in. long) from a marked glass dropper; then the central ¼- by 3-in. portion of one face of the tapered tensile specimen, which was under load, was stroked with the brush. The specimens were under load for 4 min, and then were removed from the testing machine; after 4 to 6 days, they were examined for crazing thresholds. The crazing was done in a controlled atmosphere room operating at a temperature of 23° C and 50 percent relative humidity, after conditioning the specimens for 1 week in this atmosphere.

[b] Average for 3 formed disks, 1 from each sheet of the sample.

[c] Each value is the average plus or minus the standard error for 6 specimens with 2 specimens from each sheet. The standard error was calculated taking into account the possible existence of sheet-to-sheet variation.

[d] Criterion A: That point below which there is no regular distribution of crazing cracks visible with the unaided eye; isolated cracks are disregarded.
Criterion B: That point below which no crazing cracks were visible to the unaided eye.

[e] One specimen did not craze under the load applied.

[f] Two specimens did not craze under the loads applied.

TABLE 3. *Variation with time of threshold stress for stress crazing polymethyl methacrylate formed by biaxial stretching* [a]

NBS sample	Treatment [b]	Sheet	Biaxial stretch	Stress range in reduced section of specimen	Threshold stress for the following relative humidities and times [c]											
					50-percent relative humidity [d]						95-percent relative humidity [d]					
					1 hr		10 hr		100 hr		1 hr		10 hr		100 hr	
					Unaided eye	Microscope [e]	Unaided eye	Microscope	Unaided eye	Microscope	Unaided eye	Microscope	Unaided eye	Microscope	Unaided eye	Microscope
			Percent	*lb/in.²*	*lb/in.²*	*lb/in.²*	*lb/in.²*	*lb/in.²*	*lb/in.²*	*lb/in.²*	*lb/in.²*	*lb/in.²*	*lb/in.²*	*lb/in.²*	*lb/in.²*	*lb/in.²*
L1d	F	1	48	3,750 to 2,500	>3, 750	.....	>3, 750	.....	3, 700	.....	>3, 750	.....	3, 500	.....	3, 200	.....
		2	56	3,750 to 2,500	>3, 750	.....	>3, 750	.....	[f] (3, 800)	.....	>3, 750	.....	>3, 750	.....	3, 500	.....
				Average	>3, 750		>3, 750		3, 750		>3, 750		>3, 620		3, 350	
	U	1	.....	3,750 to 2,500	3, 700	.....	3, 000	.....	(2, 300)	.....	.....	2, 800	(ca 2, 600)	.....	<2, 500	.....
		2	.....	3,750 to 2,500	3, 900	.....	3, 200	.....	2, 600	.....	(3, 100)	.....	2, 800	.....	2, 500	.....
				Average	3, 800		3, 100		2, 450		.....	.....	2, 700		<2, 500	
L2d	F	1	49	6,000 to 4,000	>6, 000	>6, 000	(5, 900)	(6, 000)	5, 100	5, 100	.....	.....	.....	.....	.....	.....
		3	54	6,000 to 4,000	>6, 000	>6, 000	ca 6, 000	ca 6, 000	ca 5, 900	ca 5, 900	>6, 000	>6, 000	(6, 200)	(>6, 000)	5, 000	5, 100
				Average	>6, 000	>6, 000	6, 000	6, 000	5, 500	5, 500	.....	.....	.....	.....	.....	.....
	U	1	----	5,000 to 3,330	ca 4, 000	.....	ca 3, 500	.....	ca 3, 200	<3, 300	ca 5, 000	.....	3, 800	3, 800	3, 300	3, 500
		3	----	5,000 to 3,330	(5, 000)	.....	4, 200	.....	3, 400	3, 500	.....	.....	4, 300	.....	3, 500	.....
				Average	4, 500		3, 850		3, 300	<3, 400	.....		4, 050	.....	3, 400	.....
P1a	F	1	57	4,000 to 2,670	>4, 000	>4, 000	>4, 000	>4, 000	>4, 000	>4, 000	>4, 000	>4, 000	>4, 000	>4, 000	>4, 000	>4, 000
		2	61	4,000 to 2,670	>4, 000	>4, 000	>4, 000	>4, 000	>4, 000	>4, 000	>4, 000	>4, 000	>4, 000	>4, 000	>4, 000	>4, 000
				Average	>4, 000	>4, 000	>4, 000	>4, 000	>4, 000	>4, 000	>4, 000	>4, 000	>4, 000	>4, 000	>4, 000	>4, 000
	U	1	----	4,000 to 2,670	>4, 000	>4, 000	3, 900	3, 500	2, 800	2, 800	(4, 400)	(4, 400)	3, 600	3, 600	2, 800	2, 800
		2	----	4,000 to 2,670	>4, 000	>4, 000	3, 800	3, 900	3, 300	3, 200	>4, 000	>4, 000	(3, 800)	(4, 000)	2, 900	2, 900
				Average	>4, 000	>4, 000	3, 850	3, 700	3, 050	3, 000	>4, 200	>4, 200	3, 700	3, 800	2, 850	2, 850
P2a	F	1	44	6,000 to 4,000	>6, 000	>6, 000	>6, 000	>6, 000	5, 700	5, 500	>6, 000	6, 000	(>6, 000)	(>6, 000)	5, 300	5, 300
		2	50	6,000 to 4,000	>6, 000	>6, 000	>6, 000	>6, 000	5, 800	5, 800	>6, 000	>6, 000	>6, 000	>6, 000	6, 000	[g] 6, 000
				Average	>6, 000	>6, 000	>6, 000	>6, 000	5, 750	5, 650	>6, 000	>6, 000	>6, 000	>6, 000	5, 650	5, 650
	U	1	----	5,000 to 3,330	.....	(4, 500)	.....	4, 000	3, 900	3, 500	>5, 000	>5, 000	4, 700	(4, 600)	4, 300	4, 100
		2	----	5,000 to 3,330	(5, 300)	>5, 000	4, 700	4, 600	4, 100	4, 000	>5, 000	>5, 000	4, 600	4, 400	4, 000	4, 000
				Average	.....	>4, 750	.....	4, 300	4, 000	3, 750	>5, 000	>5, 000	4, 650	4, 500	4, 150	4, 050

[a] Data obtained visually on tensile specimens having a reduced section about 3 in. long and tapering uniformly in width from 0.33 to 0.50 in. The specimens were subjected to dead loading in a long-time loading apparatus. The tests were made at 23° C.

[b] F, Formed; U, unformed.

[c] Values are for individual specimens.

[d] Specimens tested at 50-percent relative humidity were conditioned at 50-percent relative humidity for at least 2 weeks prior to testing. Specimens tested at 95-percent relative humidity were conditioned at 95-percent relative humidity for 1 week prior to testing.

[e] 20× Brinell microscope.

[f] Values in parentheses were extrapolated.

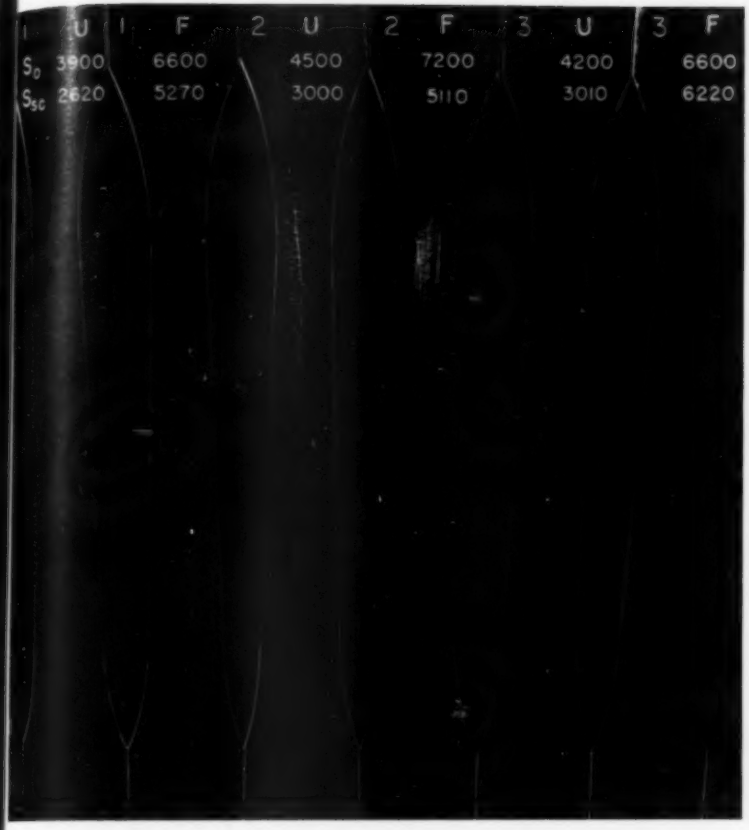

FIGURE 7. *Specimens of formed and of unformed portions of sample P2a, after stress-solvent crazing with benzene.*

The number on the top line designates the sheet from which the specimen was taken. U is unformed and F is formed material. S_0 is the stress in pounds per square inch at the minimum cross section of the specimen. S_{sc} is the threshold crazing stress according to criterion B.

stress of all samples about 40 to 50 percent. From table 4 it is also evident that the threshold stress is about 30 to 50 percent higher for the heat-resistant than for the general-purpose-grade samples. The data are not precise enough to determine with certainty any difference in threshold-crazing stress due to relative humidity or to material of a given grade.

b. Appearance of Specimens

Figure 8, taken near the end of the testing period, illustrates the appearance of the long-time tensile-loading specimens. The specimens were photographed while under load as the finest crazing cracks usually were not visible on removal of the load as noted by other workers.

TABLE 4. *Threshold-crazing stresses of polymethyl methacrylate samples after 100 hours under load* [a]

NBS sample	S_c at 50-percent relative humidity [b]			S_c at 95-percent relative humidity [b]		
	Formed (F)	Unformed (U)	$\frac{(S_c)_F}{(S_c)_U}$	Formed (F)	Unformed (U)	$\frac{(S_c)_F}{(S_c)_U}$
	lb/in.²	*lb/in.²*		*lb/in.²*	*lb/in.²*	
L1d	3,750	2,450	1.53	3,350	<2,500	>1.34
P1a	>4,000	3,050	>1.31	>4,000	2,850	>1.40
L2d	5,500	3,300	1.67	[c] 5,000	3,400	1.47
P2a	5,750	4,000	1.44	5,650	4,150	1.36

[a] Unaided eye data from table 3. The standard error of the values shown in this table is of the order of 200 lb/in.², based on the agreement between duplicates.
[b] Average for two specimens.
[c] Value for one specimen only.

The threshold-crazing-stress values give an incomplete picture of the effect of forming and other variables on the crazing behavior of the materials. Thus, the crazing on the formed specimens, where it occurs, is usually finer than that on the unformed specimens. Also, although the threshold stresses at 95- and 50-percent relative humidities did not differ appreciably in general, the nature of the crazing at these two humidities was markedly different. The cracks at 95-percent relative humidity appeared finer and more closely spaced, and were almost always noticeably shorter than those at the lower relative humidity.

For most specimens the lengths of the longest cracks in the vicinity of the minimum section were measured with the Brinell microscope. A few cracks of exceptional length, appearing to be two or more cracks joined together or to be initiated at very fine, long scratches, were disregarded. The cracks measured on the unformed specimens after 100 hr at 50-percent relative humidity were from 0.4 to 0.7 mm long; at 95-percent relative humidity they were in general about 0.1 to 0.3 mm long. The formed

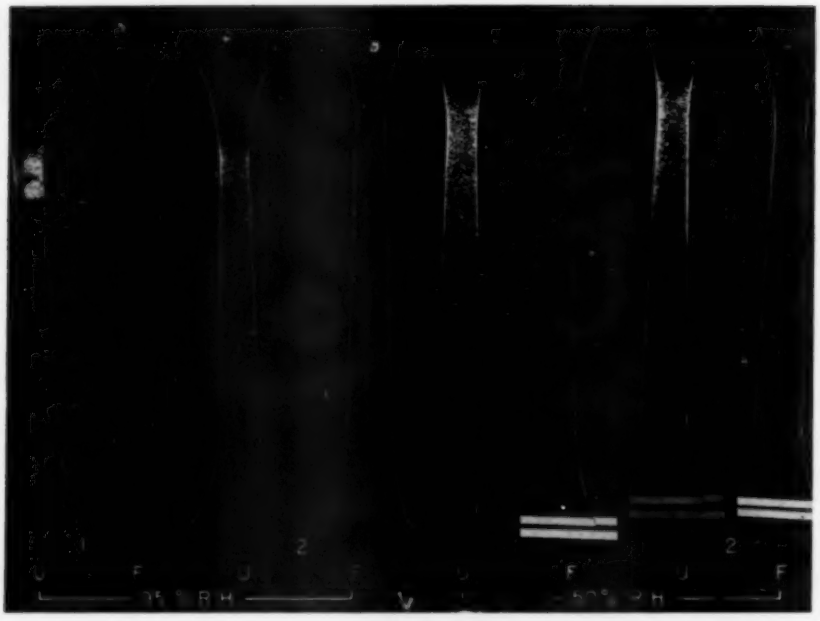

FIGURE 8. *Specimens from sample P2a, formed and unformed, after 7 days of tensile loading with 6,000 and 5,000 lb/in.² stress at the minimum sections of the formed and unformed specimens, respectively.*

specimens, in the few instances where the data were available (all on heat-resistant material), had corresponding crack lengths of close to 0.2 mm at the 50 percent and 0.1 mm at the 95-percent relative humidity.

It should be noted that the formed and unformed specimens cannot be compared on the basis of the above crack-length data because the cracks on the two sets of specimens had started at different times and the length of a crack apparently depends on the "crack lifetime", that is, the time elapsed under load after the crack appeared. Nevertheless, when the crack lifetime is taken into account the cracks on the unformed specimens seem to grow more rapidly than on the formed specimens even when the stress is appreciably higher on the latter. For example, on one formed specimen of sample P2a at 50-percent relative humidity, cracks were first observed at the minimum cross section (6,000-lb/in.² stress) at about 50 hr; and after 50 hr of crack lifetime, the longest cracks in this area were close to 0.15 mm in length. On the corresponding unformed specimens with only 5,000-lb/in.² stress at the minimum, the cracks were 0.35 to 0.4 mm long for the same crack lifetime. The difference in length is not as noticeable on specimens at 95-percent relative humidity.

Another effect of the high humidity was to increase the rate of creep markedly at the stresses used in the long-time tensile tests. Some of the specimens at the 95-percent relative humidity "necked down" at the minimum section near the end of the testing period. The formed specimens of the heat-resistant materials necked down sooner than the corresponding unformed specimens. However, it should be noted that these formed specimens had a 20-percent-higher stress than the unformed. The necking down of the formed and unformed specimens of samples L1d and P1a at the high humidity was about the same; the stress at the minimum cross section was the same for all specimens of a sample. Sample P1a is the only one of the four materials on which it was not possible to obtain values of threshold stress for stress crazing at the high relative humidity; at the loads used the material creeps before crazing can begin.

4.4. Discussion of Mechanism of Crazing

The effects of biaxial stretch-forming on the crazing behavior of polymethyl methacrylate perhaps may be explained qualitatively on a molecular basis as follows. In the unformed state the polymer molecules are assumed coiled in an approximately spherical shape; the chain segments have no preferred orientation. In the formed state the molecules should be somewhat uncoiled and in a roughly disk-like shape with the chain segments oriented predominantly in the plane of the material. The following mechanism of crazing, somewhat similar to that proposed by Maxwell and Rahm [9], is postulated. The crazing is assumed to start at the surface at submicroscopic flaws or weak points. Such weak points may be submicroscopic regions in which, by chance, the polymer chain segments are oriented normal to the applied tensile stress. With sufficient stress, a separation between portions of adjacent chains occurs; a stress concentration exists at the apex of the crack, and the latter grows until it reaches a region in which the polymer chain segments are oriented approximately in the direction of the tensile stress. The crack either does not grow or grows slowly unless the tensile stress is greatly

ncreased. Subsequent crack growth may involve upture of primary valence bonds, especially if the tress is relatively high, of the order of the tensile trength.

The process of biaxial stretch-forming, by orient- g the chain segments in the plane of the sheet, educes the proportion and size of the weak, normally riented regions and increases the regions of pre- ominantly parallel orientation. Stated differently, he stretch-forming may be said to introduce "cleavage" planes in the plane of the sheet. This rientation or introduction of cleavage planes greatly mpedes the development and growth of crazing racks. Thus, as noted previously in the long time ensile loading tests, the crazing cracks, after be- oming visible, grew more slowly on formed as ompared to the corresponding unformed specimens.

In regard to stress-solvent crazing, mechanisms ave been suggested by various authors [10, 11, 2], which, while differing in some aspects, include s a factor the concept of the solvent acting as a lasticizer. By using this concept the mechanism uggested above for stress crazing may be modified o include the influence of solvents as follows. The olvent molecules penetrating the surface of the olymer tend to surround portions of the polymer hains and reduce the forces required to separate hem. Because of this weakening influence of the olvent molecules at a surface flaw, such as a region f normal orientation of the polymer chains, the tress concentration that can be withstood is reduced nd a tiny crack develops at a lower applied stress han in the absence of solvent. The solvent mole- ules by capillarity probably fill the crack as it grows nd continue to exert a weakening influence at the pex. In this connection, it has been suggested by lopkins, Baker, and Howard [12] that another eakening influence at the apex of a crack is the film preading pressure of the crazing liquid.

The effect of forming on stress-solvent crazing ight be expected to be similar to that for stress razing. The reduction in the number and size of he regions of normal orientation and increase in the egions of parallel orientation should result in higher threshold stresses for the formed material. Also, for formed material as for unformed, the crazing stress should be lower in the presence of than in the absence of solvent, owing to the weakening influence of the solvent.

4.5. Accelerated Weathering Tests

The results of the 480-hr sunlamp-fog accelerated weathering tests are shown in table 5.

The light-transmission values for all the materials, both unformed and formed, are 92.0 ±0.1 percent initially and 92.3 ±0.3 percent after weathering. While the transmission values are slightly higher after weathering the materials, the individual differences, which do not exceed 0.5 percent, are considered within the experimental error of measurements made at different times. The haze values are approximately 0.5 ±0.2 percent for all materials both formed and unformed and before and after weathering. In this connection, the specimens were inspected visually after the weathering test, but no crazing was observed on any of them.

For all samples, the shrinkage of the unformed or control specimens was very slight, averaging 0.05 to 0.1 percent, which values are of the order of magnitude of the standard error of the shrinkage values. The formed specimens of the heat-resistant grade samples shrank only 0.2 percent; however, similar specimens of the general-purpose grade samples shrank somewhat more, the values being 1 and 2 percent for Plexiglas I–A and Lucite HC201, respectively.

Most of the specimens were slightly warped after the weathering test. In general, the formed specimens were more warped than the unformed, particularly for the general-purpose-grade materials.

The greater dimensional changes for formed pieces of the general-purpose-grade samples as compared to the heat-resistant grade are not surprising for the following reason. The specimen temperature in the test is about 60 ±5° C, which is not far below the second-order transition temperature of the general-purpose-grade samples, namely, 75° to 80° C; the

TABLE 5. *Results of accelerated weathering tests on polymethyl methacrylate formed by biaxial stretching* [a]

NBS sample	Treatment [b]	Light transmission [c]				Haze [c]				Shrinkage [d]		Warpage [e]
		Initial		After 480 hours		Initial		After 480 hours		Average	Range	Average
		Average	Range	Average	Range	Average	Range	Average	Range			
		Percent	*Percent*	*Percent*	*Percent*	*Percent*	*Percent*	*Percent*	*Percent*	*Percent*	*Percent*	
Ld1	F	92.0	91.9 to 92.1	92.3	92.2 to 92.4	0.7	0.3 to 0.9	0.7	0.5 to 0.8	2.3	1.0 to 4.3	3
	U	92.0	92.0 to 92.1	92.1	92.0 to 92.3	.4	.3 to 0.5	.3	.2 to 0.3	0.1	0 to 0.2	1
Ld2	F	92.1	92.1 to 92.2	92.6	92.5 to 92.6	.4	.3 to 0.5	.4	.3 to 0.7	.2	0.1 to 0.2	1
	U	91.9	91.9 to 91.9	92.1	91.7 to 92.5	.4	.4 to 0.4	.4	.2 to 0.5	.02	0 to 0.05	1
P1a	F	92.1	92.0 to 92.2	92.6	92.5 to 92.6	.5	.4 to 0.5	.3	.2 to 0.4	1.0	0.6 to 2.0	2
	U	92.0	91.9 to 92.1	92.5	92.5 to 92.6	.4	.4 to 0.5	.4	.3 to 0.5	0.05	0 to 0.1	0
P2a	F	92.1	92.1 to 92.1	92.5	92.5 to 92.5	.4	.4 to 0.5	.5	.3 to 0.7	.2	0.1 to 0.4	1
	U	92.1	92.1 to 92.2	92.5	92.4 to 92.5	.4	.3 to 0.5	.3	.2 to 0.3	.05	0 to 0.1	1

[a] The amount of the stretching in forming was 50 to 60 percent; the actual averages for each material are given in table 3. The weathering tests were made according to Method 6021 of Federal Specification L–P–406a, except that the testing time was 480 hr. instead of 240 hr. Each average is for three specimens, one from each of the three sheets of each material.

[b] F, Formed; U, unformed.

[c] Light transmission and haze measurements were made with a pivotable-sphere hazemeter, according to ASTM method D1003–49T, Procedure A.

[d] Distance between gage marks approximately 2 in. apart was measured before and after test with a steel scale and magnifying glass.

[e] Warpage was classified arbitrarily as follows: 0, none; 1, slight; 2, some 3, considerable.

corresponding temperature for the heat-resistant grade is about 94° to 95° C.[10]

4.6. Possible Applications of Stretch-Forming

The improvement in the crazing properties of acrylic plastic sheet produced by moderate (50 percent) biaxial stretch-forming suggests that formed enclosures made from prestretched flat sheets may have superior crazing and strength properties compared to enclosures formed from normal sheets. In an astrodome as prepared normally, as, for example, by vacuum drawing, there is a maximum amount of stretch and craze resistance at the apex and negligible stretch and minimum craze resistance at the rim. The use of prestretched sheet would hence improve the craze resistance, especially at the rim where contact with crazing liquids is quite likely.

As an alternative to using prestretched material to achieve improved craze resistance at the edge of acrylic enclosures, there is the possibility of preparing an enclosure larger and more deeply drawn than required, and then using only the central portion of the formed piece.

In view of the considerable changes in the physical properties of cast polymethyl methacrylate sheet resulting from biaxial stretching to about 50 percent, it is of interest for both practical and fundamental reasons to learn the effects of greater stretching on this material. Experiments with this objective are in progress on material stretched up to about 150 percent.

The effects of biaxial stretching on other physical properties, such as creep, abrasion resistance, natural weathering while under load, impact resistance, fracture under bullet impact, and crazing with various solvents, should also be determined.

5. Summary

Some of the effects on polymethyl methacrylate of biaxial stretch-forming to about 50 percent are as follows:

1. The strain at the onset of crazing in the standard tensile test is greatly increased; in fact, most specimens showed no crazing. The tensile strength and secant modulus of elasticity are unaffected. The elongation at failure is increased from approximately 10 percent to about 60 percent.

2. The threshold stress for stress-solvent crazing with benzene is increased about 70 to 80 percent for both general-purpose and heat-resistant grades.

3. In long-time tensile tests of up to 7 days' duration (a) the threshold stress for stress crazing is increased about 40 to 50 percent for both grades of material at both 50- and 95-percent relative humidities, and (b) the crazing cracks produced are somewhat finer and appear to grow in length more slowly.

The effect of biaxial stretch-forming on other physical properties, as well as the effects of higher degrees of stretching, should be investigated for both practical and fundamental reasons.

The considerable increase in the elongation at failure and in the stress crazing and stress-solvent crazing threshold of polymethyl methacrylate as a result of moderate (50 percent) stretch-forming suggests that formed enclosures made from prestretched flat sheets may have greatly improved crazing resistance and strength properties, possibly to the extent that acrylic glazing need not be laminated.

The courtesy of E. I. du Pont de Nemours & Co., Inc. and the Rohm & Haas Co. in furnishing material for use in this investigation is gratefully acknowledged. The authors also greatly appreciate the advice and information received from R. E. Leary and W. F. Bartoe of the two companies, respectively, and from Wendell Koch of the Air Matériel Command. The assistance of M. N. Geib, who designed the long-time loading apparatus, A. Pennington, who did much of the construction of the equipment, and of John Mandel, who advised on statistical matters, is also acknowledged.

6. References

[1] Northrop Aircraft, Inc., Mechanical properties of formed methyl methacrylate, Report L. N-2376 (April 14, 1948).

[2] J. Bailey, Stretch orientation of polystyrene and its interesting results, India Rubber World **118,** 225–231 (1948).

[3] Lockheed Aircraft Corporation, Tests of laminated type astral domes, Report 6074 (April 7, 1947).

[4] Boeing Aircraft Company, Pressure testing of sighting station domes, Report T-21254 (September 9, 1946).

[5] B. M. Axilrod and M. A. Sherman, Effect of stress-solvent crazing on tensile strength of polymethyl methacrylate, NACA Tech. Note 2444 (August 1951).

[6] G. W. Morey, Properties of glass (Reinhold Publishing Co., New York, N. Y., 1938).

[7] C. C. Hsiao and J. A. Sauer, Crazing of linear high polymers, J. Applied Phys. **21,** 1071–1083 (1950).

[8] J. A. Kies, A. M. Sullivan, and G. R. Irwin, Interpretation of fracture markings, J. Applied Phys. **21,** 716–720 (1950).

[9] B. Maxwell and L. F. Rahm, The rheological properties of polystyrene below 80° C, Ind. Eng. Chem. **41,** 1988–1993 (September 1949).

[10] B. Maxwell and L. F. Rahm, Factors affecting the crazing of polystyrene, Princeton University Plastics Laboratory Technical Report 14B (May 1949); SPE J. **6,** 7–12 (Nov. 1950).

[11] E. W. Russell, Crazing of cast polymethyl methacrylate, Nature **165,** 91–96 (Jan. 21, 1950). Report No. Chem. 447, Royal Aircraft Establishment, England (August 1948).

[12] I. L. Hopkins, W. O. Baker, and J. B. Howard, Complex stressing of polyethylene, J. Applied Phys. **21,** 206–213 (March 1950).

WASHINGTON, July 25, 1952.

[10] These values were derived from volume-temperature measurements made on these samples over the range 25° to 110° C: a mercury dilatometer was used.

Journal of Research of the National Bureau of Standards Vol. 49, No. 5, November 1952 Research Paper 2370

Mass Spectra of Fluorocarbons*

Fred L. Mohler, Vernon H. Dibeler, and R. M. Reese

Mass spectra of 22 fluorocarbons have been measured on a 180° Consolidated mass spectrometer, and the results are presented in six tables of spectral data. These include seven normal paraffins from methane to heptane; isopentane and isohexane; three pure cyclics and methylcyclohexane; four olefins; three C_4F_8 isomers; a dicyclic; and a tricyclic. These spectra are very different from the hydrocarbon analogs. In all the paraffins the most abundant ion is CF_3^+, and the molecule ions are very small or absent. Spectra of the unsaturated compounds and the cyclics are more distinctive than the normal paraffins. In the paraffins, ions of formula C_nF_{2n+1} tend to be largest, except that when one carbon is removed the largest ion is C_nF_{2n-1}. In cyclics, C_nF_{2n-1} ions tend to be largest; in the dicyclic, C_nF_{2n-3} ions are largest; and in the tricyclic, C_nF_{2n-5} ions tend to be largest. The tricyclic C_8F_{12} is probably a fused cyclobutane structure. The dicyclic is completely fluorinated methylnapthalene, $C_{11}F_{20}$, and is the heaviest compound ever run on the Bureau's mass spectrometer. In the perfluoroparaffins there is a progressive increase in the current per unit pressure for the CF_3^+ ion with increasing molecular weight of the fluorocarbon. In incompletely fluorinated molecules containing an H atom the larger ion peaks containing H will correspond with the larger peaks in the perfluoro spectrum, with H substituted for a fluorine atom.

1. Introduction

The growing interest in fluorocarbon chemistry and technology makes it worth while to obtain mass spectra of perfluorohydrocarbons as a basis for chemical analysis of unknown mixtures of fluorocarbons. Also, it is of theoretical interest to see how these spectra differ from the hydrocarbon mass spectra. The Mass Spectrometry Section of the National Bureau of Standards has for several years been collecting mass spectra of fluorocarbons as compounds become available, and the present paper gives a compilation of spectra obtained to date. A previous paper [1][1] includes data on five perfluorohydrocarbons. The present summary includes these compounds. Other laboratories have obtained mass spectra of a variety of fluorinated hydrocarbons, but no systematic compilation of spectra has been published.

Complete spectra of all the fluorocarbons included in this paper have been published in the API Catalog of Mass Spectral Data [2]. When the mass spectrum of a fluorocarbon is tabulated in the conventional manner in the order of increasing molecular weight of the ions, ions with different numbers of carbon atoms and of fluorine atoms become mixed in a confusing disorder. For that reason, spectra are presented here in order of the number of carbon atoms and the number of fluorine atoms in each ion. This is convenient for the purpose of interpreting the spectra in terms of molecular structure and for comparison with hydrocarbon spectra. For purposes of chemical analysis the conventional tables are, of course, preferable.

2. Experimental Details

Most of the mass spectra were obtained with a type 103 Consolidated mass spectrometer equipped with a micromanometer [3] to measure the pressure in the inlet reservoir. An ionizing voltage of 70 volts was used, and the metastable ions were suppressed. For the heavier compounds the suppressor voltage was adjusted to give a resolving power of about 350. The temperature of the ionization chamber was 250° C. The heaviest compounds require a magnetic field in excess of the rated capacity of the magnet, but there was no evidence of overheating in the time required to scan the spectrum. Some of the mass spectra were obtained with a type 102 mass spectrometer before the type 103 instrument was installed. There are only minor differences in spectra obtained with the two types of instrument.

We are indebted to Dr. George H. Cady, University of Washington; The M. W. Kellogg Co.; Minnesota Mining & Manufacturing Co.; the Jackson Laboratories of the E. I. du Pont de Nemours Co., Inc.; and to others acknowledged later for making available the various fluorocarbons. Most of these compounds are available only in small experimental batches. The purity was in all cases adequate for a reliable description of the spectra. Trace amounts of molecules containing one H or one Cl atom were sometimes found, but, except where noted, there was no evidence of heavier fluorocarbons as impurities. The API tables include mass peaks as small as 0.01 percent of the maximum peak. For brevity, we omit many of the small peaks in the tables to give a concise presentation of the major features.

There are no difficulties in running fluorocarbons in the mass spectrometer, although special precautions were taken in handling the *iso*-C_4F_8 because of the reported toxicity of this compound [7]. The vapor pressures are high and are of the order of magnitude of the vapor pressures of the hydrogen analogs. They are inert and are not strongly adsorbed, so they are quickly pumped out, with no serious memory effects in spite of the high molecular weight.

3. Results

Table 1 lists the larger ion peaks in the mass spectra of normal perfluoroparaffins from methane to *n*-

*This paper was presented at the Pittsburgh Conference on Analytical Chemistry and Spectrochemistry, in March 1952.

[1] Figures in brackets indicate the literature references at the end of this paper.

TABLE 1. *Mass spectra of normal perfluoroparaffins*

Ion	CF_4	C_2F_6	C_3F_8	C_4F_{10}	C_5F_{12}	C_6F_{14}	C_7F_{16}
C	7.8	1.49	2.4	0.19	0.05	0.25	0.03
F	6.7	1.22	0.98	.14	.08	.23	.05
CF	4.9	18.3	28.8	12.2	9.2	11.3	6.06
CF_2	11.8	10.1	9.3	4.16	3.12	2.50	1.86
CF_3	100	100	100	100	100	100	100
CF_4	0	------	------	------	------	------	------
C_2F_4	------	0.55	6.55	8.40	7.2	13.2	7.34
C_2F_5	------	41.3	9.0	18.3	29.5	27.8	27.0
C_2F_6	------	0.15	------	------	------	------	------
C_3F_3	------	------	0.55	1.20	2.06	4.24	2.38
C_3F_5	------	------	.23	8.37	6.54	13.9	13.3
C_3F_6	------	------	.05	2.55	1.10	1.96	.88
C_3F_7	------	------	24.6	2.14	9.73	18.9	20.5
C_3F_8	------	------	0	------	------	------	------
C_4F_7	------	------	------	0.03	3.25	2.36	2.53
C_4F_8	------	------	------	2.57	0.27	3.96	8.48
C_4F_{10}	------	------	------	0	------	------	------
C_5F_8	------	------	------	------	0	2.67	0.80
C_5F_{11}	------	------	------	------	0.77	0.08	1.20
C_5F_{12}	------	------	------	------	.03	------	------
C_6F_{11}	------	------	------	------	------	------	1.08
C_6F_{12}	------	------	------	------	------	1.11	0.02
C_6F_{14}	------	------	------	------	------	0.05	------
C_7F_{15}	------	------	------	------	------	------	.09
C_7F_{16}	------	------	------	------	------	------	0
Relative sensitivity	0.57	0.97	1.71	1.82	2.59	2.65	3.42

heptane. Ions are listed in the order of the number of carbon atoms and the number of fluorine atoms in each ion, and intensities are relative to CF_3^+ taken as 100. The last row gives the sensitivity (current per unit pressure) for the CF_3^+ ion relative to the sensitivity of normal butane at mass 43.

In each of these spectra by far the largest peak is CF_3^+, and the molecule ion peak is very small or zero. In each group of peaks containing n carbon atoms the maximum peak is C_nF_{2n+1}, except that for molecules heavier than propane, when one carbon atom is removed from the molecule the maximum peak is C_nF_{2n-1}. Thus in C_6F_{14} the largest peak containing five carbon atoms is $C_5F_9^+$. In C_7F_{16} the largest peak containing six carbon atoms is $C_6F_{11}^+$, but the largest peak with five carbon atoms is $C_5F_{11}^+$. The size of these maximum peaks decreases progressively with increasing molecular weight, and the spectra of the heavier compounds are very similar except near the heavy end, and these distinctive peaks are small. In normal hydrocarbon paraffins the maximum peaks are also C_nH_{2n+1}, except that the molecule ion peak is larger. The largest of these peaks is C_3H_7 or C_4H_9.

In these fluorocarbons the sensitivity for the CF_3^+ ion progressively increases with increasing molecular weight. The total ionization (the sum of the mass peaks times the sensitivity) increases at much the same rate.

Doubly charged ions are observed as follows: In CF_4 the intensities of CF_2^{++} and of CF_3^{++} are 3.9 and 1.25, respectively, relative to CF_3^+; in C_3F_8 the intensity of $C_3F_8^{++}$ is 0.28, and in C_5F_{12} the ion $C_5F_{10}^{++}$ is 0.09. Thus, molecules of formula C_nF_{2n+2} give ions $C_nF_n^{++}$, and in molecules where n is an even number a singly charged ion will mask the doubly charged ion. In spectra obtained with the type 102 mass spectrometer some metastable transition peaks were observed, but they were very small [1].

There are only two examples of branched fluorocarbons, perfluoroisopentane and isohexane. Table 2 shows the spectra and, for comparison, the spectra of the normal compounds from table 1. The most conspicuous difference in both the pentanes and the hexanes is found in the relative intensities of the $C_3F_7^+$ ion. It appears as if the isopropyl radical $CF(CF_3)_2$ did not contribute at all to this peak, and that the normal propyl ion $CF_3{\cdot}CF_2{\cdot}CF_2^+$ accounted for the observed ion current. In isopentane, $C_3F_7^+$ is nearly zero, and in n-pentane and isohexane, each of which contain one n-propyl radical, the relative intensity is about 9, whereas in n-hexane, which consists of two n-propyl radicals, the relative intensity is twice as great. $C_2F_5^+$ is also roughly twice as great in the normal compounds containing two terminal ethyl radicals as in the iso-compounds containing one terminal ethyl radical.

Table 3 gives mass spectra of three pure cyclics and methylcyclohexane. The spectra are very distinctive with few common characteristics. The molecule ions are small, and, with two minor exceptions, the peaks C_nF_{2n-1} are the largest peaks for n greater than 2. In the pure cyclics, production of CF_3^+ involves a rearrangement of atoms, but it is a large peak. The ion $C_2F_5^+$ also involves a rearrangement of atoms in these compounds. No doubly charged ions are observed in these spectra.

Table 4 lists mass spectra of four perfluoroolefins. The spectra are distinctive, with no obvious common characteristics, except that the molecule ions are fairly large and CF^+ is large. CF_3^+ is small in C_2F_4, where a rearrangement of atoms is involved in the ionization process. The two butenes have very

TABLE 2. *Mass spectra of perfluoroisoparaffins and normal paraffins*

Ion	nC_5F_{12}	iso-C_5F_{12}	nC_6F_{14}	iso-C_6F_{14}
CF	9.2	6.5	11.3	8.5
CF_2	3.12	2.12	2.50	1.87
CF_3	100	100	100	100
C_2F_4	7.2	3.51	13.2	7.45
C_2F_5	29.5	16.4	27.8	11.4
C_3F_5	2.06	2.76	4.24	4.67
C_3F_6	6.54	8.3	13.9	12.9
C_3F_7	1.10	1.76	1.96	0.97
C_3F_8	9.7	0.19	18.9	9.24
C_4F_7	3.25	4.53	2.36	3.64
C_4F_8	0.27	0.87	3.96	4.23
C_5F_8	0	0	2.67	3.59
C_5F_{11}	0.77	1.72	0.08	.17
C_5F_{12}	.03	0	------	------
C_6F_{11}	------	------	1.11	2.28
C_6F_{14}	------	------	0.05	0
Relative sensitivity	2.59	2.77	2.65	3.16

TABLE 3. *Mass spectra of perfluorocyclics*

Ion	Cyclo-C_4F_8	Cyclo-C_5F_{10}	Cyclo-C_6F_{12}	Methyl-cyclo-hexane
CF	54.2	23.3	21.8	10.4
CF_2	13.2	5.11	5.15	1.31
CF_3	24.6	16.2	70.3	100
C_2F_2	2.06	1.28	1.23	0.31
C_2F_3	1.92	1.88	2.14	1.20
C_2F_4	100	23.8	29.2	15.4
C_2F_5	0.04	0.24	5.59	4.93
C_3F_2	2.70	2.60	2.96	1.82
C_3F_3	6.47	9.65	15.0	10.9
C_3F_4	0.99	1.36	2.53	2.10
C_3F_5	86.7	100	100	43.8
C_4F_5	0	0.53	2.06	2.06
C_4F_6	0.12	0.93	3.96	4.30
C_4F_7	0.09	14.4	21.4	19.5
C_4F_8	0.12	0	0	0.05
C_5F_7	------	------	2.71	1.26
C_5F_8	------	4.45	20.9	2.82
C_5F_{10}	------	0.36	0.05	0
C_6F_9	------	------	0.07	2.26
C_6F_{11}	------	------	3.77	2.16
C_6F_{12}	------	------	0.70	0
C_7F_{13}	------	------	------	1.74
C_7F_{14}	------	------	------	0
Relative sensitivity	0.97	1.73	1.38	2.44

TABLE 4. *Mass spectra of perfluoro olefins*

Ion	C_2F_4	C_3F_6	1-C_4F_8	iso-C_4F_8
C	12.6	12.6	4.6	6.0
F	2.77	4.0	1.78	2.63
CF	100	100	72.9	58.9
CF_2	29.5	12.1	7.76	8.55
CF_3	2.83	77.1	36.2	100
C_2	3.03	4.06	1.02	1.39
C_2F	1.44	4.13	2.00	2.83
C_2F_2	0.99	5.04	3.09	2.45
C_2F_3	63.1	14.2	3.20	3.57
C_2F_4	33.8	36.1	4.62	6.68
C_3	------	0.77	0.86	0.92
C_3F	------	1.96	2.30	3.05
C_3F_2	------	2.59	4.33	4.19
C_3F_3	------	5.87	13.0	30.0
C_3F_4	------	1.21	4.75	11.2
C_3F_5	------	72.0	100	15.0
C_3F_6	------	28.6	0.35	6.40
C_4F_4	------	------	0.49	0.24
C_4F_7	------	------	12.1	73.3
C_4F_8	------	------	8.78	18.7
Relative sensitivity	0.55	0.56	1.22	0.74

TABLE 5. *Mass spectra of* C_4F_6 *isomers*

Ion	1-3, Butadiene	Cyclo-butene	2-Butyne
C	6.75	6.97	11.8
F	1.78	1.02	4.04
CF	49.6	64.0	53.4
CF_2	5.75	4.59	8.69
CF_3	5.52	7.68	42.1
C_2	1.85	1.77	5.14
C_2F	1.72	2.00	1.36
C_2F_2	1.10	6.48	2.45
C_2F_3	1.79	0.62	0.04
C_2F_4	0.23	3.73	0
C_3	2.13	1.55	6.38
C_3F	6.10	5.42	15.2
C_3F_2	11.5	8.56	21.5
C_3F_3	100	100	100
C_3F_4	10.5	3.77	10.8
C_3F_5	1.23	2.04	0.37
C_4F_4	4.31	1.35	14.2
C_4F_5	4.64	18.6	82.0
C_4F_6	29.9	26.2	39.5
Relative sensitivity	0.91	0.80	0.47

TABLE 6. *Mass spectra of* $C_{11}F_{20}$ *and* C_5F_{12}

Decafluoroperfluoro-1-methylnaphthalene				Tricyclic C_5F_{12}			
Ion	Relative intensity	Ion	Relative intensity	Ion	Relative intensity	Ion	Relative intensity
CF	4.72	C_3F_5	3.33	CF	64.7	C_3F	3.73
CF_2	0.94	C_3F_7	3.96	CF_2	4.19	C_3F_2	5.01
CF_3	100	C_6F_6	1.21	CF_3	98.7	C_3F_3	29.4
C_2F_4	13.2	C_6F_7	2.68	C_2F_2	2.59	C_3F_4	4.25
C_2F_5	9.66	C_6F_8	5.87	C_2F_3	1.84	C_3F_5	51.2
C_3F_2	1.34	C_7F_8	2.13	C_2F_4	11.1	C_3F_6	14.7
C_3F_3	10.4	C_7F_{11}	12.1	C_2F_5	3.02	C_3F_7	2.47
C_3F_4	2.28	C_8F_{13}	4.14	C_3F	5.18	C_4F_4	2.17
C_3F_5	33.0	C_9F_{13}	0.90	C_3F_2	20.7	C_4F_5	3.94
C_3F_7	2.57	$C_{10}F_{15}$	1.07	C_3F_3	79.2	C_4F_6	27.3
C_4F_4	2.44	$C_{10}F_{16}$	1.16	C_3F_4	11.8	C_4F_7	100
C_4F_5	4.16	$C_{10}F_{17}$	1.22	C_3F_5	34.3	C_4F_8	21.9
C_4F_6	4.49	$C_{11}F_{19}$	2.11	C_4F	7.06	C_7F_7	9.73
C_4F_7	13.3	$C_{11}F_{20}$	0.17	C_4F_2	11.1	C_7F_8	14.8
C_5F_8	1.95			C_4F_3	23.3	C_7F_9	61.6
				C_4F_4	8.49	C_7F_{10}	2.14
				C_4F_5	40.3	C_8F_{11}	35.8
						C_8F_{12}	3.02
Relative sensitivity, 2.65				Relative sensitivity, 0.51			

distinctive spectra, and both are different from the isomer cyclo-C_4F_8 given in table 3. The relative intensities of $C_3F_5^+$, $C_3F_3^+$, $C_2F_4^+$, and CF_3^+ are strikingly different in the three spectra. C_2F_6 gives a relatively large doubly charged ion peak $C_3F_5^{++}$ of intensity 2.17, and $C_3F_3^{++}$ has intensity 0.16. In 1-butene $C_3F_5^{++}$ of intensity 0.11 is observed.

Table 5 lists mass spectra of three C_4F_6 isomers: 1,3-Butadiene, $CF_2{=}CF{-}CF{=}CF_2$; cyclobutene, $CF_2{-}CF{=}CF{-}CF_2$; and 2-butyne, $CF_3{-}C{\equiv}C{-}CF_3$. In these compounds $C_3F_5^+$ is the maximum peak. The relative intensities of $C_4F_6^+$, $C_4F_5^+$, and CF_3^+ are distinctively different in the three compounds.

Table 6 includes mass spectra of a dicyclic and a tricyclic fluorocarbon. The dicyclic compound is completely fluorinated 1-methylnaphthalene, $C_{11}F_{20}$, prepared by E. T. McBee of Purdue University. This compound of molecular weight 512 is the heaviest compound ever run on the Bureau's mass spectrometer. Two small peaks ascribed to $C_{12}F_{19}^+$ and $C_{11}F_{21}^+$ indicate that there is some heavier impurity present. The maximum peak of each carbon group has the formula C_nF_{2n-3} for n greater than 4. The ions $C_2F_5^+$ and $C_3F_7^+$ involve rearrangement in the ionization. There are also many small peaks not included in table 6 that come either from rearrangement or from impurities.

The C_8F_{12} compound was furnished by W. T. Miller of Cornell University and was described by Prober and Miller in 1949 [4]. When hexafluorobutadiene is heated, one of the products is a saturated fluorocarbon of formula C_8F_{12}. It has a freezing point of 40° C and a boiling point of 80° C. They state that "preliminary X-ray diffraction studies are consistent with the (following) structure":

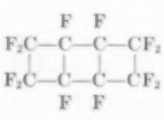

The mass spectrum of table 6 can also be described as consistent with this structure. While the ions CF_3^+ and $C_2F_5^+$ involve rearrangements in the ionization process, if this is the structure, other spectra show that rearrangements to give these ions are very common in fluorocarbon spectra. It is perhaps significant that $C_2F_4^+$ is the largest C_2 ion, $C_4F_6^+$ the largest C_4 ion, and $C_6F_8^+$ is fairly large. The spectrum shows a very uniform distribution of intensity from CF^+ to $C_8F_{11}^+$. The largest peaks in each carbon group are C_nF_{2n-5} beyond $n{=}4$.

4. Conclusions

The fluorocarbons included in this investigation cover a wide variety of compounds, but, with the exception of the normal perfluoroparaffins, there are not enough compounds of any chemical class to permit broad generalizations. The normal perfluoroparaffins show a marked regularity in their spectra that is quite different from the regularities found in the hydrocarbon analogs. CF_3^+ is by far the most abundant ion and accounts for half or more of the total ionization. Another research [5] shows that the appearance potential of this ion is the same (14.3 to 14.4 ev) in C_2F_6, C_3F_8, C_4F_{10}, and C_5F_{12}. (The value given in the reference for C_4F_{10} is not correct.) As production of CF_3^+ is the predominant ionization process, it is significant that the sensitivity, or current, per unit pressure increases progressively with increasing molecular weight.

In the ionization process a valence electron is removed, and this weakens the ionized bond. Then there are two possibilities, (1) either the molecule dissociates at the point where it was initially ionized or (2) the electrons rearrange themselves before there is time for dissociation and the dissociation occurs at some other bond than at the point initially ionized. On the first hypothesis, the probability of producing CF_3^+ should be the same for all normal compounds heavier than ethane, for in each case one of two terminal C—C bonds has to be ionized. (We have seen that the ionization potential remains the same.) This is not the case, and the progressive increase in the probability of ionization indicates that whenever the molecule is initially ionized there is a high probability of breaking a terminal C—C bond to give CF_3^+. Large molecules with many valence bonds afford a larger target area than small molecules. Wallenstein, Wahrhaftig, and Eyring [6] have advanced this second hypothesis concerning the ionization process to explain the relative intensities in hydrocarbon mass spectra, but in hydrocarbons radicals other than CH_3 are preferentially ionized.

It has been noted that in normal perfluoroparaffins ions of formula C_nF_{2n+1} give the largest peak in each carbon group, except that in fragment ions with one carbon removed from the molecule C_nF_{2n-1} is the largest peak. In hydrocarbons, C_nH_{2n+1} is the largest, with rare exceptions. In the cyclics the ions C_nF_{2n-1} tend to be the largest for n greater than 2. In the dicyclic, $C_{11}F_{20}$, the ions C_nF_{2n-3} are largest, and in the tricyclic, C_8F_{12}, ions of formula C_nF_{2n-5} tend to be largest. In this respect patterns of fluorocarbons are simpler than hydrocarbons. In hydrocarbons there is a close resemblance between patterns of the 1-olefin and the isomeric cyclic. There is no such resemblance between cyclo-C_4F_8 and perfluoro-1-butene.

Identification and analysis of mixtures of perfluoroparaffins will be difficult because of the almost complete absence of molecule ions and the low intensity of all the heavier ions in these spectra. Unsaturated molecules and cyclics have very distinctive spectra and possibilities of analysis will be favorable when spectra of more compounds become available.

As there are gaps of several mass units between fluorocarbon peaks, impurities other than fluorocarbons are usually conspicuous. A common trace impurity will be molecules that are not completely fluorinated and contain one or two H atoms. The previous paper on mass spectra of fluorocarbons [1] includes a spectrum of cyclo-C_5F_9H, and it is found

hat large peaks containing an H atom correspond losely in relative intensity to large peaks in the yclo-C_5F_{10} spectrum, with H substituted for one of he F atoms. We have qualitative evidence based n hydrogen impurities rather than pure compounds hat this is a quite general relation and also holds hen 2 H atoms are substituted for 2 F atoms in a olecule. Thus, if a trace of H is present, peaks ontaining H will not be adjacent to the large fluoro- arbon peaks but will be 18 mass units less than the rge peaks. With traces of chlorine in the fluoro- arbon the larger peaks containing Cl will be 16 and 8 mass units heavier than the larger fluorocarbon eaks.

When any HF or F_2 is formed in a reaction this eacts with glass to give SiF_4. The SiF_3^+ ion of mass 5 is by far the largest peak in the SiF_4 spectrum, nd this will be a common impurity peak.

5. References

[1] F. L. Mohler, E. G. Bloom, J. H. Lengel, and C. E. Wise, Mass spectra of some cyclic and straight chain fluorocarbons, J. Am. Chem. Soc. **71,** 337 (1949).

[2] Catalog of mass spectral data, API Project 44, Carnegie Institute of Technology, Pittsburgh, Pa.

[3] V. H. Dibeler and F. Cordero, J. Research NBS **46,** 1 (1951) RP2167.

[4] M. Prober and W. T. Miller, Jr., J. Am. Chem. Soc. **71,** 598 (1949).

[5] V. H. Dibeler, R. M. Reese, and F. L. Mohler, Phys. Rev. **87,** 213 (1952) abstract.

[6] M. B. Wallenstein, A. L. Wahrhaftig, and H. Eyring, AECU Report 1484.

[7] W. H. Pearlson, Minnesota Mining & Manufacturing Co., private communication.

Washington, September 8, 1952.

Journal of Research of the National Bureau of Standards Vol. 49, No. 5, November 1952 Research Paper 2371

A Method of Computing Exact Inverses of Matrices With Integer Coefficients[1]

J. Barkley Rosser[2]

In theory, the problem of computing the exact inverse of a matrix A with integer coefficients is completely solved by solving exactly the simultaneous equations $Ax=y$, in which both x and y are variable vectors. This solution can be carried out by any one of numerous well-known procedures, resulting in expressions for the components of x as linear combinations of the components of y. The coefficients of these linear combinations are just the components of A^{-1} because we have $x=A^{-1}y$.

In actual practice, if the order of A is at all large, the exact components of A^{-1} will be fractions whose numerator and denominator each have a large number of digits, and the usual methods of solution become extremely laborious due to the necessity for carrying an even larger number of significant digits throughout most of the computation. In the method presented herein, the number of significant digits involved builds up gradually, and only the final stages of the computation involve a large number of digits. Moreover, the method can be readily adapted to use on IBM equipment, and so all but the final stages (in which many significant digits must be carried) can be readily mechanized.

1. Illustration of a Solution by Previous Methods

Suppose we require the exact inverse of

$$A=\begin{vmatrix} 152 & -128 & 183 & 83 & -141 & -27 \\ 103 & -89 & 156 & -91 & 135 & -96 \\ 72 & 195 & 75 & 113 & -187 & 178 \\ 157 & -192 & -37 & -138 & 71 & -179 \\ 34 & 190 & -120 & 102 & 37 & 65 \\ 191 & 77 & -154 & 117 & -131 & -112 \end{vmatrix}$$

To invert this, we write

$$\begin{aligned} 152x_1-128x_2+183x_3+\ 83x_4-141x_5-\ 27x_6&=y_1 \\ 103x_1-\ 89x_2+156x_3-\ 91x_4+135x_5-\ 96x_6&=y_2 \\ 72x_1+195x_2+\ 75x_3+113x_4-187x_5+178x_6&=y_3 \\ 157x_1-192x_2-\ 37x_3-138x_4+\ 71x_5-179x_6&=y_4 \\ 34x_1+190x_2-120x_3+102x_4+\ 37x_5+\ 65x_6&=y_5 \\ 191x_1+\ 77x_2-154x_3+117x_4-131x_5-112x_6&=y_6. \end{aligned} \tag{1}$$

Eliminating x_1 from the last five of these by use of eq 1 gives

$$\begin{aligned} 344x_2-\ 4863x_3+22381x_4-35043x_5+11811x_6&=103y_1-152y_2 \\ -4857x_2+\ 222x_3-\ 1400x_4+\ 2284x_5-\ 3625x_6&=\ 9y_1-\ 19y_3 \\ 9088x_2+34355x_3+34007x_4-32929x_5+22969x_6&=157y_1-152y_4 \\ -16616x_2+12231x_3-\ 6341x_4-\ 5209x_5-\ 5399x_6&=\ 17y_1-\ 76y_5 \\ -36152x_2+58361x_3-\ 1931x_4-\ 7019x_5+11867x_6&=191y_1-152y_6. \end{aligned} \tag{2}$$

[1] The preparation of this paper was sponsored (in part) by the Office of Naval Research.
[2] National Bureau of Standards and University of California at Los Angeles.

The multipliers that were used in eliminating x_1 are apparent from the coefficients of the y's on the right sides of the reduced equations.

We now use eq 2 to eliminate x_2 from the four equations that follow it. The multipliers we use for eq 2 are, respectively, 4857, 1136, 2077, and 4519. We get

$$\begin{aligned}
&-235\ 43223x_3+1082\ 22917x_4-1694\ 18155x_5+561\ 19027x_6=5\ 03367y_1-7\ 38264y_2-6536y_3 \\
&-70\ 01633x_3+\ 239\ 62515x_4-\ 383\ 92901x_5+124\ 29629x_6=1\ 10257y_1-1\ 72672y_2+6536y_4 \\
&-95\ 74518x_3+\ 462\ 12674x_4-\ 730\ 08298x_5+242\ 99290x_6=2\ 14662y_1-3\ 15704y_2-3268y_5 \\
&-194\ 66374x_3+1010\ 56706x_4-1586\ 61134x_5+538\ 84190x_6=4\ 73670y_1-6\ 86888y_2-6536y_6.
\end{aligned} \tag{3}$$

We now use eq 3 to eliminate x_3 from the three equations that follow it. The multipliers we use for eq 3 are, respectively, 3 68507, 1 67974, and 10 24546. We get

$$\begin{aligned}
&1018\ 85427\ 75664x_4-1485\ 84797\ 36168x_5+527\ 84896\ 85096x_6=4\ 88729\ 40000y_1 \\
&\qquad -5\ 80946\ 41224y_2-24085\ 61752y_3-80988\ 68712y_4 \\
&-90\ 90003\ 96128x_4+\ 169\ 74292\ 29652x_5-\ 61\ 00170\ 01012x_6=\ -41112\ 09360y_1 \\
&\qquad +\ 63889\ 07320y_2-10978\ 78064y_3+13498\ 11452y_5 \\
&-1434\ 17256\ 47920x_4+2302\ 30153\ 46048x_5-927\ 22912\ 23488x_6=-7\ 12099\ 03008y_1 \\
&\qquad +9\ 47491\ 69752y_2-66964\ 32656y_3+80988\ 68712y_6.
\end{aligned} \tag{4}$$

We now use eq 4 to eliminate x_4 from the two equations that follow it. The multipliers we use for eq 4 are, respectively, 63 21634 and 997 39385. We get

$$\begin{aligned}
&26343\ 37340\ 69713\ 22772x_5-9854\ 75613\ 37432\ 23540x_6=17\ 65250\ 77603\ 04880y_1+85\ 44010\ 53886\ 36424y_2 \\
&\qquad -93\ 01742\ 24170\ 60256y_3-51\ 19808\ 38113\ 15408y_4+95\ 64239\ 81708\ 51884y_5,
\end{aligned} \tag{5}$$

$$\begin{aligned}
&1\ 49345\ 83813\ 20139\ 98936x_5-1\ 30525\ 23686\ 92201\ 70136x_6=-171\ 10024\ 03515\ 99936y_1 \\
&\quad +919\ 23447\ 01231\ 65744y_2-714\ 71168\ 36351\ 59272y_3-807\ 77618\ 45306\ 22120y_4+573\ 85438\ 90251\ 11304y_6.
\end{aligned}$$

We now use eq 5 to eliminate x_5 from the equation that follows it. The multiplier we use for eq 5 is 13 52291 10622. We get

$$\begin{aligned}
&1\ 78080\ 76167\ 83302\ 24294\ 95529\ 75104x_6=646\ 84381\ 45668\ 50109\ 91756\ 88544y_1 \\
&\quad -1037\ 27853\ 59149\ 81148\ 61699\ 71008y_2+446\ 95683\ 03519\ 19158\ 33166\ 05736y_3 \\
&\quad +1234\ 46556\ 51847\ 48058\ 62839\ 54504y_4+1293\ 36364\ 42399\ 49987\ 74131\ 11848y_5 \\
&\quad -1368\ 83204\ 20859\ 69018\ 78357\ 06376y_6.
\end{aligned} \tag{6}$$

Dividing this through by the common factor 191 28479 63417 03768, we get

$$\begin{aligned}
&930\ 97185\ 49728x_6=3\ 38157\ 46308y_1-5\ 42269\ 20056y_2+2\ 33660\ 40527y_3+6\ 45354\ 77403y_4+6\ 76145\ 55311y_5 \\
&\qquad -7\ 15598\ 97507y_6.
\end{aligned} \tag{7}$$

Substituting this back into eq 5, 4, 3, 2, and 1, we get

$$\begin{aligned}
&930\ 97185\ 49728x_5=\ \ 1\ 88884\ 62180y_1+\ \ 99087\ 63656y_2-2\ 41312\ 82729y_3 \\
&\qquad +\ \ 60486\ 42243y_4+5\ 90937\ 51511y_5-2\ 67697\ 43115y_6, \\
&930\ 97185\ 49728x_4=\ \ 5\ 46840\ 79248y_1-1\ 05392\ 26192y_2-4\ 94982\ 08180y_3 \\
&\qquad -3\ 20138\ 43300y_4+5\ 11496\ 67628y_5-\ \ 19658\ 85132y_6, \\
&930\ 97185\ 49728x_3=-\ \ 29934\ 79728y_1+4\ 29235\ 11632y_2+\ \ 43989\ 17764y_3 \\
&\qquad -3\ 68561\ 73708y_4-2\ 89478\ 23484y_5+1\ 30251\ 85404y_6 \\
&930\ 97185\ 49728x_2=-4\ 95059\ 83764y_1+5\ 01313\ 85144y_2+2\ 21002\ 58797y_3 \\
&\qquad -3\ 77781\ 95727y_4-3\ 87417\ 30707y_5+4\ 19819\ 57079y_6 \\
&930\ 97185\ 49728x_1=\ \ 1\ 68307\ 83936y_1-\ \ 41475\ 04752y_2+2\ 21089\ 12392y_3 \\
&\qquad +4\ 71153\ 69576y_4+4\ 11243\ 40200y_5-1\ 67986\ 90584y_6
\end{aligned}$$

From these results one can easily write down A^{-1}.

We hardly need to stress the fact that the procedure outlined above is not a really practicable method to find A^{-1}. In the present case, we did carry the computation through to the bitter end, just to show how unwieldy it becomes, but it required 38 hours of computing time by a trained professional computer. We might note further that the computation would have been even more unwieldy and extensive if we had not deviated from a strict mechanical procedure by removing common factors from our multipliers when combining equations. Precisely, what we did do in this direction is described below.

In general, if we wish to eliminate x_i from two equations $ax_i + \ldots$, $bx_i + \ldots$, the mechanical way to proceed is to multiply the first equation by b and the second equation by $-a$, and add. However, in order to mitigate somewhat the frightful increase in the sizes of the coefficients in the later stages of the process, we have in every such step of the present computation determined the greatest common factor, c, of a and b, and have multiplied the first equation by b/c and the second by $-(a/c)$, and added. For example, in the case of eliminating x_5 from eq 5 and the equation following it, a is a 20-digit number and b is a 21-digit number. However, the common factor, c, is a 10-digit number, so that our multipliers, b/c and $-(a/c)$, are 12- and 11-digit numbers, respectively. If we had used b and $-a$ as multipliers, the coefficients in eq 6 would each have had about nine more digits.

Similarly, in the multipliers used with eq 4, a six-digit factor was removed, and in the multipliers used with eq 3 a two-digit factor was removed. Without such removal of factors, the coefficients of eq 6 would each have had about 15 more digits, so that it is doubtless worth while to carry out such a determination of common factors. Nevertheless, this portion of the computation can be quite a chore, especially when (as in the present case) the greatest common factor of a 20-digit number and a 21-digit number is required. Also, if determination of common factors is carried out, mechanization of the process is more much difficult.

One could effect a further saving in the number of digits carried by extracting common factors from each of the equations derived in the course of the computation, instead of only from eq 6. However, this entails a great increase in labor with only a moderate decrease in the number of digits in the various equations. In the present case, if all possible common factors would be extracted from previous equations, one would still obtain as the equation corresponding to eq 6 an equation with a 23-digit coefficient for x_6, and there would be much additional labor in the determination and extraction of common factors.

2. A New Method of Solution

We treat the same matrix A as in the previous section. If G is the inverse of A, then GA is the unit matrix. To find G, we find in succession B, C, D, E, and F with the properties that BA has its first column the same as the unit matrix, CA has its first two columns the same as the unit matrix, DA has its first three columns the same as the unit matrix, and so on up to GA, which has all its columns the same as the unit matrix.

Our method for finding B, C, . . ., G is a modification of the algorithm set forth in a previous note.[3] In addition, we use the following well-known property of matrix multiplication. If W and V are matrices with $WA=V$, then if we form W^* and V^* from W and V by performing the same elementary transformation on the rows of each, we will have $W^*A=V^*$. By an elementary transformation on the rows, we mean one of (a) Multiplying the ith row by a constant α. (b) Interchanging the ith and jth rows. (c) Adding α times the ith row to the jth row.

By a sequence of such transformations, we can reduce V to the unit matrix, and so the same sequence of transformations performed on W will reduce it to A^{-1}. This fact is the basis of various methods for computing A^{-1}. The novelty in our method lies in the fact that we are able to use mainly transformation (c) with an occasional transformation (b) until the final stage of the reduction, and also that we have a mechanical procedure for keeping the sizes of the numbers small until the final stages of the reduction.

[3] J. Barkley Rosser, A note on the linear Diophantine equation, Am. Math. Mo., 48 662 (1941).

As indicated earlier, we carry out the reductions on V in a certain order. First we reduce the first column of V to be the first column of the unit matrix. Then W has been reduced to the B mentioned earlier. Then, restricting ourselves to transformations that leave the first column of V unchanged, we reduce the second column to be the second column of the unit matrix. Then W has been reduced to the C mentioned earlier. Proceeding in this way, column by column, we eventually reduce V to I and W to A^{-1}.

To get started, let us take W to be the unit matrix, I. Then V is A. We first seek transformations that will bring the first column of V to the desired form. So we temporarily ignore all other columns of V, and consider only the first column, which is (I). This is to be reduced to form (II).

(I)	(II)
152	1
103	0
72	0
157	0
34	0
191	0

One can do this in many ways, but we follow the way that is proposed in the note referred to in footnote 3, since this is quite mechanical but keeps the sizes of the numbers involved reasonably small. Specifically, we apply the elementary transformation (c) to those two rows containing the two numbers of maximum absolute value. Thus we first add -1 times the fourth row to the sixth, getting (III). Then we add -1 times the first row to the fourth, getting (IV). Then we add -1 times the second row to the first, getting (V).

(III)	(IV)	(V)
152	152	49
103	103	103
72	72	72
157	5	5
34	34	34
34	34	34

Clearly, if we were trying to reduce the sizes of the numbers as rapidly as possible, we would now add -2 times the first row to the second. However, this presupposes that good judgment is to be applied at the various steps. One of the advantages of the procedure we are describing is that it gives quite good results even when applied quite mechanically. To illustrate, we ignore the smart transformation, and proceed according to rule, adding -1 times the ith row to the jth for the following values of i and j:

i	3	1	5	5	2	3	1	2	2	1	4	5	1	1
j	2	3	1	6	5	2	3	1	3	2	1	4	5	4

We then have

2
1
0
0
1
0

We now have a situation that occasionally arises, in which the largest number is at least twice as great as the next largest. In such case, our multiplier can conveniently be different from the -1 used uniformly so far. Thus we could conclude by adding -2 times the second row to the first, then -1 times the second row to the fifth, and, finally, by interchanging the first and second rows. However, we could equally well continue mechanically, since exactly the same result would ensue if we twice add -1 times the second row to the first row, and then add -1 times the second row to the fifth, and, finally, interchange the first and second rows.

Applying the transformations listed to the unit matrix transforms it into B, which is

$$\begin{Vmatrix} 1 & 1 & -4 & 0 & 1 & 0 \\ -1 & -3 & 10 & -1 & -3 & 0 \\ -3 & 2 & 3 & 0 & 1 & 0 \\ -2 & 2 & -3 & 2 & 0 & 0 \\ -2 & -1 & 3 & 1 & 1 & 0 \\ 0 & 0 & 0 & -1 & -1 & 1 \end{Vmatrix}$$

and has the property that the first column of BA is the same as the first column of the unit matrix. Moreover, the coefficients of B are quite small, which is why there is little increase in the sizes of our numbers as yet.

We now seek to bring the second column of BA into agreement with the second column of the unit matrix by means of elementary transformations. In order not to change the form of the first column, we must avoid the following transformations: (a) Multiplying the first row by a constant different from unity; (b) interchanging the first and jth rows; (c) adding α times the first row to the jth row for $\alpha \neq 0$.

However, the remaining transformations are quite adequate to effect the desired reduction. The second column of BA is

$$\begin{Vmatrix} -807 \\ 1967 \\ 981 \\ -891 \\ 928 \\ 79 \end{Vmatrix}$$

Confining attention to this column only, we see that the following sequence of transformations is called for. We add α times the ith row to the jth row for the following succession of α, i, and j:

α	-2	-1	$+1$	-1	11	-1	-1	-1	-1	$+1$	$+1$	-1	$+1$	$+1$	-1	-1	-1	-1	4	$+1$
i	3	5	4	4	6	6	3	5	6	4	3	5	4	2	2	2	2	6	4	2
j	2	3	5	1	4	1	6	3	5	6	4	3	5	4	1	3	5	2	6	4

Performing these transformations on B gives C, namely,

$$\begin{Vmatrix} -2 & 6 & -5 & 0 & 7 & -1 \\ 6 & -6 & 7 & 8 & 7 & -12 \\ 3 & 5 & -4 & -6 & 2 & 1 \\ 12 & -9 & 8 & -6 & -10 & -1 \\ -9 & 15 & -7 & -9 & -5 & 10 \\ 23 & -13 & 1 & -65 & -80 & 56 \end{Vmatrix}$$

The first two columns of CA are identical with those of the unit matrix. The third column is

$$\begin{Vmatrix} -491 \\ 1399 \\ 857 \\ 2968 \\ -439 \\ 5637 \end{Vmatrix}$$

In dealing with this, we must now curtail transformations on the first two rows. Nevertheless, we can reduce it to the desired form by adding α times the ith row to the jth row for the following succession of α, i, and j:

α	−1	−1	−1	−3	+1	+1	−1	+1	−1	−2	−1	−1	−1	+1	−1	−1	−1	+1	−1	−1	−1	−1	−1	−1	−1	−1	−2
i	4	6	3	3	5	5	5	3	4	3	6	6	4	4	6	4	3	3	6	3	3	6	6	3	3	6	3	3
j	6	4	2	6	3	2	1	5	3	4	3	2	6	1	4	6	4	5	3	6	1	3	2	6	4	3	1	6

Performing these transformations on C gives D, namely,

$$\begin{Vmatrix} -293 & 815 & -1464 & -5481 & -6270 & 5967 \\ 65 & -187 & 350 & 1317 & 1509 & -1434 \\ 283 & -796 & 1373 & 5057 & 5745 & -5493 \\ -68 & 158 & -351 & -1447 & -1721 & 1597 \\ -24 & 79 & -49 & -51 & 5 & 36 \\ -744 & 2095 & -3608 & -13278 & -15079 & 14421 \end{Vmatrix}$$

The first three columns of DA are identical with those of the unit matrix. The fourth column is

$$\begin{Vmatrix} 5\ 51061 \\ -1\ 33644 \\ -5\ 03483 \\ 1\ 51308 \\ -2958 \\ 13\ 21462 \end{Vmatrix}$$

In dealing with this, we must now curtail transformations on the first three rows. Nevertheless, we can start out to reduce it to the desired form by adding α times the ith row to the jth row for the following succession of α, i, and j:

α	−1	+2	+1	−3	−1	−1	+1	+1	+1	+1	−1	+1	−1	+1	+1	−3	+1	−2	+1	+2
i	6	5	4	6	6	6	6	5	5	4	4	4	6	5	4	6	6	6	6	5
j	3	6	5	4	3	1	2	6	3	5	1	2	4	6	5	4	1	2	3	6

α	−8	−3	+3	+1	−1	−1	−2	+1	−1	−3	+1	−2	+1	+3	−1	−1	+2	+1	+1	+1	+1
i	4	4	4	4	6	6	4	4	6	4	4	4	4	5	5	5	4	4	5	5	6
j	6	1	3	2	4	1	6	3	4	6	1	2	3	4	1	2	5	1	4	2	5

We now have the fourth column reduced to

$$\begin{Vmatrix} -1 \\ 0 \\ -1 \\ 0 \\ -2 \\ 0 \end{Vmatrix}$$

We cannot reduce the -2 in the fifth row to unity except by dividing by 2, which would introduce fractions. We would prefer to delay the introduction of fractions until the last possible moment. Accordingly, we multiply the first and third rows by 2, then subtract the fifth row from the first and third, then multiply the fifth row by -1, and, finally, interchange the fourth and fifth rows.

We have now changed the first and third columns so that they are no longer the first and third columns of the unit matrix, but have a 2 where the unit matrix has a unity. Also our fourth column has the same property. This can readily be corrected by multiplying the appropriate rows by one-half, but we will postpone this step until we can no longer avoid fractions.

Performing the indicated transformations on D gives the matrix

$$\begin{Vmatrix} -32262 & 147945 & -111285 & -133369 & -13466 & 99868 \\ -12391 & 60699 & -46328 & -54117 & -3115 & 39630 \\ 3330 & -20337 & 16173 & 17547 & -1298 & -11972 \\ -36052 & 168729 & -127507 & -151577 & -13242 & 112718 \\ -14752 & 74554 & -57273 & -66137 & -2494 & 47933 \\ 83708 & -393352 & 297521 & 353125 & 29905 & -262237 \end{Vmatrix}$$

This is not exactly the matrix E as we defined it earlier, but is close enough so that we shall call it E. The first four columns of EA are essentially the first four columns of the unit matrix, merely having 2 in place of unity in the first, third, and fourth columns. The fifth column of EA is

$$\begin{Vmatrix} 222\ 81663 \\ 94\ 55740 \\ -34\ 73233 \\ 256\ 87577 \\ 117\ 87645 \\ -600\ 10368 \end{Vmatrix}$$

We now reduce this by adding α times the ith row to the jth row for the following succession of α, i, and j:

α	$+5$	-2	-2	-1	$+11$	-3	-2	$+2$	-1	-181	-43	-37	-32	-5	7	3	3	-3
i	5	5	5	5	6	6	6	6	6	5	5	5	5	5	6	6	6	6
j	6	4	1	2	5	3	2	4	1	6	3	1	2	4	5	4	1	2
α	$+2$	5	-2	$+2$	-2	$+1$	2	1	-1	$+1$	-1	-1	$+1$	-1	$+4$	-1	$+2$	$+1$	$+1$
i	6	5	5	5	5	5	6	6	6	5	5	5	6	6	5	5	6	6	6
j	3	6	2	1	3	4	5	2	3	6	4	2	5	1	6	1	5	3	4

We now multiply the second, third, and fourth rows by 3, then add -1 times the sixth row to the second and $+1$ times the sixth row to the third and fourth. Finally, we interchange the fifth and sixth rows.

We could perform these transformations directly on E to get a matrix that we will call F. However, it is computationally easier to proceed as follows. We perform the transformations on the unit matrix, getting the matrix.

$$\begin{Vmatrix} 1 & 0 & 0 & 0 & 29\ 53877 & 5\ 80221 \\ 0 & 3 & 0 & 0 & 108\ 36604 & 21\ 28600 \\ 0 & 0 & 3 & 0 & -346\ 28689 & -68\ 02003 \\ 0 & 0 & 0 & 3 & -339\ 84487 & -66\ 75463 \\ 0 & 0 & 0 & 0 & -90\ 19777 & -17\ 71726 \\ 0 & 0 & 0 & 0 & -200\ 03456 & -39\ 29215 \end{Vmatrix}.$$

Then, if we multiply E on the left by the matrix above, we get the same matrix F that we would get by performing the indicated transformations on the rows of E. This matrix F follows.

$$\begin{Vmatrix} 49935\ 13702 & -80075\ 96989 & 34504\ 23435 & 95298\ 44107 & 99845\ 26301 & -1\ 05671\ 28268 \\ 1\ 83192\ 29419 & -2\ 93767\ 10487 & 1\ 26582\ 40724 & 3\ 49612\ 33901 & 3\ 66292\ 83279 & -3\ 87666\ 19778 \\ -5\ 85396\ 37006 & 9\ 38741\ 43339 & -4\ 04497\ 80947 & -11\ 17196\ 52341 & -11\ 70499\ 53243 & 12\ 38798\ 74958 \\ -5\ 74506\ 12736 & 9\ 21277\ 84365 & -3\ 96972\ 85793 & -10\ 96413\ 09887 & -11\ 48724\ 50163 & 12\ 15753\ 13514 \\ -1\ 52478\ 89704 & 2\ 44515\ 11094 & -1\ 05360\ 03125 & -2\ 90997\ 52301 & -3\ 04881\ 42192 & 3\ 22671\ 40121 \\ -3\ 38157\ 46308 & 5\ 42269\ 20056 & -2\ 33660\ 40527 & -6\ 45354\ 77403 & -6\ 76145\ 55311 & 7\ 15598\ 97507 \end{Vmatrix}$$

The matrix FA is

$$\begin{Vmatrix} 2 & 0 & 0 & 0 & 0 & 137\ 47502\ 92848 \\ 0 & 3 & 0 & 0 & 0 & 504\ 34158\ 21303 \\ 0 & 0 & 6 & 0 & 0 & -1611\ 63837\ 57000 \\ 0 & 0 & 0 & 6 & 0 & -1581\ 65675\ 30712 \\ 0 & 0 & 0 & 0 & 3 & -\ 419\ 78538\ 73419 \\ 0 & 0 & 0 & 0 & 0 & -930\ 97185\ 49728 \end{Vmatrix}.$$

At this point, we can read off the determinant of A. Most of the transformations that we used in forming F are such as to leave the determinant unchanged. Compiling those that do change the determinant, we find that the determinant of F is 108. So the determinant of A is $-5585\ 83112\ 98368$.

One can readily write down the inverse of FA, namely, a matrix whose components are fractions with the common denominator 930 97185 49728 and the following numerators

$$\begin{Vmatrix} 465\ 48592\ 74864 & 0 & 0 & 0 & 0 & 68\ 73751\ 46424 \\ 0 & 310\ 32395\ 16576 & 0 & 0 & 0 & 168\ 11386\ 07101 \\ 0 & 0 & 155\ 16197\ 58288 & 0 & 0 & -268\ 60639\ 59500 \\ 0 & 0 & 0 & 155\ 16197\ 58288 & 0 & -263\ 60945\ 88452 \\ 0 & 0 & 0 & 0 & 310\ 32395\ 16576 & -139\ 92846\ 24473 \\ 0 & 0 & 0 & 0 & 0 & -1 \end{Vmatrix}$$

Finally, we compute A^{-1} from the equation $A^{-1}=(FA)^{-1}F$. This gives the same matrix for $A)^{-1}$ that was computed in section 1.

The computations outlined in section 2 required 23 hours of computing time by a professional computer. This time included the time needed to train the computer in the unfamiliar method.

3. Remarks on Computational Details

One advantage of the procedure outlined in section 2 is the ease in making numerical checks. Since all the operations are on rows, one can easily carry an extra check column which is the sum of all the columns with which one is dealing. However, this is not needed, for other checks are possible, as follows. The computation of B is easily checked by computing the first column of BA and seeing if it agrees with the first column of the unit matrix. Then one can check C by computing the first two columns of CA and seeing if they agree with the first two columns of the unit matrix; and so on.

Not only does this furnish a convenient check, but when a check is not forthcoming, one can often find the error by this method. For example, in computing E, two mistakes were made, and the resulting matrix was

$$\begin{Vmatrix} -32262 & 1\ 47945 & -1\ 11285 & -1\ 32919 & -13466 & 99868 \\ -12391 & 60699 & -46328 & -54117 & -3115 & 38872 \\ 3330 & -20337 & 16173 & 17997 & -1298 & -11972 \\ -36052 & 1\ 68729 & -1\ 27507 & -1\ 51127 & -13242 & 1\ 12718 \\ -14752 & 74554 & -57273 & -66587 & -2494 & 47933 \\ 83708 & -3\ 93352 & 2\ 97521 & 3\ 52225 & 29905 & -2\ 62237 \end{Vmatrix}$$

which differs from E in most elements of the fourth column (where the original error had snowballed) and in the second element of the sixth column. When we multiplied this matrix on the right by A, we got

$$\begin{Vmatrix} 70652 \\ -1\ 44778 \\ 70650 \\ 70650 \\ -70650 \\ -1\ 41300 \end{Vmatrix}$$

as the first column, instead of twice the first column of the unit matrix. So, except for the second row, our errors are all multiples of 70650, which is $(450)\times(157)$. As 157 is the fourth element in the first column of A, it seems clear that there are errors in the fourth column of what purports to be E, and that these errors are multiples of 450. With this information, the mistake in computing in the fourth column was quickly discovered and eliminated. Now multiplication on the right by A verified all but the second row, and a trivial amount of detective work on the second row of the product sufficed to locate the error in the second row and give its magnitude.

In setting up the computation for use on IBM machinery, we notice that the majority of the steps consist of adding α times a row vector to another row vector, and that commonly α is a small integer. It is not difficult to wire a multiplier so that if we insert a deck with a card containing α followed by cards with the components of the two vectors interleaved, the multiplier will punch cards with the components of the resulting vector. At various stages in the procedure, some columns are computed for the product of two matrices, of which the first has as rows the row vectors that we are manipulating, and of which the second is always A.

Such a matrix multiplication can also be wired up for the multiplier. After the matrix multiplication, one then makes a list of α's and rows to be operated on by inspection from a column. This is most conveniently done by hand, which permits the exercise of judgment at this point. However, one can proceed perfectly mechanically, as we did in the illustrative example. Indeed, it is not clear that one can really do much better by exercising judgment than we did with our purely mechanical procedure. Once the list of α's and rows to be operated on is compiled, the respective operations can be quickly performed on IBM machinery. With only a multiplier, one must keep each row as a deck, and the row decks have to be interleaved and separated repeatedly. If a card programmed calculator is available, one may put an entire row on a single card (unless the matrix is of really high order) and the operations are greatly speeded.

The matrix A that we used was constructed from a table of random numbers in an effort to furnish an example that might be considered typical.

With an increase in the order of the matrix to be inverted, the method presented herein becomes even more of an improvement over the standard methods. The method was first devised in the summer of 1948 while working with Dr. N. G. Gunderson at Cornell University on a problem in number theory, in which we required the exact solution of 15 equations in 16 unknowns (one unknown was transposed to the right-hand side, and a solution obtained in terms of it). Fortunately, many of the coefficients were zeros. Even so, the usual methods of solution led us to hopelessly large numbers, whereas a solution was carried out by the method of this paper without encountering any integer of more than 12 digits.

Some of the procedural details of the present method were devised by Dr. Gunderson. The computations for the present paper were carried out by Lillian Forthal, Nancy Mann, and Gerald Kimble, under the direction of Marvin Howard.

Los Angeles, August 14, 1950.